JAERI-Review
98-014

PROGRESS REPORT ON SAFETY RESEARCH ON RADIOACTIVE WASTE MANAGEMENT FOR THE PERIOD APRIL 1996 TO MARCH 1998

October 1998

(Eds.) Toshihiko OHNUKI, Susumu MURAOKA and Tsunetaka BANBA

日 本 原 子 力 研 究 所
Japan Atomic Energy Research Institute

Progress Report on Safety Research on Radioactive Waste Management for the Period April 1996 to March 1998

(Eds.) Toshihiko OHNUKI, Susumu MURAOKA and Tsunetaka BANBA

Department of Environmental Safety Research
Nuclear Safety Research Center
Tokai Research Establishment
Japan Atomic Energy Research Institute
Tokai-Mura, Naka-gun, Ibaraki-ken

This report summarizes the research and development activities on radioactive waste management at the Engineered Barrier Materials Laboratory, Natural Barrier Laboratory and Environmental Geochemistry Laboratory of the Department of Environmental Safety Research, JAERI during the fiscal year of 1996 and 1997 (April 1, 1996 − March 31, 1998).

The topics are as follows:

(1) In the research and development of waste forms and engineered barrier, studies on development of ceramic waste forms, the leaching behaviors from glass waste at reduced condition and sorption behaviors on backfill materials have been carried out.

(2) In studies on shallow land disposal, studies on the migration behaviors of radionuclides in the presence of humic acid have been carried out.

(3) In the studies on geological disposal, the studies on diffusivity in rock formation, in-situ migration and diffusion experiments, sorption mechanism, fixation mechanism, natural analogue study and geochlonology have been carried out.

放射性廃棄物処理処分の安全性研究に関する平成8,9年度報告書

日本原子力研究所東海研究所安全性試験研究センター環境安全研究部
（編）大貫 敏彦・村岡 進・馬場 恒孝

人工バリア研究室、天然バリア研究室及び地質環境研究室において、平成8年度及び9年度に実施した放射性廃棄物処理処分の安全性研究に関する研究成果をまとめたものである。主な内容としては以下のとおりである。

(1) 廃棄物固化体及び人工バリア材の研究開発では、セラミック固化体の開発に関する研究、還元雰囲気におけるガラス固化体からの浸出挙動に関する研究及び緩衝材への収着挙動に関する研究を行った。

(2) 浅地中埋設に関する研究では、放射性核種の移行に及ぼす腐植物質の影響に関する研究を行った。

(3) 深地層処分に関する研究では、岩石中の拡散挙動に関する研究、原位置における移行と拡散に関する研究、収着機構及び固定機構を解明する研究、ナチュラルアナログ研究及び炭素同位体を用いた年代測定に測定に関する研究を行った。

東海研究所：〒319-1195 茨城県那珂郡東海村白方白根2－4

Contents

目　　　次

This is a blank page.

Introduction

This report seeks to summarize the work implemented in the Engineered Barrier Materials Laboratory, Natural Barrier Laboratory and Environmental Geochemistry Laboratory of the Department of Environmental Safety Research, JAERI during the fiscal year of 1996 and 1997 (April 1, 1996 – March 31, 1998). These three laboratories have been conducting the studies on the development of new waste forms and performance of engineered and natural barriers for the containment of the disposed waste. The overall goal of the studies in the laboratories is to construct the methodology for assessing the impact of waste disposal.

The progress report series have been issued in the following numbers:

JAERI-M 82-145, 83-076, 84-090, 86-131, 87-131, 88-201, 89-192, 91-019, 92-022, 93-037, 94-027, JAERI-Review 96-005 and 97-007.

This is a blank page.

－ 3 －

1. Research and Development of Waste Forms and Engineered Barrier

1.1 Np-doped Yttria-Stabilized Zirconia Waste Form for high concentrated TRU Nuclides from Partitioning.

K.Kuramoto

INTRODUCTION

For the management of high concentrated TRU nuclides arising from a partitioning process of high-level liquid waste, it is very important to isolate them from the biosphere for a long time.   The TRU nuclides are to be conditioned by being fixed into a suitable solid form, and then to be disposed in an underground repository over thousands years.   In the previous works[1], to decide matrix for conditioning the TRU nuclides characteristic examinations waste forms were carried out with emphases on phase stability, chemical durability and compactness using TRU simulants-doped yttria-stabilized zirconia (YSZ), alumina-compound and YSZ-alumina composite. From the results it was concluded that YSZ was superior to the other matrices.   For the property evaluation of waste forms for the conditioning of the TRU nuclides, it is necessary to investigate the initial properties using as-fired specimen and the long-term stability related to disintegration and α-decay damage for a long time.   In the present study, the initial properties of phase stability, mechanical property and compactness are investigated and evaluated using Np-doped YSZ waste forms (Np-YSZ) with Np content.   In addition effect of sintering atmospheres on the properties are also examined.

EXPERIMENTAL PROCEDURE

The compositions of Np-YSZ are listed in Table I.   The YSZ (TZ-8Y; Tosoh Co.Ltd.) powder and designed amount of Np nitrate solution were mixed and calcined at 900 °C in alumina crucibles, followed by a ball milling to obtain fine powder.   The

powder mixtures were pelletized at 130 MPa and sintered at 1500 °C for 80 hours in a stream of air (Np-YSZ_{OX}) or 3 % H_2+Ar (Np-YS_{RE}) using a resistance furnace.

To evaluate phase stability, crystalline phases in Np-YSZ were identified by X-ray diffraction (XRD) method. The measurement was carried out with Cu Kα radiation in air at room temperature at 40 kV and 40 mA. Lattice parameters of phases formed in Np-YSZ were determined by Nelson-Riley method[2].

To evaluate mechanical property, Vickers hardness[3], Young's modulus[4] and fracture toughness[3] of Np-YSZ were measured. A Vickers pyramid indenter and a knoop indenter were used with a load of 4.9 N on specimen surface polished with up to 1 μm of diamond paste.

To evaluate compactness, density measurement of as-fired pellet Np-YSZ were carried out at a room temperature using the water displacement method.

RESULTS AND DISCUSSIONS

Phase Stability

From the results of XRD measurement, only a fluorite-type structure phase was identified in Np-YSZ_{OX} doped up to 40 mol% (equal to 60 wt%). And lattice parameter of the fluorite-type structure of Np-YSZ_{OX} enlarges in proportion to the content of Np as shown in Fig. 1. From the identification of XRD patterns and the linearity of the lattice parameters, the Np-YSZ_{OX} has a wide range solubility for Np. Therefore, it is evaluated that the Np-YSZ has an excellent phase stability in respect of Np. In the same results as mentioned above, the results of XRD patterns and the lattice parameters of Np-YSZ_{RE} were identical with the Np-YSZ_{OX}. So it is cleared that sintering atmosphere did not effect on the phase stability of Np-YSZ, and further on the valence of Np in Np-YSZ. Here, from the data of the library computer code ORIGEN2[5] and mass balance of the partitioning process[6], about 900 g of TRU oxides is produced from 1 ton of UO_2 spent fuel . This means that 1 ton-spent fuel can

be conditioned by 1.5 kg of TRU-YSZ waste form (600 g of YSZ and 900 g of TRU oxides, about 200 cm^3). In addition, the valence of Np in YSZ waste forms is suspected as 4+ based on the following discussions by comparison with Ce-doped YSZ waste forms (Ce-YSZ). In the case of Ce-YSZ sintered in oxidizing atmosphere, Ce exists as tetra-valent[7] and the lattice parameter enlarges in proportion to the content of Ce (solid line) as shown in Fig. 1. On the other hand, in the case of reducing atmosphere, Ce is tri-valent and the lattice parameter is in proportion to the content of Ce and only the fluorite-type structure phase is identified in specimens when the content is within the solubility limit of Nd (dotted lines). Once the content of Ce exceeds the solubility limit and the additional pyrochlore structure phase is formed, the lattice parameter is kept constant. It should be noted that the gradient of lattice parameter of the reducing atmosphere is larger than that of oxidizing atmosphere because of the ionic radii difference of Ce^{3+} and Ce^{4+} as shown in Table II[8]. Judging from the results that lattice parameters, especially the gradient, of Np-YSZ$_{OX/RE}$ is almost the same as that of Ce^{4+}-YSZ and there is no solubility limit of Np-YSZ$_{OX/RE}$ in the range of 0 to 40 mol% of Np content, it is suggested that the valence of Np in Np-YSZ may be 4+ regardless of the different sintering atmospheres.

Mechanical Property

Figure 2 shows Vickers hardness, Young's modulus and fracture toughness of Np-YSZ with Np content, where the values of Ce-, Nd- and Ce+Nd-YSZ specimens, borosilicate glass and SYNROC were also illustrated. It is revealed that the values of Young's modulus and fracture toughness of Np-YSZ are similar to each other regardless of Np contents and the sintering atmosphere, and that Vickers hardness of Np-YSZ are also the same as each other except 10 mol% Np-YSZ$_{RE}$. This low value is due that quite low relative density causes fragility of this specimen . In addition, it is confirmed that Vickers hardness, Young's modulus and fracture toughness of Np-YSZ is

not significantly different from those of Ce-, Nd- and Ce+Nd-YSZ. This result leads to the suggestion that the mechanical property of YSZ waste forms doped similar elements chemically and physically will be similar. And, because the mechanical property of Np-YSZ is more than those of a borosilicate glass[9] and a SYNROC[10], it is evaluated that the mechanical property of Np-YSZ is good enough for waste forms.

Compactness

Figure 3 shows the ratio of apparent density and theoretical density (relative density) of Np-YSZ as a function of Np content. Relative density of all Np-YSZ is over 90 % regardless Np content except 10 mol% Np-YSZ$_{RE}$. This leads to the confirmation that compact waste forms can be formed even in glove boxes and to an evaluation that the Np-YSZ is compact enough.

CONCLUSION

The main results of the present study are as follows:

(1) Phase stability of Np-doped YSZ waste forms are excellent.

(2) Mechanical property of Np-doped YSZ waste forms are good enough as a waste form.

(3) Compact Np-doped YSZ waste forms can be formed.

And followings are suggested that:

(4) 1 ton of spent fuel can be conditioned by 1.5 kg-200 cm^3 of YSZ waste form.

(5) Np in YSZ waste form is tetra-valent.

REFERENCE

(1) Kuramoto,K.,et al.,: Proc.of International Conference on Evaluation of Emerging Nuclear Fuel Cycle System (Global'95), 1838, (1995).

(2) "X-Ray Method": ed.by Whiston,C.,John Wiley & Sons, (1985).

(3) JIS,: R 1607 (in Japanese), (1995).

(4) Marshall,D.B.,et al.,: J.Am.Ceram.Soc., C-175, (1982).

(5) Croff,A.G.,: Nucl.Technol., 62, 335, (1983).

(6) Morita,Y.,et al.,: Radioac.Waste Res., 2, 75 (in Japanese), (1996).

(7) Muraoka,S.,et al.,: JAERI-M 94-027, 31, (1994).

(8) Shannon,R.D.: Acta.Cryst., A32, 751 (1976).

(9) Lutze,W.,et al.,: "Radioactive Waste Forms for the Future", ed.by Lutze,W.,et al.,
699, Elsevier Science Publishing Company, (1988).

(10) Ringwood,A.E.,et al.,: "Radioactive Waste Forms for the Future", ed.by
Lutze,W.,et al., 233, Elsevier Science Publishing Company, (1988).

Table I Compositions of Np-doped YSZ waste forms in mol%*

Sample	TRU NpO$_2$	Matrix ZrO$_2$	YO$_{1.5}$
10 mol% Np-YSZox/re#	10.00	77.13	12.78
20 mol% Np-YSZox/re	20.00	68.56	11.44
30 mol% Np-YSZox/re	30.00	59.99	10.01
40 mol% Np-YSZox/re	40.00	51.42	8.58

* The compositions of constituents are indicated by contents of each cation in the total cations for each samples.
# OX and RE means samples formed in oxidizing and reducing atmosphere, respectively.

Table II Ionic Radii of Ce and Np ions in 6 fold-coodination in nm

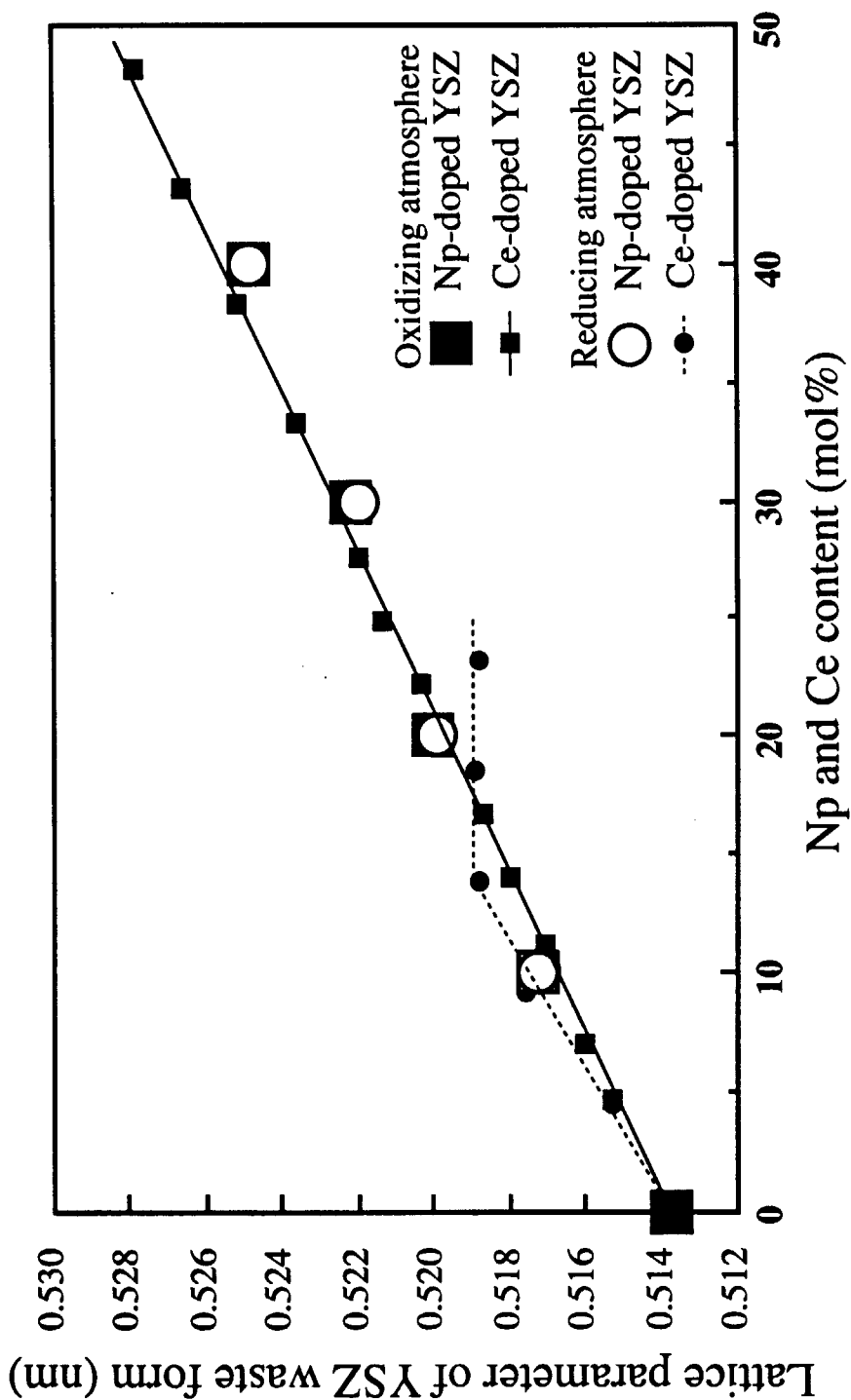|	M3+	M4+
Ce	0.101	0.087
Np	0.101	0.087

Fig. 1 Variation of the lattice parameters of the fluorite-type strcture of the Np-doped and Ce-doped yttria-stabilized zirconia (YSZ) with Np and Ce content, respectively.
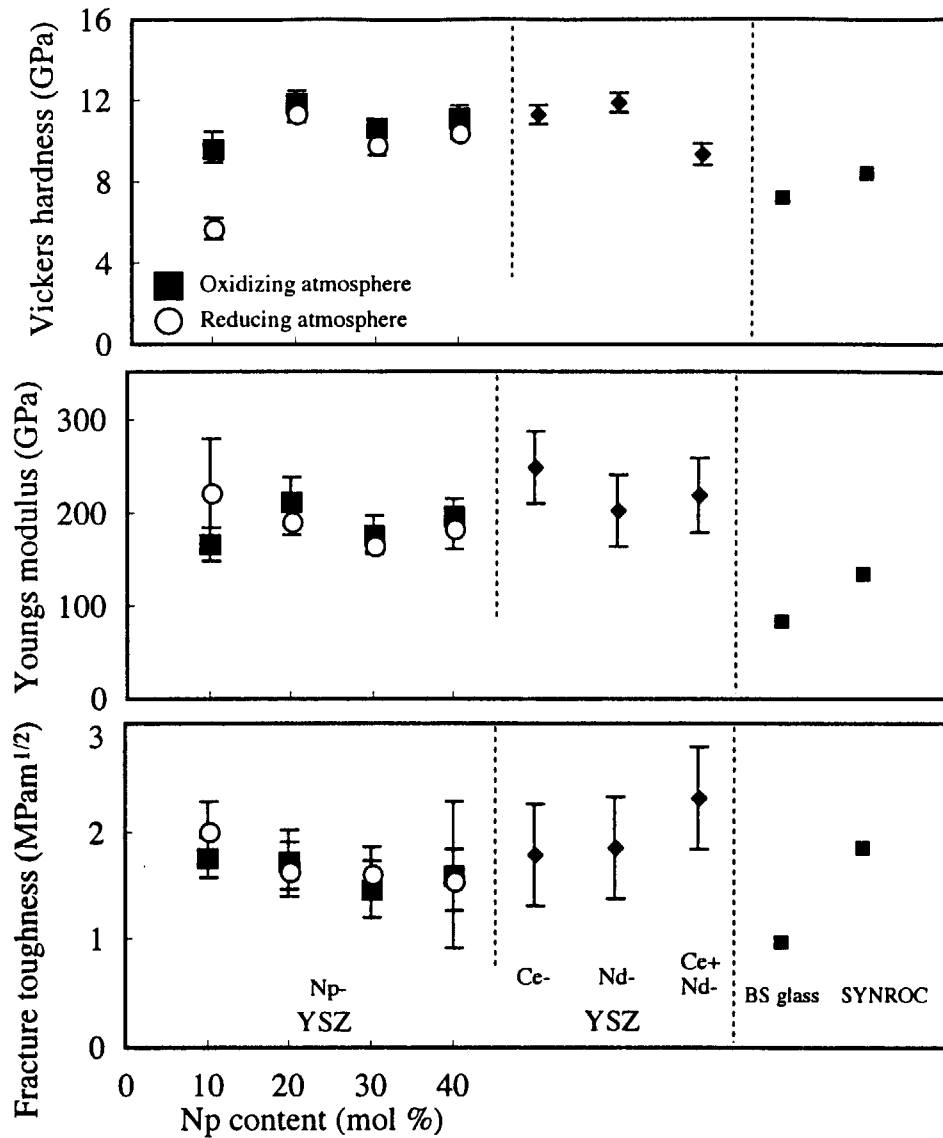
Fig. 2 Mechanical property of Np-doped YSZ waste forms with Np content, and that of Ce-, Nd- and Ce+Nd-YSZ specimen, and BS glass and SYNROC.
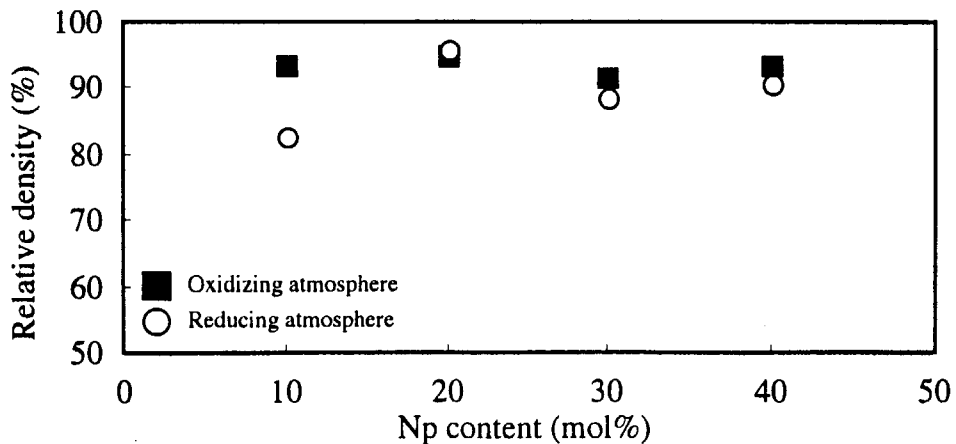
Fig. 3 Relative density of Np-doped YSZ waste forms with Np content.

1.2 Volume Swelling of Cm-doped Perovskite due to α-Decay Damage

H. Mitamura

INTRODUCTION

Synroc was developed as a matrix for immobilizing high-level radioactive waste. After repository emplacement, the nuclear waste form will experience long-term self-irradiation and accumulate damage due primarily to alpha-decay events. This radiation damage can deleteriously affect stability of the waste form. In Synroc, actinide nuclides would be incorporated in the actinide-host phases, perovskite and zirconolite. As microencapsulation by more durable phases could mask radiation-damage effects on the less durable phase, single phase material is useful for getting direct information on this point. In the present study, macroscopic and microscopic volume swelling of Cm-doped perovskite due to α-decay damage was investigated through density measurement and X-ray diffractometry.

EXPERIMENTAL

The Cm-doped perovskite cylinders were made by hot-pressing at 1250°C under the pressure of 29 MPa for 2 hours.[1] For the measurement of macroscopic volume swelling, the density of a Cm-doped cylinder was periodically measured at 30°C using the water displacement method. For microscopic volume swelling, a thin semicircular section was subjected to X-ray diffractometry. X-ray diffraction data were periodically collected using Cu Kα radiation at intervals of 0.05° over 2θ range of 15 to 120°. Obtained X-ray data were refined using Rietveld analysis.[2]

RESULTS AND DISCUSSION

Density Change

The density of Cm-doped perovskite gradually decreases with increasing dose. Change in density was well fitted by an exponential relationship. The fitting gave 4.08 $g \cdot cm^{-3}$ as an initial density of Cm-doped perovskite. Using this initial density, density change was obtained as a function of α-decay dose (Fig. 1). Data from Cm-doped Synroc and zirconolite are also included in Fig. 1 as references. At a dose of 2.5×10^{18} α decays$\cdot g^{-1}$, the fractional density decrease of the Cm-doped perovskite is 3.4 %. In Synroc, this dose corresponds to a disposal age of 2×10^5 years. Perovskite density changes most and zirconolite density least. This phenomenon could be due to the fact that perovskite had the largest unit-cell volume expansion in all Synroc constituent minerals.

Unit-Cell Volume Swelling

Figure 2 shows a Rietveld plot for as-damaged Cm-doped perovskite. The accumulated dose of the sample is 5×10^{17} α decays$\cdot$g^{-1}. The observed data are shown by crosses (+) and the calculated pattern is the continuous line overlying them. The lower curve is the difference between the observed data and the calculated pattern. Vertical markers indicate the position of all Bragg reflections. The resultant profile (R_p), weighted profile (R_{wp}) and Bragg (R_p) factors are 8.5, 11.3 and 3.9, respectively. Generally speaking, the better the profile fitting is, the lower these factors are.

Figure 3 shows change in elongation of cell parameters as a function of α-decay dose. The results means that expansion of the unit cell is anisotropic and the 'a' parameter changes most and the 'c' parameter least. At a dose of 2.5×10^{18} α decays$\cdot$g^{-1}, elongation of a-, b-, and c- parameters are 1.06, 0.76, 0.58%, respectively. Anisotropic expansion of the unit cell could be due to an anisotropic response to an essentially isotropic stress center because the structure of perovskite is based on a pseudo-cubic subcell.

Figure 4 shows change in volume and swelling of the true unit cell as a function of α-decay dose. When the expansion of the unit cell is assumed to satisfy an exponential relation, the fitting gave the initial unit cell volume of 0.2232 nm^3 and the solid line in Fig. 4. At a dose of 2.5×10^{18} α decays$\cdot$g^{-1}, swelling of the true unit cell reaches 2.4 %. This value is by 1% lower than the density change at the same dose. As optical microscopy found some macrocracks on the Cm-doped perovskite sample, a difference between the macroscopic and microscopic volume swellings may be probably attributed to occurrence of microcracking due to anisotropic swelling of the unit cell.

CONCLUSION

The main results of the present study are as follows:

(1) Perovskite density changes most and zirconolite density least. At a dose of 2.5×10^{18} α decays$\cdot$g^{-1}, the fractional density decrease of the Cm-doped perovskite was 3.4 %.

(2) At a dose of 2.5×10^{18} α decays$\cdot$g^{-1}, swelling of the true unit cell reaches 2.4 %. A difference between the density change and unit cell volume swelling may be probably attributed to occurrence of microcracking due to anisotropic swelling of the unit cell.

REFERENCES

[1] H. Mitamura et al., pp. 1405-12 in Scientific Basis for Nuclear Waste Management Vol. XVIII, Materials Research Society, PA, 1995.

[2] T. J. White, H. Mitamura and T. Tsuboi, pp. 871-78 in Scientific Basis for Nuclear Waste Management Vol. XVIII, Materials Research Society, PA, 1995.
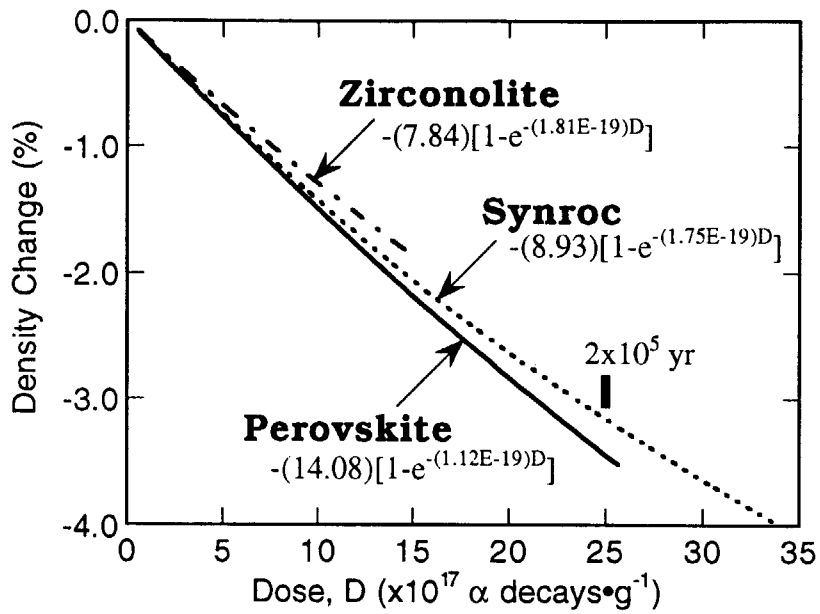
Fig. 1 Density change in Cm-doped perovskite. Data from Cm-doped Synroc and zirconolite are also included as references.
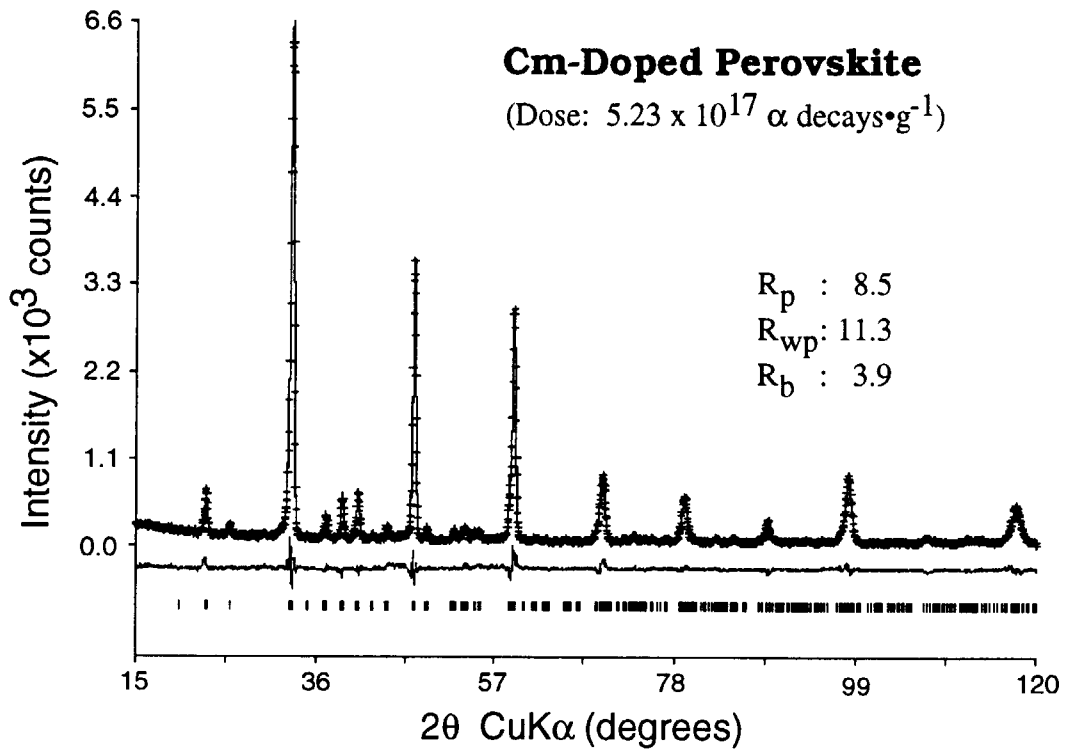
Fig. 2 Rietveld plot for Cm-doped perovskite. The observed data are shown by crosses (+) and the calculated pattern is the continuous line overlying them. Vertical markers indicate the position of all Bragg reflections.
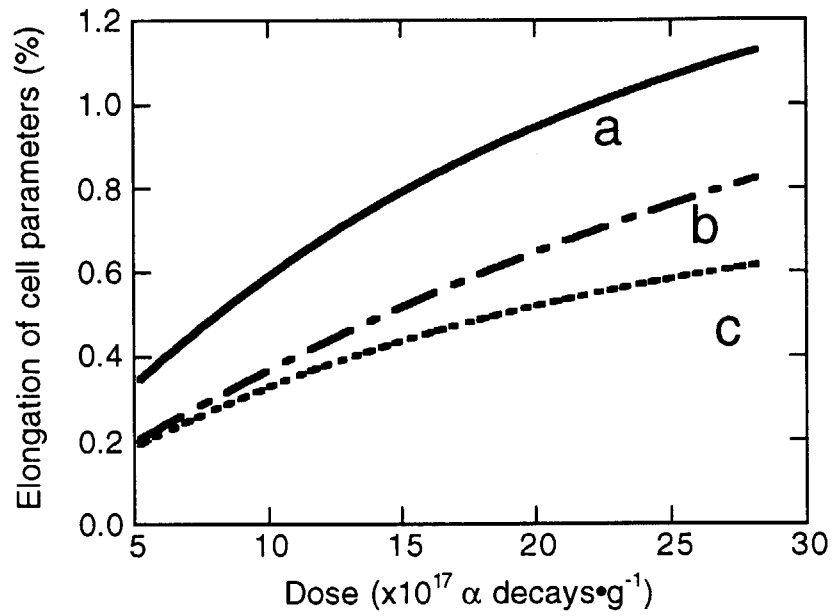
Fig. 3 Change in elongation of cell parameters as a function of α-decay dose.

$$\delta V/V_0 = (3.7)\{1-\exp(-4.2 \times 10^{-19}D)\}$$
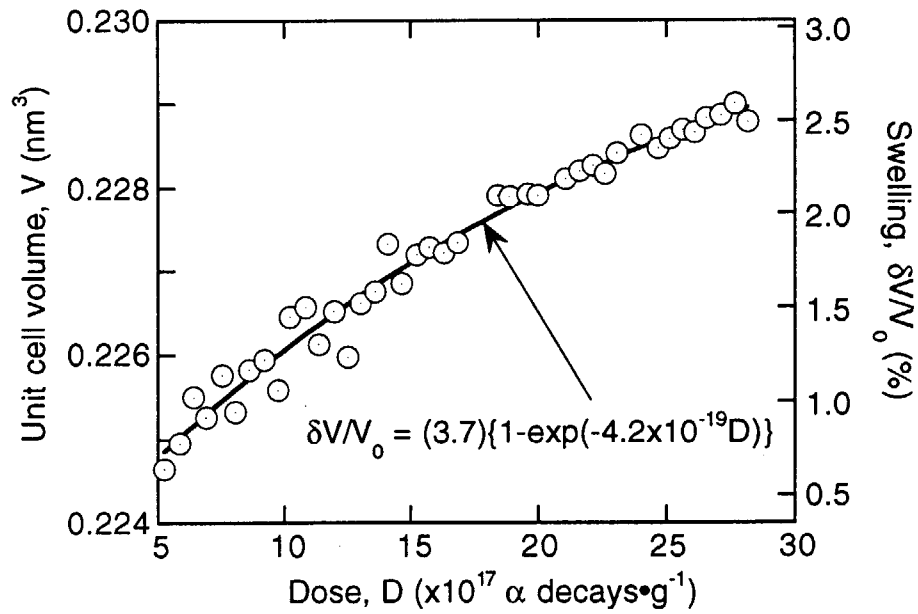
Fig. 4 Changes in volume and swelling of unit cell as a function of α-decay dose.

1.3 EFFECTS OF WATER REDOX CONDITIONS AND PRESENCE OF MAGNETITE ON LEACHING OF Pu FROM HLW GLASS

T. Maeda

INTRODUCTION

The purpose of this study is to understand the effects of redox conditions and of the presence of iron corrosion products (magnetite) on the release of actinides from HLW glass, for evaluating the release of actinides from the repository. Static corrosion tests were performed on a simulated borosilicate HLW glass doped with Pu, in deionized water and in the presence of magnetite, under oxidizing and reducing conditions. The corrosion tests under oxidizing conditions were performed in air, while the corrosion tests under reducing conditions were performed in a mixed gas atmosphere (Ar+5%H2) where the solution Eh was maintained at -0.5 V vs. SHE. After the corrosion tests, the solution was passed through filters with different pore size in order to investigate the particle size distribution of Pu colloids, and the solution concentrations of Pu and other glass constituent elements were measured.

EXPERIMENTAL

A powdered simulated waste glass of borosilicate type doped with Pu (238PuO2; 0.22wt%) was used as glass specimen. Static corrosion tests with grain sizes from 75μm to 150μm were performed in deionized water at 90℃, in the presence of magnetite under oxidizing and reducing conditions. Synthetic magnetite with grain size under 5μm and the specific surface area of 7.9 m²/g was used. The glass specimen (1.6g), the magnetite (1.6g) and deionized water (50ml) were placed in a Teflon container with a S/V ratio of 2600 m⁻¹ and kept at 90℃ for periods of up to 90 days. For corrosion tests under reducing conditions performed in (Ar+5%H2) atmosphere, the pH and Eh of the initial solution (deionized water) were measured to be 6.7 and -0.35 V vs. SHE at 25℃, respectively. Details of the test methods are given elsewhere[1]. Analogous corrosion tests without addition of magnetite were performed under both redox conditions for comparison. At the end of the corrosion tests, the Teflon container was cooled to room temperature and the solution pH and Eh were measured immediately. The leachate was passed through filters with pore sizes of 450nm, 5nm and 1.8nm, and concentrations of Pu and major glass constituents in the filtrates were measured by α-spectrometry and ICP-AES.

RESULTS and DISCUSSION

Fig.1 shows the solution pH and Eh as a function of corrosion time. Fig.2

shows normalized concentrations (NC) of Pu and major glass constituents in the leachates. It was observed that the presence of magnetite caused an increase of NC of soluble elements(B, Na) under both redox conditions. The higher B, Na release indicates that the presence of magnetite enhances glass corrosion. The enhancement under reducing conditions was small compared to that under oxidizing conditions. It is noted that the NC of soluble elements continued to increase at a relatively high rate when magnetite was present under oxidizing conditions. Fig.3 shows the solution concentrations of Pu after filtration with three different pore sizes. It was observed that the presence of magnetite caused an increase of the Pu concentrations in the 5 nm filtrates under both redox conditions. However, both the presence of magnetite and the water redox conditions had no remarkable influence on the Pu concentrations in the 1.8 nm filtrates. In all cases, the Pu concentrations in the 1.8 nm filtrates reached approximately 10^{-9} mol/l, and those in the 5 nm filtrates were higher than those in the 1.8 nm filtrates. There was no remarkable difference in the Pu concentrations between the 5 nm and the 450 nm filtrates. The Pu concentrations in the 1.8 nm filtrates were assumed to correspond to dissolved species, and the difference between the 1.8 nm and 5 nm filtrates might be attributed to insoluble suspended fractions (colloidal particles). Therefore, it is concluded that Pu colloidal particles with the size from 1.8 nm to 5 nm are dominant in all leachates, and that significantly higher colloid concentrations are found in leachates from corrosion tests conducted in the presence of magnetite.

REFERENCES

[1]Y.Inagaki, A.Sakai, et al., Mat.Res.Soc.Symp.Proc.Vol.465(1997)213.
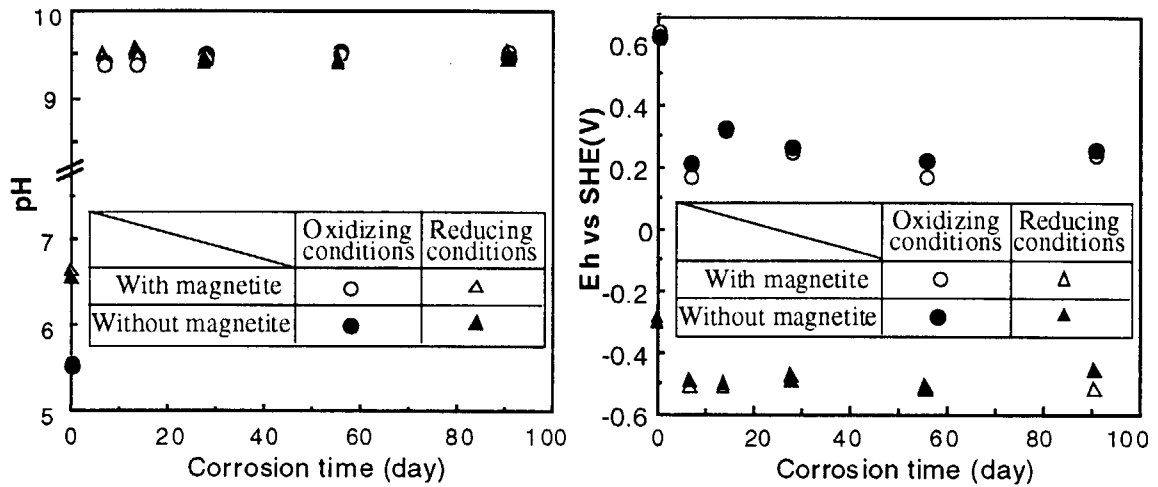
Fig.1. Solution pH and Eh as a function of corrosion time
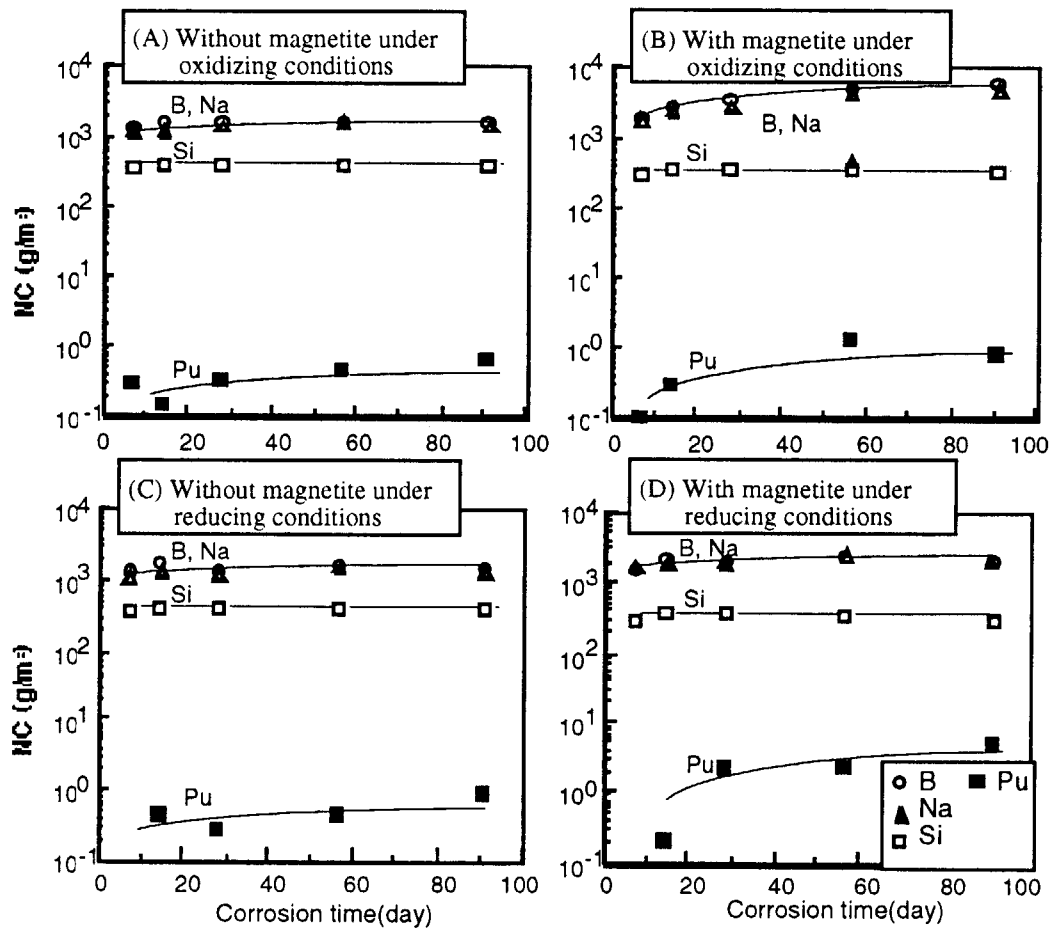
Fig.2. Normalized concentrations (NC) of Pu and major glass constituents calculated from the concentrations in 450 nm filtrates.
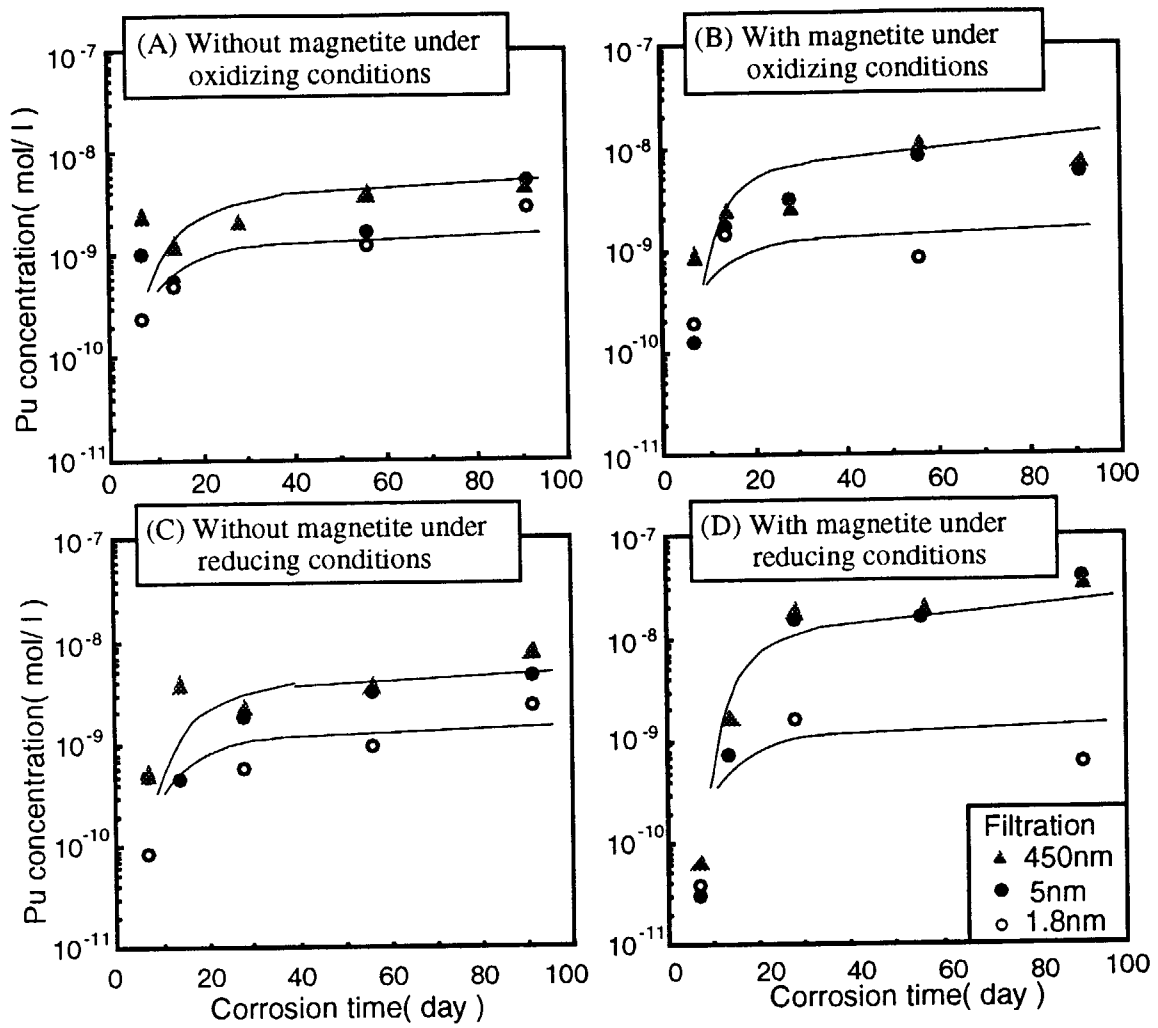
Fig.3. Solution concentrations of Pu after filtration
with three different pore sizes.

1.4 Sorption Characteristics of Americium on Buffer Material

N. Kozai

1. Introduction

Sodium-rich type bentonite has been proposed as a candidate of a buffer material for radioactive waste disposal because the sorption potential of bentonite for radionuclides is expected to retard their dispersion to the geosphere. Bentonite contains several kinds of minerals such as smectite and quartz. In particular, smectite has high sorption capacities for nuclides.

We investigated sorption characteristics of americium on smectite. Americium has been recognized as an important element for radioactive waste disposal because of its long half life and high toxicity. In this study, two types of smectite (homoionic Na^+ type and Ca^{2+} type) were used to examine the effect of replacement of Na^+ of smectite for Ca^{2+} by the contact of ground water, which contains Ca^{2+} abundantly, on the sorption of americium.

2. Experimental methods

2.1 Materials preparation

A trivalent (Am(III)) americium solution obtained from the Commissariat à l'Énergie Atomique (CEA) was diluted with 0.01 M $NaClO_4$ to yield a working solution having a americium concentration of about 5×10^{-10} M.

Smectite was Kunipia F (Kunimine Industries Co. Ltd.), which was mainly montmorillonite and contained quartz as a minor contaminant (<1 weight %). Before use, the smectite was converted to homoionic Na^+, or Ca^{2+} form (Na-smectite, or Ca-smectite) by submerging in 1 M NaCl, or 1 M $Ca(CH_3COO)_2$ solution for 3 times. Na-smectite was repeatedly washed using deionized water until Cl^- in a supernatant was not detected by $AgNO_3$ solution. Ca-smectite was repeatedly washed using deionized water for the same times as Na-smectite. These types of smectite were then dried, ground, and sieved under 74μm.

2.2 Sorption - desorption experiments

For the sorption experiments, the pH of the americium solution was adjusted in the range of 2 to 8 using HCl and NaOH solutions. A portion (0.06 g) of the powdered smectite was soaked in 6 cm³ aliquots of the americium solution and stored in a sealed polycarbonate tube for 10 days

at 20°C. This smectite-solution mixture was agitated once a day throughout the experiment. No further pH adjustment of the solution was carried out. At completion of the americium-smectite contact, a supernatant was collected by centrifugation for 1 hour at 1.2×10^4 rpm (2.6×10^4 G) and its pH measured. The americium concentration of the supernatant was determined by a combination of a liquid scintillation analyzer with alpha/beta discrimination (Packard Tri-Carb^{TM} 2550TR/AB) and a liquid scintillation cocktail (Packard Ultima-Gold XR).

Subsequently, the sequential extraction experiment was conducted in two steps. First, 6 cm^3 of 1 M KCl solution was added to the contacted smectite (previously collected by centrifugation), and then kept for 2 days at 20°C. At the conclusion of the extraction, the KCl solution was separated by centrifugation and the americium concentration in the supernatant was determined. Second, an acid extraction using 1 M HCl was undertaken in the same way as the extraction using 1M KCl. Extraction by each solution was carried out twice to confirm the complete desorption of americium in each extraction step.

3. Estimation methods

The relation between the quantity of americium before and after the sorption-desorption experiment is expressed by

$$C_0 \cdot V = C \cdot V + Q, \qquad (1)$$

$$Q = Q_K + Q_H + Q_R, \qquad (2)$$

where C_0 = initial concentration of americium in solution (mol $\cdot$ cm^{-3}), C = concentration of americium in solution after the sorption experiment (mol $\cdot$ cm^{-3}), Q = total amount of americium sorbed on smectite (mol), Q_K = the amount of americium desorbed by KCl from smectite (mol), Q_H = the amount of americium not desorbed by KCl but desorbed by HCl from smectite (mol), Q_R = the americium remained on smectite after the desorption (mol), and V = volume of solution (cm^3).

To evaluate the distribution of americium between solution and smectite, the sorption ratios of the amount of americium sorbed on smectite to the initial amount of americium in the solution were defined as:

$$P_T = \frac{Q}{C_0 \cdot V} \cdot 100 \ (\%), \qquad (3)$$

$$P_K = \frac{Q_K}{} \cdot 100 \ (\%), \qquad (4)$$

$$P_H = \dfrac{\dfrac{C_0 \cdot V}{Q_H}}{C_0 \cdot V} \cdot 100 \ (\%), \qquad (5)$$

$$P_R = \dfrac{\dfrac{C_0 \cdot V}{Q_R}}{C_0 \cdot V} \cdot 100 \ (\%), \qquad (6)$$

where P_T = the percent fraction of all of the americium sorbed on smectite, P_K = the percent fraction of the sorbed americium desorbable with KCl, P_H = the percent fraction of the sorbed americium stable with KCl but desorbable with HCl, and P_R = the percent fraction of the sorbed americium remained on smectite after the desorption procedure.

The distribution coefficient of americium for smectite (Kunipia F) was calculated by the following equation:

$$K_d = \dfrac{Q}{C_0 \cdot W}, \qquad (7)$$

where K_d = distribution coefficient ($cm^3 \cdot g^{-1}$) and W = weight of smectite (g).

4. Results and discussion

As shown in Fig. 1 nearly 100% of americium was sorbed on Na- and Ca-smectite in the pH range of 2 to 8: K_d of americium ranged from 2×10^3 to more than 10^4 $cm^3 \cdot g^{-1}$. At pH <3, sorption ratio for Ca-smectite, P_T was slightly lower than that for Na-smectite.

All of the americium sorbed were completely desorbed by 1M KCl and 1M HCl solutions (P_R = 0). As lowering the pH the fraction of the sorbed americium desorbable with KCl increased, and this fraction became dominant below around pH 5. Cation species of americium, such as Am^{3+} and $AmOH^{2+}$, becomes dominant as lowering the pH and Am^{3+} is predominant below around pH 5 [1]. The fraction of the americium desorbable with KCl from Ca-smectite, P_K, was slightly lower than that from Na-smectite in all of the experimental pH range. Because the association of Ca2+ with smectite is stronger than that of Na+ with smectite, less ion exchange

reaction occurs generally on Ca-smectite than on Na-smectite. Thus, the americium desorbable with KCl is believed to be cation species of sorbed by ion-exchange mechanism.

On the other hand, the other fraction of americium, which was not desorbed by KCl, increased with pH. This fraction became predominant above pH 7 where hydrolysis or carbonate species of americium, which possess a monovalent positive charge, a neutral charge, or a negative charge, is dominant. Surface coordination with the reactive hydroxyl groups of smectite or precipitation on the surface of smectite may be a possible reaction of those species. We will further examine this fraction in a future study.

Though P_T was nearly 100 % for both Na- and Ca-smectite in the pH range of 5 to 8, P_K value for Na-smectite was higher than that of Ca-smectite; the difference of P_K between Na- and Ca-smectite was equal to the increased fraction of P_H for Ca-smectite. A possible explanation for this may be that a part of americium-smectite association is changeable between ion-exchange and other mechanisms according to the type of exchangeable cation of smectite.

Reference
[1] Denise S. et al., Radiochimica Acta 51, 189-193 (1990).
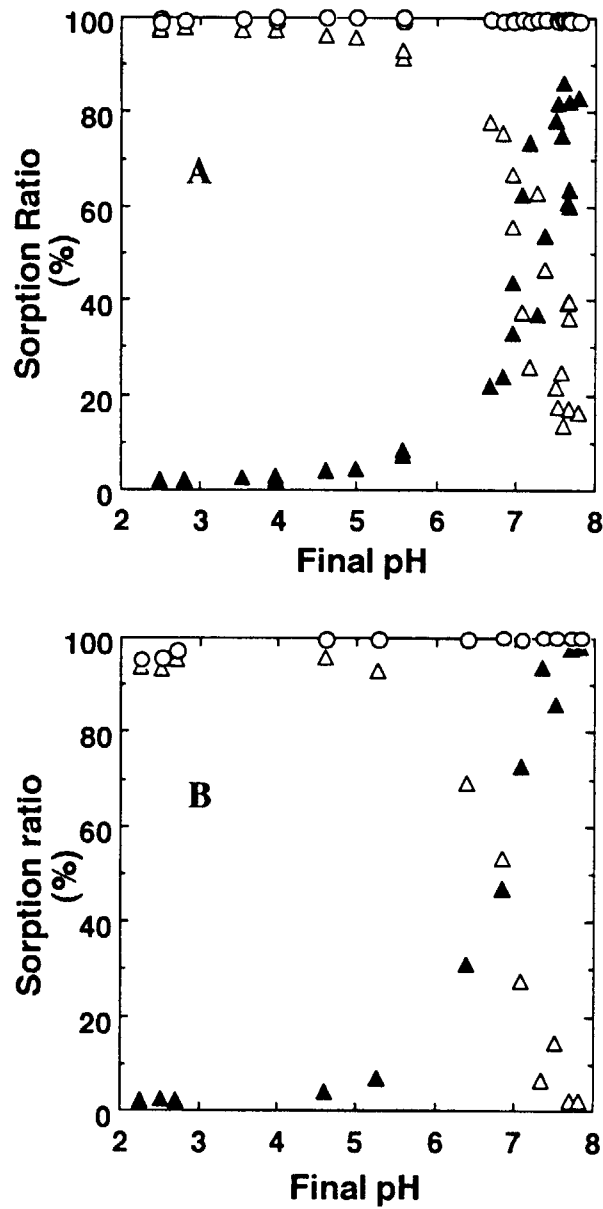
Fig.1 Sorption ratios of ameicium onto smectite
A: Na-smectite, B: Ca-smectite
○: P_t, △: P_K, ▲: P_H

This is a blank page.

2. Study on Shallow Land Disposal

2.1 Influence of Molecular Size of Humic Acid on Distribution Coefficient of Radionuclides for Ando Soil

Tadao Tanaka, Seiya Nagao, Yoshiaki Sakamoto, Toshihiko Ohnuki,

Shiwei Ni and Muneaki Senoo

Introduction

Much of the dissolved organic matter in natural water consists of humic substances, which are formed during microbial degradation of biomass in soil and water. The generic humic substance "humic acid (HA)" is very stable to further degradation. Humic acid has substantial chelation properties for metals, especially the transition metals. The resulting product "humic complexes" acts as a pseudocolloid of radionuclides. From a geochemicalpoint of view, it is important to know the stability of humic complexes with radionuclides released from a radioactive-waste repository.

We have performed sorption experiments of ^{60}Co, ^{85}Sr and ^{241}Am on an ando soil in the presence of humic acid, in order to clarify the effects of concentration and molecular size of HA on sorption behavior of the radionuclides onto the ando soil. The ando soil, which was known to be a soil having a high content of humic substances, will sorb also humic complexes, so it is available to study on influence of sorption ability of HA on the sorption behavior of the radionuclides.

Experimental

The ando soil collected in Ibaraki prefecture, Japan was used in this experiment. Before use for the experiments, the ando soil was sieved and a grain size fraction between 37 and 1000 μ m was collected by washing out with deionized water, and then air-dried. Humic acid purchased from Aldrich Chemical Co. was further purified to remove insoluble humin, fulvic acid and ash following the procedure described by Nash et al.[1].

The 2.5 g ando soil samples were contacted with 50 ml of HA solutions spiked with ^{60}Co, ^{85}Sr or ^{241}Am, yielding a final activity of about 1×10^3 Bq/ml. The ionic strength of the solutions was adjusted to 0.01 M with NaNO$_3$, the pH to 5.5 with 0.1 M HCl and NaOH, and the temperature was controlled at 25 ℃ by using a water jacket. The solutions with the ando soil were gently agitated for 7 days. The pH of the solutions was kept at 5.5~6.0 throughout the experiments. Blank tests not containing the ando soil were also carried out. The supernatant was sampled and ultrafiltered using Millipore filters of 5,000, 30,000 and 100,000 molecular weight cutoff (MW).

Concentrations of the radionuclide in each filtrate were measured by using an ORTEC γ-ray detector, and those of the HA were determined as dissolved organic carbon concentration by using a Shimadzu UV-240 spectrophotometer[2]. Distribution coefficient, Kd (ml/g), of M between liquid and solid phases was calculated.

Results and Discussion

(a) Influence of humic acid concentration on the distribution coefficient

In the case without any ultrafiltrations, the influence of HA concentration on the distribution coefficient Kd of the radionuclides is shown in Fig.1 together with that of HA. The HA was well sorbed onto the ando soil. The Kd values of HA decreased with increasing HA concentration. The Kd of ^{60}Co was constant at 580 ml/g, that is the Kd at the absence of HA, except for 131 mg/L where the Kd decreased from 580 to 340 ml/g. The Kd of ^{241}Am was 350 ml/g at the absence of HA, and decreased with increasing HA concentration, similar to that of HA. On the other hand, the Kd of ^{85}Sr was 52 ml/g at the absence of HA, and gradually increased with the HA concentration. These results suggest that the effects of HA on the Kd are different among the three radionuclides.

(b) Size distribution of humic acid in solutions

Concentration of HA in each size fraction at the blank tests and after the sorption experiments is shown in Fig.2. At the blank tests, in the fraction larger than 100,000 MW (>100,000 MW), approximately 20 % of the HA were detected. About half of the HA was present in the molecular size range from 30,000 to 100,000 MW (30,000-100,000 MW). The amounts of HA detected in the fraction from 5,000 to 30,000 MW (5,000-30,000 MW) and that less than 5,000 MW (<5,000 MW), were 20 and 10 %, respectively.

After the sorption, the HA of >100,000 MW remained in the solutions, while that smaller than 30,000 MW was little. This shows that the ando soil preferably sorbs the HA of smaller sizes. The HA of 30,000-100,000 MW increased with HA concentration. This increase reduced the Kd of HA in Fig.1.

(c) Effects of molecular size of humic acid on the sorption of ^{60}Co

Concentration of ^{60}Co in each size fraction at the blank tests and after the sorption experiments is shown in Fig.3(a). At the absence of HA, all ^{60}Co in the solutions was present in the fraction of <5,000 MW. In the solutions at the blank tests, the ^{60}Co concentration in the fraction of 30,000-100,000 MW increased with the HA concentration. This indicates that the HA of 30,000-100,000 MW effectively contributes to an interaction with ^{60}Co.

The ^{60}Co concentration in all fractions was reduced to near 0 after the sorption at different HA concentrations. Hence the Kd of ^{60}Co in Fig.1 is not apparently affected by the HA concentration. Additionally, the fact that the concentration of ^{60}Co associated with the HA of >100,000 MW was reduced after the sorption in spite that the HA was not sorbed on the ando soil, suggests that most of ^{60}Co in the fraction of >100,000 MW is dissociated from HA (*Reaction b* in Fig.4) and the resulting cationic ^{60}Co is sorbed on the ando soil (*Reaction c*).

(d) Effects of molecular size of humic acid on the sorption of ^{85}Sr

In the solution at the blank tests, the concentration of ^{85}Sr in the fraction of <5,000 MW significantly decreased with increasing HA concentration, while that in the fraction of 30,000- 100,000 MW increased similar to that of ^{60}Co (Fig.3(b)). This shows that a portion of the ^{85}Sr in the solution can be attracted by the HA of 30,000-100,000 MW. However, the authors have previously found that a binding between ^{85}Sr and the HA of 30,000-100,000 MW is broken so easily, and such a binding is not based on coordination bond, but on a binding such as electrostatic force[3].

The concentration of ^{85}Sr in the fraction of 30,000-100,000 MW significantly reduced after the sorption, whereas considerable amounts of the cationic ^{85}Sr in the fraction of <5,000 MW remained after the sorption. The cationic ^{85}Sr should be removed by the sorption from the fraction of <5,000 MW onto the ando soil (*Reaction c* in Fig.4). When the cationic ^{85}Sr is removed from the solution, it might be mainly supplied again by dissociating the humic compounds in the fraction of 30,000-100,000 MW (*Reaction b*). The dissociation of the humic compounds proceeds until the equilibrium in the solution achieves. Hence it seems that the humic compounds of ^{85}Sr in the fraction of 30,000-100,000 MW are apparently sorbed on the ando soil. However, the cationic ^{85}Sr is weakly sorbed on the ando soil, as indicated by the small Kd value at the absence of HA, so that it remained in the solution after the sorption. The cationic ^{85}Sr remaining in solution can associate with the HA which either is sorbed onto the ando soil (*Reaction f*) or is dissolved (*Reaction a*). The sorption processes of *Reactions e* and *f* possibly causes the increase in the Kd of ^{85}Sr with increasing HA concentration, as shown in Fig.1.

(e) Effects of molecular size of humic acid on the sorption of ^{241}Am

In the solution at the blank tests, most ^{241}Am formed humic compounds even in extremely low HA concentration region, since ^{241}Am, that is a trivalent element, has a large complexing stability with HA and other organic ligands (Fig.3(c)). The ^{241}Am

selectively interacted with the HA in size range larger than 30,000 MW. This indicates that ^{60}Co and ^{85}Sr preferentially form smaller humic compounds but ^{241}Am forms larger ones. The concentration of ^{241}Am in the fraction of 30,000-100,000 MW increased with the HA concentration. Thus the ^{241}Am effectively interacts with the HA of 30,000-100,000 MW. Contrary to this, the concentration of ^{241}Am in the fraction of >100,000 MW decreased gradually with increasing HA concentration. This suggests that ^{241}Am interacts more strongly with the HA of 30,000-100,000 MW than that of >100,000 MW.

The concentration of ^{241}Am in the fraction of 30,000-100,000 MW was significantly reduced by the sorption, but it slightly increased with the HA concentration after the sorption. This increase means a decrease of sorption amounts of ^{241}Am on the ando soil, so that the Kd of ^{241}Am decreased with increasing HA concentration, as shown in Fig.1. The size distribution profile of ^{241}Am remaining in the solution after the sorption (in Fig.3(c)) was similar to that of HA (in Fig.2). This indicates that the sorption behavior of ^{241}Am is dominated by the sorption of HA which involves ^{241}Am (*Reaction e*). Therefore, the agreement in the Kd values between ^{241}Am and HA in the presence of HA (in Fig.1) is probably attributable to the strong complexation of ^{241}Am with HA.

Conclusion

Values of distribution coefficient Kd in the sorption of ^{241}Am, which forms stable compounds with HA of 30,000-100,000 MW in the solutions, on the ando soil decreased with increasing HA concentration, as well as the Kd of HA. On the other hand, the Kd of ^{60}Co was little affected by the presence of HA and that of ^{85}Sr increased with the HA concentration, because ^{60}Co and ^{85}Sr preferentially but weakly interact with the HA fractions smaller than 100,000 MW. Large size of the humic compounds might be mechanically retained in the interstitial network. Therefore, the migration of cationic radionuclide in geologic media in the presence of HA can be partly accelerated by formation of the humic compounds and/or partly retarded by sorption of the humic compounds.

References
(1) Nash,K., Fried,S., Friendman,A.M., Sullivan,J.C.: Redox behavior, complexing, and
      sorption of hexavalent actinides by humic acid and selected clays.
Environ.Sci.Technol.,
      15, 834-837 (1981).
(2) Tanaka,T., Ni,S.:Influence of humic acid on migration of ^{60}Co, ^{85}Sr and ^{137}Cs in

coastal sandy soil. *JAERI-M 93-185*, Japan Atomic Energy Research Institute, (1993).

(3) Tanaka,T., Senoo,M.: Sorption of ^{60}Co, ^{85}Sr, ^{137}Cs, ^{237}Np and ^{241}Am on soil under coexistence of humic acid. In: *Scientific Basis for Nuclear Waste Management XVIII*

(Murakami,T. and Ewing,R.C., ed.). Materials Research Society, 1995, pp.1013-1020.
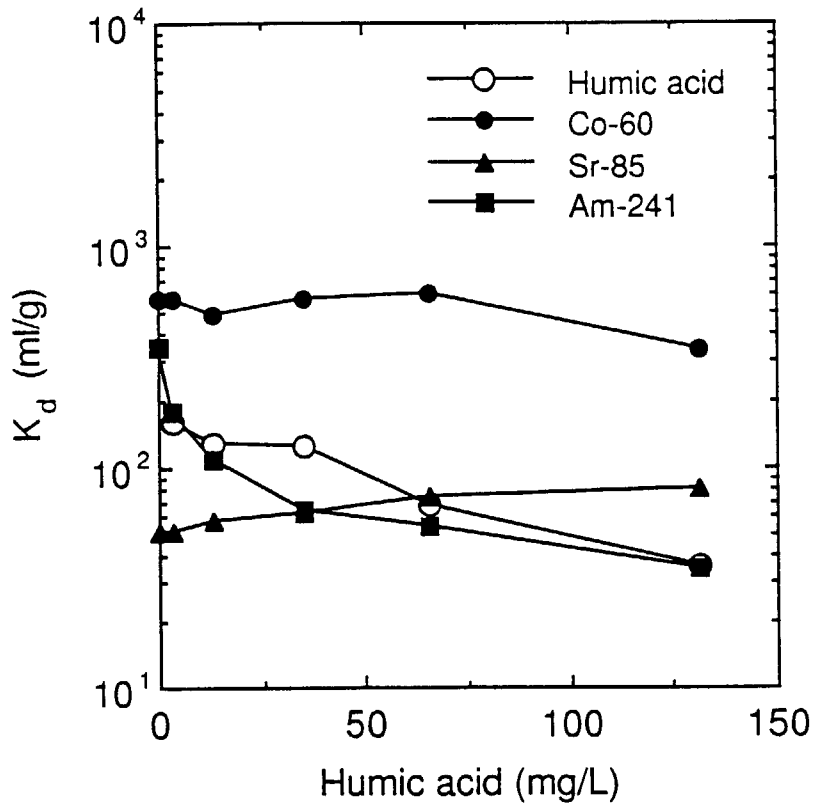
Fig.1 The dependence of the distribution coefficient Kd of radionuclides and humic acid
     as a function of the initial humic acid concentration.
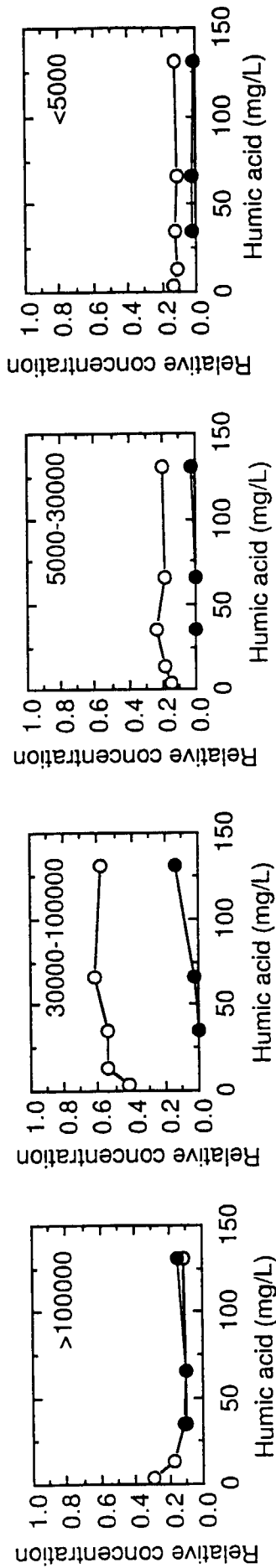
Fig.2 Concentration of humic acid in each size fraction at blank tests and after the sorption experiments; relative concentration is normalized to the initial one in the solution at the blank tests, ○: blank test, ●: after sorption.
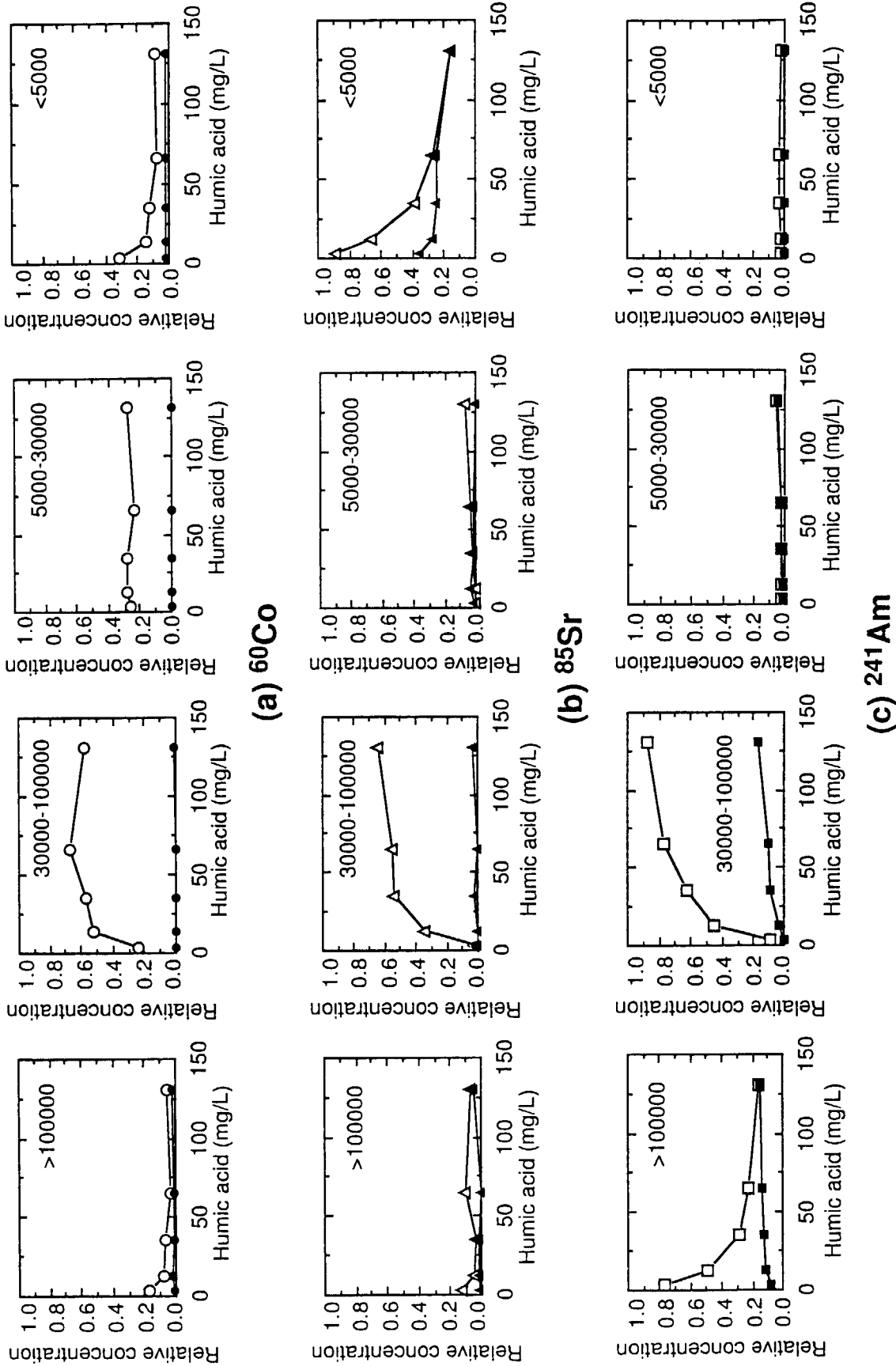
Fig.3 Concentration of radionuclides in each size fraction at blank tests and after the sorption experiments; relative concentration is normalized to the initial one in the solution at the blank tests, ○,△,□: blank test, ●,▲,■: after sorption.
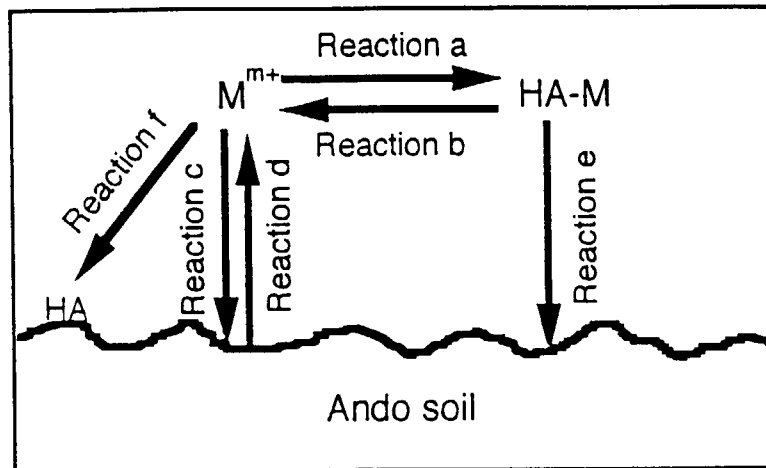
Fig.4 Reaction process predicted in the sorption experimental system;
M represents a radionuclide.

2.2 Migration Behavior of Eu(III) in Sandy Soil in the Presence of Dissolved Organic Materials

S.Nagao[1], R.R.Rao[*], R.W.D.Killey[*] and J.L.Young[*],

[*] Atomic Energy of Canada Limited, Chalk River Laboratories, Environmental Research Branch, Chalk River, Ontario K0J 1J0, Canada

INTRODUCTION

The natural organics present in groundwater, especially humic substances, could affect radionuclide mobility by changing the solubility and sorption properties of radionuclides through redox processes and /or complexation. Recent studies have shown the important role played by soluble and colloidal humic substances in the transport behavior of actinides from the observation of field studies[1,2]. It appears necessary to evaluate the migration behavior (sorption, coagulation/dissolution, filtration etc.) of aquatic humic substances loaded with actinide ions in the geosphere. The purpose of this study was to investigate the effects of groundwater DOM on the migration of actinides at the average concentration (range from 0.2 to 15 $mgC \cdot L^{-1}$) of DOM present in most groundwater. The migration of Eu(III), as a model nuclide for trivalent actinides, in the presence of the DOM was studied by column experiment with a constant feed method. To understand migration behavior of actinide-humus complexes in detail, humic substances from a commercial reagent and a river water were used as reference organics.

2. Experimental

Materials

Sandy soil was collected at Stn. PLS-63 of the depth interval of 2.44 to 3.96 m from the Glass Block site at the Chalk River Laboratories of AECL. The physico-

chemical properties of the sand had been reported by Jackson and Inch[3] and Killey et al.[4]. The core sample obtained was air-dried after removing the silty clay part at the top of 10 cm and then homogenized.

10,000 L of groundwater was collected from the well, which is screened at a depth of 2.8 to 3.6 m, located near Stn. PLS-63. The chemical properties of groundwater at this area were reported by Champ et al. [1], Jackson and Inch[3] and Killey et al.[4]. The DOM was concentrated from the groundwater by a reverse osmosis-nanofiltration system. The organics were then freeze-dried. Other three humic substances with different origin were used as reference organics in this study for comparing their effects on the mobility of Eu(III) as follows: 1) A commercial HA was purchased from Aldrich Co. Ltd.; 2) Suwannee River HA and 3) River FA purchased from the International Humic Substances Society (IHSS). Aromatic-carbon content of the DOMs is 11% for the groundwater DOM (Nagao *et al.*, unpublished data), 28% for the River FA, and 40% for the River HA and Aldrich HA[5,6]. Proton exchange capacity of carboxyl groups is 7.9 meq/g for the groundwater DOM (Nagao *et al.*, unpublished data), 6.0 meq/g for the River FA, and 5.1 meq/g for the River HA and 4.8meq/g for the Aldrich HA[5,7]. The structure of the DOMs may be different due to the different origin.

Column experiment

Migration behavior of Eu(III) in the absence and presence of DOM in the sandy soil was studied by the column experiment with a constant feed method. The column is made of polyvinyl chloride, and is 2.5 cm in diameter and 2.5 cm in length. Solutions of ^{152}Eu (Amersham Canada) in the absence and presence of DOM at pH 5.5 and ionic strength of 0.01M $NaClO_4$ was continuously introduced to the top of the column by the micro tube pump at constant flow rate of 1 mL·min^{-1}. The effluent was automatically collected into glass test tubes for 12 minutes with the fraction collector. The concentrations of ^{152}Eu and DOMs in the influent were 510 cpm·mL^{-1} and 10 mg·mL^{-1}

(weight unit), respectively. The influent solution was prepared before 7 days of each column experiment, and stored in the refrigerator until the experiment. Column effluent fractions were analyzed for concentrations of ^{152}Eu (γ spectrometry) and DOMs (UV spectrometry) and for pH (pH meter). Average pH is 5.9 for the Eu, 5.7 for the Eu-groundwater DOM, 6.1 for the River FA, 6.0 for the River HA and 5.9 for the Aldrich HA. Variation of pH at each column experiment was 0.1-0.3. Migration behavior of the DOMs in the absence of Eu was also performed by the similar procedures. Hydraulic properties of the column were characterized by a radiotracer experiment using non-sorbing tracer of tritium (HTO). After the column experiments, the sand packed in the column was collected each 0.5 cm- interval. The segments were air-dried and then weighted.

RESULTS AND DISCUSSION

Breakthrough curves of tritium, and Eu in the absence and presence of DOM

Breakthrough curves of tritium and Eu(III) are shown in Fig.1. In the absence of DOM, Eu was not detected even after 90 pore volumes were eluted from the column. Europium elution was observed, however, when any of the DOMs were present. The relative concentration of Eu at the Eu-Groundwater DOM system rapidly increased from 0.10 at 11 mL to 0.31 at 32 mL, and then gradually increased. Europium in the presence of the other organics gradually increased with increasing the effluent volume.

All of the experiments the relative concentration of Eu was not reached to the unity. Maximum relative concentrations of Eu was observed in the order: River FA< Groundwater DOM < River HA=Aldrich HA. The amount of Eu passed through the column is 30% for the Eu-River FA system, 48% for the Eu-Groundwater DOM system, and 53-55% for the Eu-Aldrich and Eu-River HA systems. These results indicate that

the elution pattern of Eu in the presence of DOMs can be divided into three groups: 1) the River HA and Aldrich HA systems; 2) the River FA system; 3) the Groundwater DOM system.

Profiles of Eu content in the sand column

The extent of sorption of Eu in the sand column was further elucidated through the measurement of ^{152}Eu-activity along the column (Fig. 2). The Eu content at the Eu-River HA and Eu-Aldrich HA experimental systems was almost constant through the column and agreed with each other. The profiles of Eu at the Eu-River FA and Eu-Groundwater DOM systems showed a decrease along the column. The trend of variation is similar, but the Eu content at the Eu-River FA system is higher than that at the Eu-Groundwater DOM at 0-1.5 cm interval. The types of Eu profiles correspond to the elution patterns of Eu obtained by the breakthrough curves as shown in Fig.1. The sum of Eu sorbed on the sand at the Eu migration experiment was slightly lower than that at the Eu-organics migration experiments because the Eu concentration in the influent solution at the Eu experiment was about 20% lower than that of the Eu-organics experiments.

These results suggest that differences in characteristics of DOM may be reflected in mobility of Eu-DOM complexes in sandy soil.

REFERENCES

(1) D.R.Champ et al. (1984) J. Water Poll. Res. Canada **19**, 35 (1984).

(2) N.A.Marley et al. (1993) Environ. Sci. Technol. **27**, 2456 (1993).

(3) R.E.Jackson and K.J. Inch (1980) National Hydrology Research Inst., NHRI Paper No.7, 1980.

(4) R.W.D.Killey et al. (1995) AECL Report RC-1513.

(5) J.I.Kim et al. (1990) Fresenius J. Anal. Chem. **338**, 245 (1990).

(6) R.C. Averett et al. (1989) U. S. Geological Survey, Open-File Report 87-557.

(7) E.M.Thurman (1985) In. *Humic Substances in Soil, Sediment, and Water. Geochemistry, Isolation, and Characterization* (G.R.Aiken, D.M.McKnight, R.L.Wershaw, P. MaCarthy, eds.), John Wiley & Sons, pp.87-103.
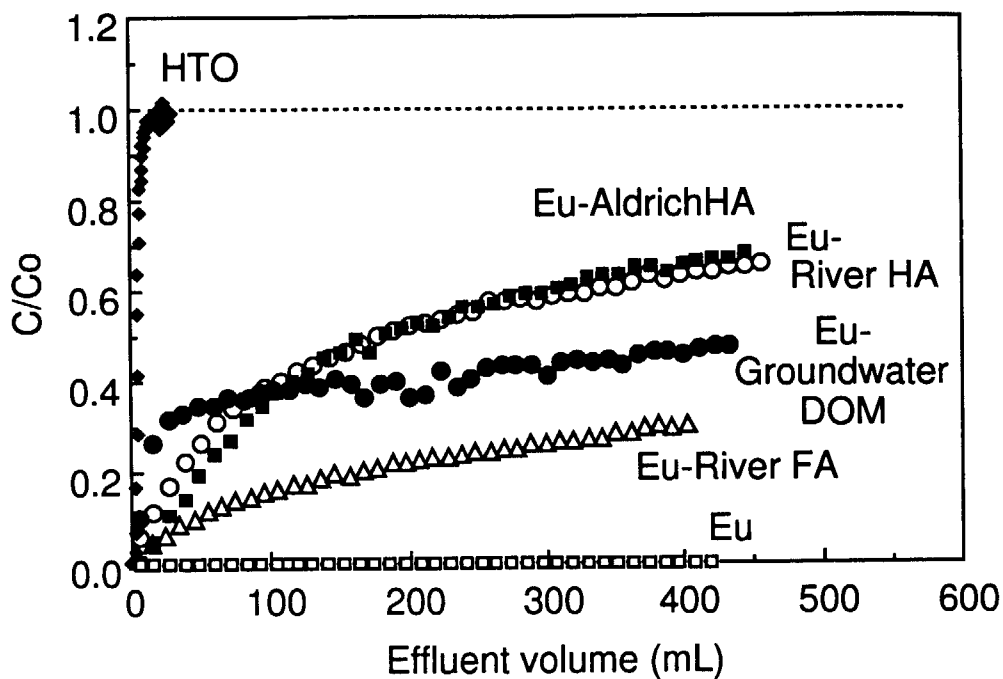
Fig.1 Breakthrough curves of tritium (HTO) and Eu(III) in the absence and presence of DOM. Flow rate was 0.85-0.96 mL·min⁻¹. pH of the influent was 5.2-5.5.
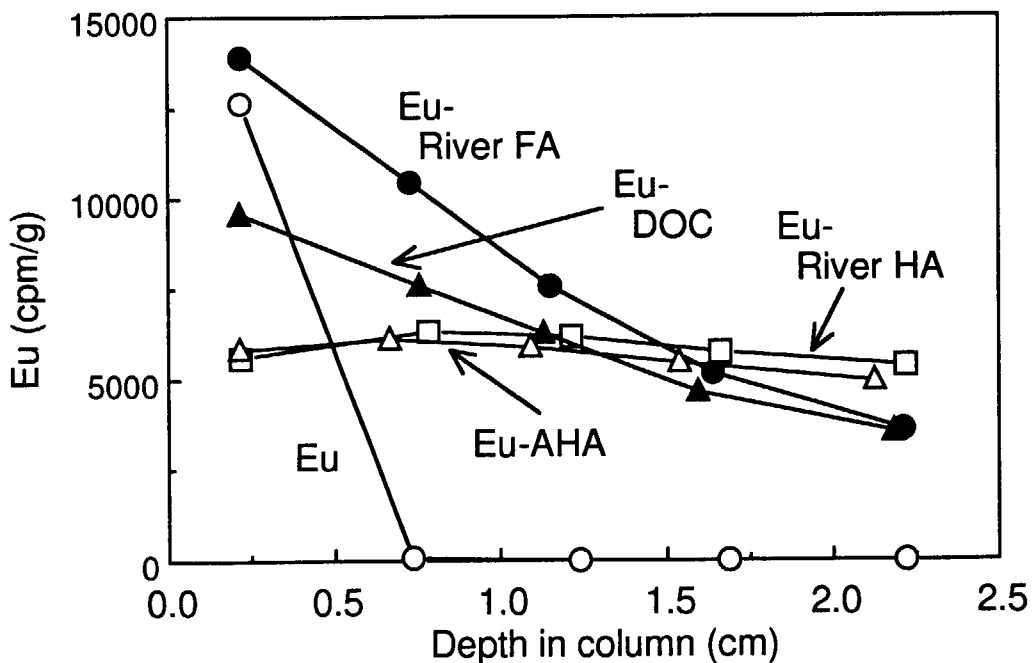
Fig.2 Profiles of ^{152}Eu in the column packed with the sand after the migration experiments.

— 43 —

3. Studies on Geological Disaposal

3.1 Diffusivity of U, Pu and Am carbonate complexes in a granite from Inada, Ibaraki, Japan studied by through diffusion

Tetsuji Yamaguchi, Shinichi Nakayama

Abstract

The diffusivities of uranium, plutonium and americium in Inada granite have been determined using through-diffusion method. Experiments were performed at (25 ± 1) ℃ in a 0.1 mol L^{-1} $NaHCO_3$ solution where the actinides are present as carbonate or hydroxy-carbonate complexes. Effective diffusivity (D_e) values of $(1.42\pm0.24)\times10^{-13}$ m^2/s and $(5.1\pm2.0)\times10^{-14}$ m^2/s were obtained for uranium and plutonium, respectively. Diffusion through 5 mm thick granite was not observed for americium within the experimental period of 366 days. The D_e value for uranyl carbonate species obtained in these experiments was found to be four times higher than the previously obtained D_e value for the uncomplexed uranyl ion.

1. Introduction

After emplacement of high level radioactive waste in a deep underground repository, radionuclides, including long-lived actinides, may be leached from the wastes and may subsequently be transported through the surrounding rock mass. Major water bearing fractures in the rock mass are considered to form the main transport paths. Sorption onto mineral surfaces and diffusion into the pores or micro fissures in the rock matrix are important processes leading to the retardation of the transport of actinides and other contaminants through the geosphere. To assess the extent of actinide migration, it is important to quantify the diffusion of actinides into the rock matrix and to understand the diffusion mechanisms. Granite was used in these experiments, as it is being considered as a potential host rock for the disposal of high level wastes.

The diffusivity of an ion through the interconnected pore space in a rock matrix is often assumed to be proportional to its bulk diffusivity in solution (D_v) and to the geometric parameters of the rock: ε (porosity), δ (constrictivity) and τ^{-2} (τ : tortuosity) (Neretnieks, 1980). It may therefore be possible to apply this theoretical relationship to actinide aqueous actinide species such as UO_2^{2+}, Th^{4+}, and several trivalent actinides whose bulk diffusivities in solution are known (Li & Gregory, 1974; Fourest et al., 1995). But this approach can no be used to estimate D_e for actinide complexes in groundwater because data on their bulk diffusivity is not available. In this study, the effective diffusivity of uranium in Inada granite was obtained under condition that favored the formation of a uranyl tri-carbonate species. The result was compared with previously obtained D_e value for UO_2^{2+} (Yamaguchi et al., 1997a). The diffusion of plutonium and americium carbonate complexes through Inada granite was examined simultaneously with uranium and the results are compared.

2. Experimental

The rock used in this study was a biotitic granite obtained from the Inada mine in the Ibaraki prefecture, eastern Japan. The chemical and mineral compositions are given elsewhere (Yamaguchi et al., 1993; Idemitsu et al., 1992). The porosity and the pore size of the granite have been given by Yamaguchi et al., (1997b). The procedures for preparing

5-mm thick, 40 mm diameter granite disks have been described in a previous paper (Yamaguchi et al., 1993). The diffusion experiment was performed in triplicate using three granite disks, C15, C17 and C19.

The acrylic diffusion cell used in this study is shown in Fig. 1. A granite disk was fitted tightly into the central support member of the cell and the space between the rock disk and the acrylic central support member sealed with a silicone gasket. The granite disk was soaked in deionized water under vacuum for a couple of days to evacuate all air from the interconnected pores. The granite disks were kept in a 0.1 mol L^{-1} $NaHCO_3$ solution at pH = 9 under atmospheric pressure for 30 days to pre-equilibrate the disks with the solution at the same pH. The central support member containing the granite disk was sandwiched between the two reservoirs, each with a capacity of 116 mL. Solutions were prepared from reagent grade chemicals (Wako Pure Chemical Ind., Ltd., Tokyo) and deionized water (Milli-Q Labo System, Millipore).

Uranium-233 and americium-241 were prepared as 8.6×10^{-4} mol L^{-1} (7.1×10^4 Bq mL^{-1}) and 1.8×10^{-6} mol L^{-1} (5.6×10^4 Bq mL^{-1}) stock solution in 0.1 mol L^{-1} HCl. Plutonium-239 was prepared as 4.2×10^{-4} mol L^{-1} (2.3×10^5 Bq mL^{-1}) Pu(IV) stock solutions in 10 mol L^{-1} HNO_3 as described in a previous paper (Yamaguchi et al., 1994). The starting solution was prepared by combining 100 mL of 0.1 mol L^{-1} Na_2CO_3, 275 mL 0.1 mol L^{-1} $NaHCO_3$, 3 mL of the ^{233}U stock solution, 0.95 mL of the ^{239}Pu stock solution and 1 mL of ^{241}Am stock solution in a polypropylene bottle. To maintain the Pu in the tetravalent state, 0.26 g $NaNO_2$ was added to this mixture. The pH was adjusted to 9.3 by adding dilute NaOH and HCl. The initial concentrations of total carbonate and NO_2^- in the source solution were 0.1 and 0.01 mol L^{-1}, respectively. The Eh and concentration of ^{233}U, ^{239}Pu and ^{241}Am were determined and the oxidation state of Pu was determined by TTA extraction as described in a previous paper (Yamaguchi et al., 1994). To measure the concentrations of actinides in the source solution, a 50 μ L aliquot was withdrawn and diluted to 2 mL to prevent the salt from interfering with alpha spectrometry of the samples. A 50 μ L aliquot of this diluted solution was evaporated on a stainless planchet and its activity determined by alpha spectrometry. The solution was stored for 40 days in atmosphere at room temperature to ensure that the concentrations of the actinides remained constant. The pH, Eh, total carbonate concentration and concentrations of the actinides were determined

again, and the TTA extraction was performed.

A blank solution was prepared by adding 0.26 g of $NaNO_2$ to a 380 mL volume of 0.1 mol L^{-1} $NaHCO_3$ solution and adjusting the pH of the solution to 9.3. The diffusion experiments were started by placing the actinide-containing solution in the source reservoir and the blank solution in the other, or measurement, reservoir. The experiment was performed in triplicate at (25 ± 1) °C. At 10 day intervals, a 50 μL aliquot was taken from the measurement reservoir to determine the concentrations of the actinide elements. The 50 μL aliquot removed from the measurement reservoir was replaced by an equal volume of the blank solution to maintain the balance between the water levels in the two reservoirs and to avoid actinide transport through the granite by advective flow. The concentrations of U, Pu and Am, pH, Eh and total carbonate concentration of the solution in one of the source reservoirs were determined at the 55th and the 366th day. At the termination of each experiment, the inner wall of the measurement reservoir was rinsed with 10 mol L^{-1} HNO_3 to determine the amount of diffusing species adsorbed on the cell walls.

3. Results

Figure 2 shows the time dependence of the concentrations of ^{233}U, ^{239}Pu and ^{241}Am in the measurement reservoirs. No americium was observed in the measurement reservoirs throughout the experiments. The concentrations of U and Pu increase linearly with time after 150 days. For all three cells, the increase in relative uranium concentration was greater than that of plutonium. The relative uranium concentration in cell C17 was the largest of the 3 runs and that of C19 the smallest. This order is the same for Pu concentration. The amount of uranium, plutonium and americium sorbed on the acrylic wall of the reservoirs were found to be 3% of the inventory in the solutions in the reservoirs and can be ignored. The concentrations of all three actinides in the source reservoir remained virtually constant, as shown in Table 1, suggesting no significant removal occurred by precipitation and/or sorption on reservoir walls or on the surfaces of the granite disks.

The method described by Crank (1975) was used to analyze the data presented in this paper. After plotting the concentration of diffusing species in the measurement reservoir against time, values for D_e, are obtained from the slope, and the rock capacity factor, $(\varepsilon + \rho R_d)$, from the intercept on the concentration axis of the extrapolated linear portion, where r is the bulk density of the rock and R_d is the distribution coefficient. The effective diffusivity and the rock capacity factor are presented in Table 2 with literature data.

4. Discussion

4.1. Uranium

The D_e value obtained for uranium in this experiment was $(1.42\pm0.24)\times10^{-13}$ m²/s on an average of three experiments. This value is four times larger than the previously obtained value for the uncomplexed uranyl ion, UO_2^{2+}, $(3.6\pm 1.2)\times10^{-14}$ m²/s (Yamaguchi et al., 1997a). The previous experiment had been performed in 0.1 mol L⁻¹ KCl solution at pH 4, while this experiment was in 0.1 mol L⁻¹ NaHCO₃ at pH 9.3. In aerated solutions, the dominant oxidation state of uranium is hexavalent. The stability constants of the carbonate and hydroxy-carbonate complex species expected to be present around pH 9.3 are shown in Table 3. Complexation of UO_2^{2+} by nitrite anion is negligible (Brown and Wanner, 1987). Speciation of uranium(VI) under the conditions under which this experiments was performed was calculated using the data listed in Table 3. More than 99.9 % of the uranium was calculated to be present as a monomeric tri-carbonate complex, $UO_2(CO_3)_3^{4-}$ throughout the experiment. The structure of the complex species is shown elsewhere (Weigel, 1985). The bond length between the uranium atom and the nearest oxygen atoms of the carbonate groups is 0.244-0.246 nm (Weigel, 1985). The bond length between the carbon atom and the oxygen atoms in the carbonate group is 0.122-0.134 nm (Weigel, 1985). Based on these bond length, the size of this species was graphically estimated to be 0.42±0.03 nm. The radius of the ions can be correlated with diffusivity (Yamaguchi et al., 1997a) using the relationship

$$D^0 = RT(r/r_s) \ / \ (6 \ \pi N \ \eta^0 r) \qquad\qquad (1)$$

where D^0 : Diffusion coefficient of ion at infinite dilution (m^2/s)

        R : Gas constant (= 8.314 J/mol/K)

        T : Absolute temperature (K)

        r : Hydrated ion radius (m)

        r/r_s : Correction factor

        N : Avogadro's number (= 6.02×10^{23} mol^{-1})

        η^0 : Viscosity of water (8.902×10^{-4} Ns/m^2 at 25 _)

The diffusivity of $UO_2(CO_3)_3^{4-}$ was estimated to be $(7.2 \pm 0.5) \times 10^{-10}$ m^2/s assuming no significant hydration occurs. In this calculation, the correction factor r/r_s is 1.23 (Nightingale, 1959). An empirical correlation between D_e and D_v has been reported (Yamaguchi et al., 1997a) and is shown in Fig. 3. The value for $UO_2(CO_3)_3^{4-}$ obtained in this experiment is consistent with the previous results as shown in this figure.

It is noteworthy that the results show that the diffusivity of the $UO_2(CO_3)_3^{4-}$ complex is larger than that of the "master" species, UO_2^{2+}, both in bulk of the solution and in the pores of the granite. A similar effect of complexation on the diffusivity of metal ions has been observed for Fe^{2+} and Fe^{3+} complexes with CN^- (Dean, 1978). The diffusivity of $Fe(CN)_6^{4-}$ at infinite dilution, 7.3×10^{-10} m^2/s, is larger than that of Fe^{2+}, 7.1×10^{-10} m^2/s and the diffusivity of $Fe(CN)_6^{3-}$ at infinite dilution, 8.8×10^{-10} m^2/s, is larger than that of Fe^{3+}, 5.9×10^{-10} m^2/s.

4.2. Plutonium

The D_e value obtained for the plutonium complex in this experiment was $(5.1 \pm$

2.0)x10^{-14} m^2/s based on an average value obtained in the triplicate experiment. This value is lower by a factor of three compared with the uranium. The chemical speciation of Pu was calculated using the data presented in Table 3 and the result of the TTA extraction. The stability constants for U(VI) in Table 3 were used for carbonate complex species of Pu(VI) by analogy. A hydroxy-carbonate complex of Pu(IV), $Pu(OH)_2(CO_3)_2^{2-}$ is presumed to be dominant under the employed condition and a carbonate complex of Pu(VI) $PuO_2(CO_3)_3^{4-}$ minor species. The diffusivity of $Pu(OH)_2(CO_3)_2^{2-}$ in bulk of the solution is not known and cannot be estimated using equation(1) because the hydration of this species is not known.

4.3. Americium

In aerated solutions, the dominant oxidation state of americium is trivalent. Based on the data for Am species presented in Table 3, a tri-carbonate complex species, $Am(CO_3)_3^{3-}$ is presumed to be dominant under the employed condition. No diffusion of americium through the granite was detected. This suggests that either the effective diffusivity is very small or the sorption distribution coefficient very large. An upper limit to the apparent diffusivity, D_a, of americium in the granite can be estimated as follows. An intercept, t_D, on the time axis of the extrapolated linear portion in the plot of the concentration of diffusing species in the measurement reservoir against time is

$$t_D = (\varepsilon + \rho R_d) l^2 / 6 D_e = l^2 / 6 D_a \tag{2}$$

The absence of americium in the measurement reservoir at the 366th day implies that t_D is greater than 366 days or D_a is less than 1.3x10^{-13} m^2/s. For comparison, the apparent diffusivities of uranium and plutonium in this experiment determined using Eq.(2), were (4.6±1.0)x10^{-13} and (4.4±0.9)x10^{-13} m^2/s, respectively. The apparent diffusivity of americium was smaller for uranium and plutonium. A similar low diffusivity for americium in rock has been observed elsewhere (Ittner and Torstenfelt, 1988; Andersson et al., 1992; Torstenfelt, 1982; Muuronen et al., 1986; Suksi et al., 1987; Berry, 1987).

5. Conclusion

Effective diffusivities for $UO_2(CO_3)_3^{4-}$ and $Pu(OH)_2(CO_3)_2^{2-}$, in Inada granite, of $(1.42\pm0.24)\times10^{-13}$ m^2/s, and $(5.1\pm2.0)\times10^{-14}$ m^2/s, respectively, have been obtained in a 0.1 mol L^{-1} NaHCO$_3$ solution at pH 9.3. The effective diffusivity of $UO_2(CO_3)_3^{4-}$ in the granite was found to be four times larger than that of the uncomplexed UO_2^{2+} obtained previously in 0.1 mol L^{-1} KCl at pH 4. The effective diffusivity of $UO_2(CO_3)_3^{4-}$ in granite and the estimated bulk diffusivity of this species, $(6.6\pm0.4)\times10^{-10}$ m^2/s, are consistent with an empirical correlation between D_e and D_v obtained previously. The effective diffusivity of $Pu(OH)_2(CO_3)_2^{2-}$ is about 1/3 of that of $UO_2(CO_3)_3^{4-}$. No through diffusion of americium was observed in this study.

Acknowledgements

Reference

Andersson, K., Evans, S. and Albinsson, Y., 1992. Diffusion of radionuclides in sediments. Radiochim. Acta, 58/59: 321.

Bennet, D.A., Hoffman, D., Nitsche, H., Russo, R. E., Torres, R. A., Baisden, P. A., Andrews, J. E., Palmer, C. E. A. and Silva, R. J., 1990. Hydrolysis and carbonate complexation of dioxoplutonium(V). Radiochim. Acta, 56: 15.

Berry, J.A., Bourke, P.J., Green, A. and Littleboy, A.K., 1987. Sorption of radionuclides on hard rocks. AERE-R-12844, 15 pp.

Brown, P. L. and Wanner, H., 1987. Predicted formation constants using the unified theory of metal ion complexation, OECD-NEA, Paris, 102 pp.

Choppin, G. R. and Mathur, J. N., 1991. Hydrolysis of actinyl(VI) cations. Radiochim. Acta, 52/53: 25.

Crank, J., 1975. The mathematics of diffusion. (2nd ed.) Oxford Univ. Press, London, 414 pp.

Dean, A., 1978. Lange's Handbook of Chemistry (McGraw-Hill, New York).

Fourest, B., Morss, L. R., Blain, G., David, F. and M'Halla, J., 1995. Determination of limiting ionic conductivity of $Am^{3+}_{(aq)}$ and $Cf^{3+}_{(aq)}$. Radiochim. Acta, 69: 215.

Idemitsu, K., Furuya, H., Murayama, K. and Inagaki, Y., 1992. Diffusivity of uranium(VI) in water-saturated Inada granite, Sci. Basis Nucl. Waste Manage. XV (Sombret, C. G., ed.), Mater. Res. Soc., Pittsburgh, Pennsylvania, pp.625-632.

Ittner, T. and Torstenfelt, B., 1988. Diffusion of neptunium, plutonium and americium in granitic rock. Radiochim. Acta, 44/45: 171.

Kita, H., Iwai, T. and Nakashima, S., 1989. Diffusion coefficient measurement of an ion in pore water of granite and tuff. J. Jpn. Soc. Eng. Geol. (in Japanese), 30: 84.

Kumata, M., Iwai, T., Sagawa, T., Suzuki, T. and Nishiyama, K., 1990. Diffusion experiment of a radionuclide in granitic rock cores, JAERI-M 90-179 (in Japanese), JAERI, Tokai, Japan, 21 pp.

Li, Y. H. and Gregory, S., 1974. Diffusion of ions in sea water and in deep-sea sediments. Geochim. Cosmochim. Acta 38: 703.

Lierse, Ch. 1985. Chemical behaviour of plutonium in natural aquatic system: hydrolysis, carbonate complexation and redox reaction., Ph. D. Thesis (in German), Technische Universität München, München.

Muuronen, S., Kämäräinen, E-L., Jaakkola, T., Pinnioja, S. and Lindberg, A., 1986. Sorption and diffusion of radionuclides in rock matrix and natural fracture surfaces studied by autoradiography. Mat. Res. Soc. Symp. Proc. Vol. 50, pp. 747-754.

Neretnieks, I., 1980. Diffusion in the rock matrix: An important factor in radionuclide retardation? J. Geophys. Res., 85: 4379.

Nightingale, E. R., 1959. Phenomenological theory of ion solvation. Effective

radii of hydrated ions, J. Phys. Chem., 63: 1381.

Nitsche, H. and Silva R., 1996. Investigation of the carbonate complexation of Pu(IV) in aqueous solution. Radiochim. Acta, 72: 65.

Silva, J. et al., 1995. Chemical Thermodynamics of Americium (North-Holland, Amsterdam).

Suksi, S., Kämäräinen, E-L., Siitari-Kauppi, M. and Lindberg, A., 1987. Sorption and diffusion of cobalt, nickel, strontium, iodine, cesium and americium in natural fissure surfaces and drill core cups studied by autoradiography, _. YJT-87-17, 69 pp.

Torstenfelt, B., 1982. Mobilities of radionuclides in fresh and fractured crystalline rock. SKBF-KBS-TR-82-26, 25 pp.

Wanner, H. and Forest, I., 1992. Chemical thermodynamics of uranium, North-Holland, Amsterdam, 715 pp.

Weigel, F., 1985. The carbonates, phosphates and arsenates of the hexavalent and pentavalent actinides. in Handbook on the Physics and Chemistry of the Actinides (Freeman, A. J. and Keller, C., eds.) Vol. 3, North Holland, Amsterdam 1985, pp. 243-288.

Yamaguchi, T., Sakamoto, Y. and Senoo, M., 1993. Consideration on effective diffusivity of strontium in granite, J. Nucl. Sci. Technol., 30: 796.

Yamaguchi, T., Sakamoto, Y. and Ohnuki, T., 1994. Effect of complexation on solubility of Pu(IV) in aqueous carbonate system, Radiochim. Acta, 66/67: 9.

Yamaguchi, T. and Nakayama, S., 1996. Consideration on thermodynamic data for americium(III) aqueous carbonate system. Radioactive Waste Research (in Japanese), 3: 49.

Yamaguchi, T., Sakamoto, Y., Nakayama, S. and Vandergraaf, T. T., 1997a. Effective diffusivity of the uranyl ion in a granite from Inada, Ibaraki, Japan. J. Contaminant Hydrology, 26: 109.

Yamaguchi, T., Isobe, H. and Nakayama, S., 1997b. Analysis of Microporous Structure in Granite. Radioactive Waste Research (in Japanese), 3: 99.

Table 1 pH, Eh, and concentration of total carbonate, U, Pu and Am in the source reservoir.

Time after starting diffusion run	As prepared[a]	0	55	366
pH	9.27	9.27	9.22	9.30
Eh (mV vs NHE)	297.8	306.8	317.8	339.8
total carbonate (mol l^{-1})	0.10	0.10	0.09	0.08
U (mol l^{-1})	6.7×10^{-6}	6.7×10^{-6}	6.5×10^{-6}	6.3×10^{-6}
Pu (mol l^{-1})	1.0×10^{-6} (88%[b])	1.0×10^{-6} (81%[b])	1.0×10^{-6} (79%[b])	9.9×10^{-7} (70%[b])
Am (mol l^{-1})	4.7×10^{-12}	4.9×10^{-12}	5.0×10^{-12}	4.6×10^{-12}

a: The source solution was prepared 40 days prior to the start of the diffusion run to ensure that the concentrations of U, Pu and Am had remained constant values.

b: percentage of Pu extracted by TTA.

Table 2 Effective diffusivity (D_e) and rock capacity factor ($\varepsilon + \rho R_d$) of species in Inada granite, and hydrated radious (r_b) in aqueous solution.

Species	D_e(m²/s)	$\varepsilon + \rho R_d$	Solution	Temperature	Reference	r_b(nm)
$UO_2(CO_3)_3{}^{4-}$	$(1.56\pm0.06)\times10^{-13}$	0.266 ± 0.047	0.1 M NaHCO₃	25℃	This work	0.42 ± 0.03[a]
	$(1.43\pm0.05)\times10^{-13}$	0.323 ± 0.034	pH = 9.3			
	$(1.28\pm0.15)\times10^{-13}$	0.37 ± 0.08				
	avg. $(1.42\pm0.24)\times10^{-13}$					
$Pu(OH)_2(CO_3)_2{}^{2-}$	$(6.94\pm0.11)\times10^{-14}$	0.125 ± 0.006	0.1 M NaHCO₃	25℃	This work	no available data
	$(5.34\pm0.12)\times10^{-14}$	0.125 ± 0.007	pH = 9.3			
	$(2.95\pm0.18)\times10^{-14}$	0.085 ± 0.007				
	avg. $(5.1\pm2.0)\times10^{-14}$					
$Am(CO_3)_3{}^{3-}$	not determined		0.1 M NaHCO₃ pH = 9.3	25℃	This work	no available data
$UO_2{}^{2+}$	avg. $(3.6\pm1.2)\times10^{-14}$	0.011 ± 0.010	0.1 M KCl pH = 4	room temp.	Yamaguchi et al.,1997a	0.58[b]
$NpO_2{}^{+}$	avg. $(2.5\pm0.4)\times10^{-13}$	0.010 ± 0.006	ground water pH=7.2~7.5 I = 0.077	room temp.	Kumata et al., 1990	no available data
I^{-}	avg. $(2.3\pm0.4)\times10^{-12}$	0.06 ± 0.06[c]	0.1 M KI	room temp.	Kita et al., 1989	0.33[d]
Sr^{2+}	avg. $(2.7\pm0.6)\times10^{-13}$	0.013 ± 0.008	0.1 M KCl・ pH=4	25℃	Yamaguchi et al.,1993	0.42[d]
uranine	avg. $(4.4\pm0.9)\times10^{-14}$	0.03 ± 0.04	1% uranine solution	room temp.	Kumata et al., 1990	0.55 ± 0.05[b]

a: See text.

b: Yamaguchi et al., 1997a

c: re-estimated value (Yamaguchi et al., 1997a)

d: Nightingale, 1959

e: multi-tracer diffusion experiment of Ba, Co, Mg, Ni, Sr

Table 3 Equilibrium constants for actinide hydrolysis and carbonate complexes in 0.1 mol/kg ionic strength solution.

Species	Log β [a]	reference
UO_2^{2+}		
$UO_2(OH)^+$	-5.4 ± 0.3	Wanner and Forest, 1992
$UO_2(OH)_2^0$	-12.43 ± 0.09 [c]	Choppin and Mathur, 1991
$UO_2(OH)_3^-$	-19.2 ± 0.4	Wanner and Forest, 1992
$UO_2(OH)_4^{2-}$	-33 ± 2	Wanner and Forest, 1992
$(UO_2)_2(OH)^{3+}$	-2.5 ± 1.0	Wanner and Forest, 1992
$(UO_2)_2(OH)_2^{2+}$	-5.84 ± 0.04	Wanner and Forest, 1992
$(UO_2)_3(OH)_4^{2+}$	-12.3 ± 0.3	Wanner and Forest, 1992
$(UO_2)_3(OH)_5^+$	-16.21 ± 0.12	Wanner and Forest, 1992
$(UO_2)_3(OH)_7^-$	-31 ± 2	Wanner and Forest, 1992
$(UO_2)_4(OH)_7^+$	-22.8 ± 1.0	Wanner and Forest, 1992
$UO_2CO_3^0$	9.24 ± 0.04	Wanner and Forest, 1992
$UO_2(CO_3)_2^{2-}$	16.06 ± 0.12	Wanner and Forest, 1992
$UO_2(CO_3)_3^{4-}$	21.60 ± 0.05	Wanner and Forest, 1992
$(UO_2)_3(CO_3)_6^{6-}$	54.0 ± 1.0	Wanner and Forest, 1992
$(UO_2)_2(OH)_3CO_3^-$	-20.0 ± 0.5	Wanner and Forest, 1992
$(UO_2)_3O(OH)_2HCO_3^+$	-18.8 ± 0.5	Wanner and Forest, 1992
$(UO_2)_{11}(OH)_{12}(CO_3)_6^{2-}$	-78.2 ± 2.0	Wanner and Forest, 1992
PuO_2^+		
PuO_2OH^0	-9.73 ± 0.10	Bennet et al., 1990
$PuO_2CO_3^-$	-4.60 ± 0.04	Bennet et al., 1990
Pu^{4+}		
$PuOH^{3+}$	-2.0 ± 0.3	Lierse, 1985
$Pu(OH)_2^{2+}$	-4.1 ± 0.6	Lierse, 1985
$Pu(OH)_3^+$	-7.5 ± 0.5	Lierse, 1985
$Pu(OH)_4^0$	-13.1 ± 0.5	Lierse, 1985
$Pu(OH)_2(CO_3)_2^{2-}$	16.6 ± 0.6	Yamaguchi et al., 1994
$Pu(OH)_4(CO_3)_2^{4-}$	-5.40 ± 0.48	Yamaguchi et al., 1994
$PuCO_3^{2+}$	14.0	Nitsche and Silva, 1996
$Pu(CO_3)_2^0$	26.0	Nitsche and Silva, 1996
$Pu(CO_3)_3^{2-}$	32.6	Nitsche and Silva, 1996
$Pu(CO_3)_4^{4-}$	34.5	Nitsche and Silva, 1996
$Pu(CO_3)_5^{6-}$	33.9	Nitsche and Silva, 1996
Am^{3+}		
$AmOH^{2+}$	-6.8 ± 0.7	Silva et al., 1995
$Am(OH)_2^+$	-14.8 ± 0.6	Silva et al., 1995
$Am(OH)_3^0$	-26.3 ± 0.5	Silva et al., 1995
$Am(CO_3)^+$	6.5 ± 0.8	Yamaguchi and Nakayama, 1996
$Am(CO_3)_2^-$	10.2 ± 1.0	Yamaguchi and Nakayama, 1996
$Am(CO_3)_3^{3-}$	13.8 ± 0.6	Yamaguchi and Nakayama, 1996
$Am(OH)CO_3^0$	-1.7 ± 0.2	Yamaguchi and Nakayama, 1996
$Am(OH)_2CO_3^-$	-10.0 ± 0.9	Yamaguchi and Nakayama, 1996
$AmOH(CO_3)_2^{2-}$	2.4 ± 0.2	Yamaguchi and Nakayama, 1996

(a) equilibrium constant for $mM^{l+} + nH_2O + qCO_3^{2-} = M_m(OH)_n(CO_3)_q^{lm-n-2q} + nH^+$
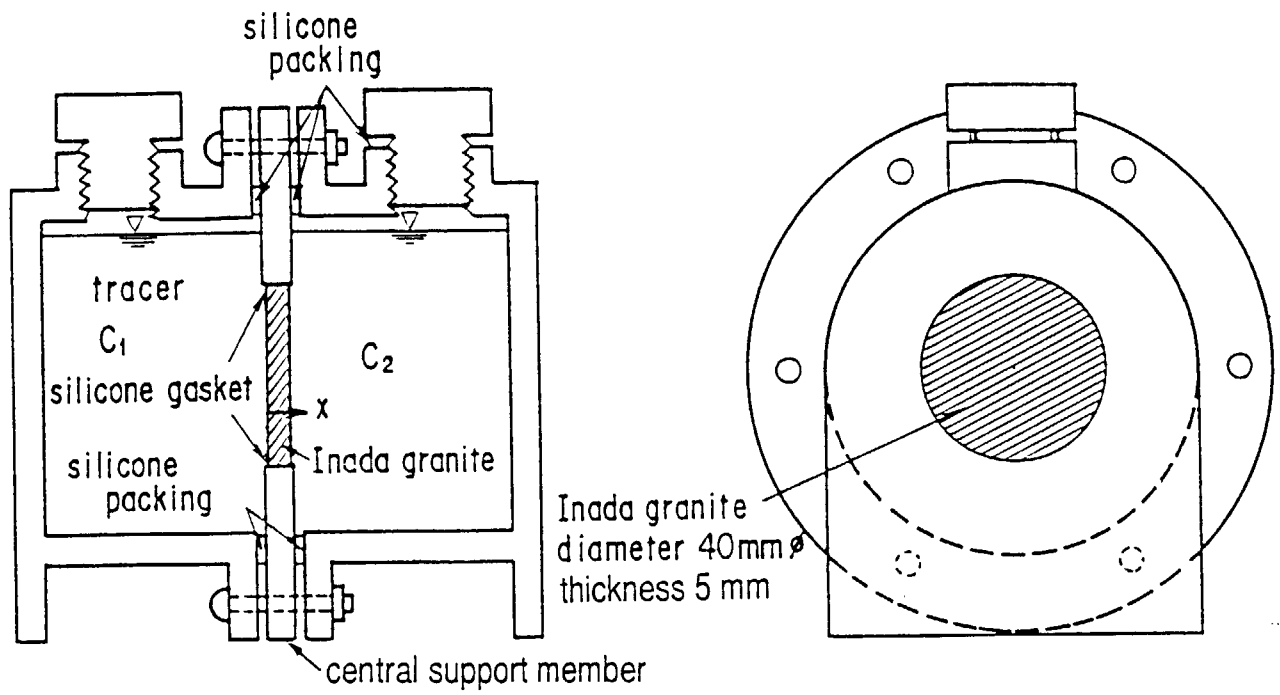
Fig. 1 Diffusion cell used in experiment
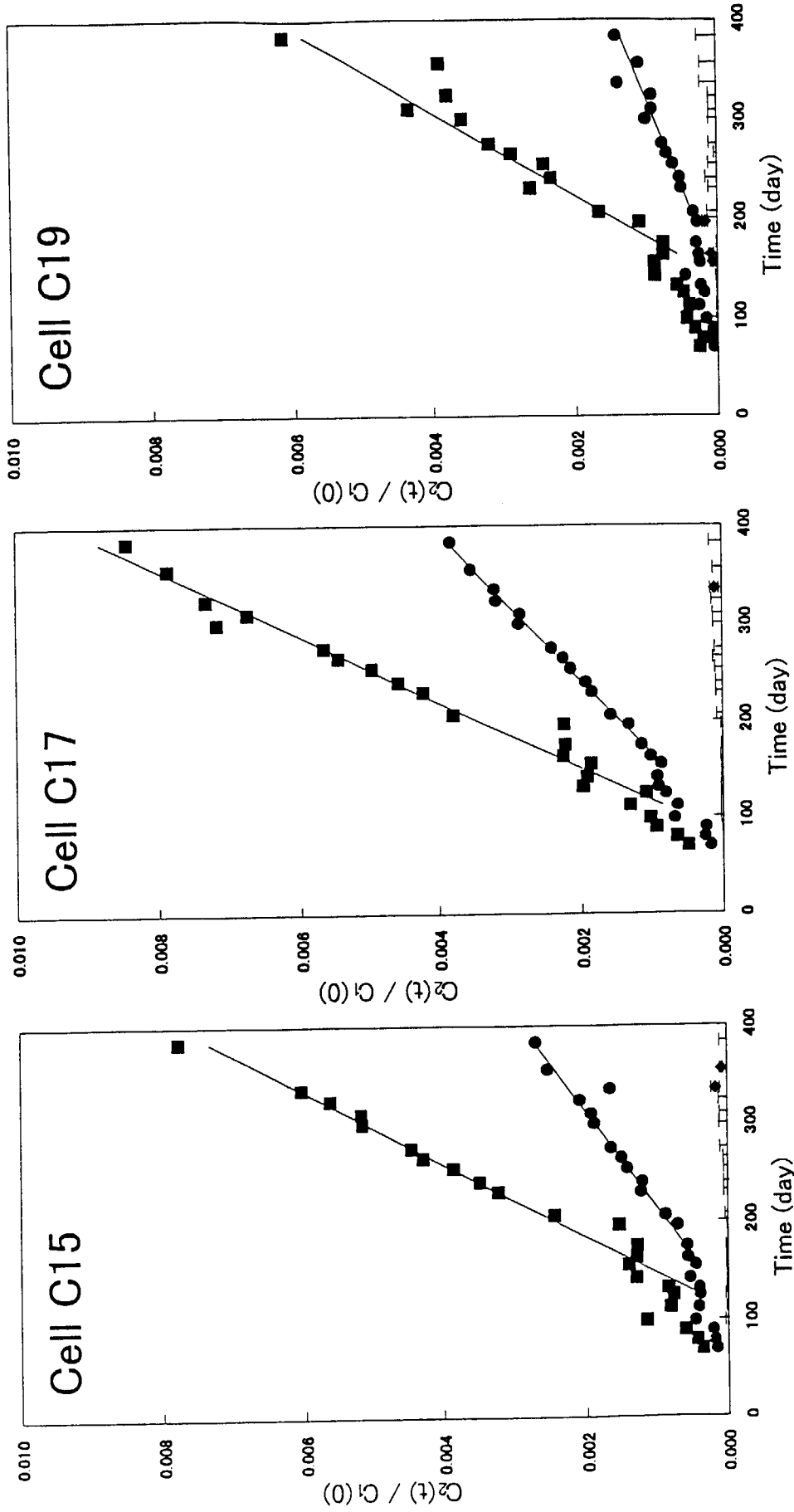
Fig. 2 Diffusion curves of uranium (O), plutonium (■) and americium (◆) through 5-mm thick Inada granite disk in triplicate. When the concentration of americium was under the detection limit, maximum possible concentration was shown by the bars.
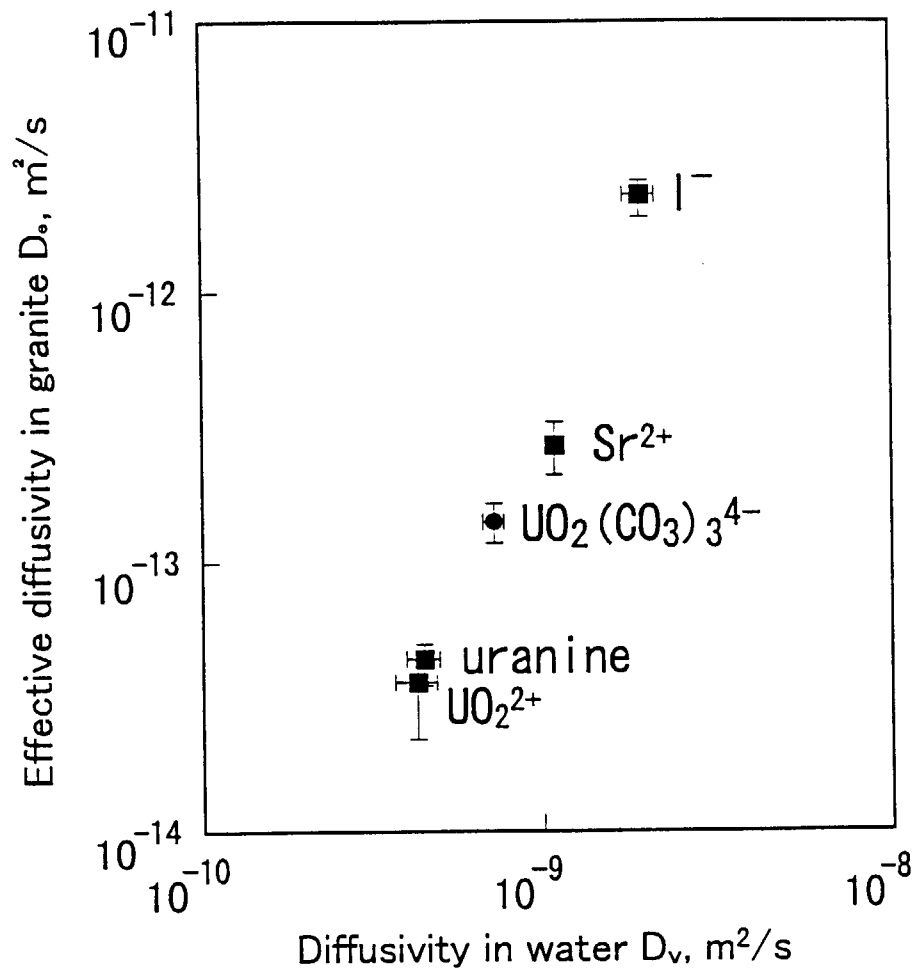
Fig. 3 Correlation between effective diffusivity of species in Inada granite and diffusivity in solution.

3.2 EXPERIMENTAL STUDY ON NEPTUNIUM MIGRATION UNDER
IN SITU GEOCHEMICAL CONDITIONS[1]

M.Kumata and T.T.Vandergraaf[2]

INTRODUCTION

Geochemical processes, including oxidation-reduction and colloid formation, are strongly dependent on the in-situ geochemical conditions and play an important role in the transport of radionuclides through geological media.   Therefore, experiments aimed at predicting the transport of radionuclides through the geosphere should be performed under realistic or in-situ conditions. For this reason, a specially designed facility was constructed at the 240 level of the Underground Research Laboratory (URL) near Pinawa, Manitoba, under a cooperative JAERI-AECL program. This facility contains an experimental system, designed to maintain the original geochemical conditions of the geological material and the groundwater used in the migration experiments[1].

Neptunium-237 has been identified as one of the most important radionuclides in the geological disposal of high-level vitrified wastes.   Neptunium exists under laboratory conditions as relatively poorly sorbing Np(V) species but, under the chemically reducing conditions expected in the geosphere, may exist as Np(IV).   Our previous work with neptunium migration showed strong sorption of Np on the surfaces of iron-bearing minerals under reducing conditions[2].   To further study the transport behaviour of Np under in-situ conditions, migration experiments were performed over a range of groundwater flow rates in columns of crushed rock in the URL.

EXPERIMENTAL

Highly altered granitic rock was obtained from core material from a borehole intersecting a major subhorizontal fracture zone at a depth of 250 m in the URL.   The granite was wet crushed and wet sieved using groundwater obtained from the same borehole into the fracture.   The 180-850 μm size fraction, representative of the grain size of the host granite, was selected and packed in 20 cm-long, 2.54 cm-diameter Teflon-lined stainless steel columns.   A "speciation train," consisting of two colloid filter membranes (pore size of 1000 nm and 50 nm), and anion and cation exchange resin columns were connected to   the outlet   of each column.   The injection solution for the migration

---

[2] Whiteshell Laboratories, AECL, Pinawa, Manitoba Canada, R0E 1L0

experiment containing Np(V) and ^{3}HHO was prepared under an N_2 atmosphere with an O_2 concentration of < 0.5 ppm in a controlled atmosphere chamber in a surface laboratory at the Whiteshell Laboratories[2] as follows: Groundwater from an expansion tank in the URL that was connected directly to the borehole into the fracture zone was shipped in sealed containers to the controlled atmosphere chamber. Aliquots of stock ^{237}Np solutions as Np(V) in acid were added to this groundwater and the pH adjusted to that of the groundwater in the fracture zone (8.9±0.2) with dilute NaOH. The concentration of ^{237}Np in the injection solution was 2.7×10^{-5} mol/L or 1.7×10^5 Bq/L. Approximately 30 mL volumes of groundwater containing ^{3}HHO and ^{237}Np were injected into the columns at flow rates of 0.3, 1 and 3 mL/h, followed by elution with groundwater at the same flow rates, for a period of 95 days. Total volumes of eluted solution were 0.68, 2.28 and 6.84 liters, respectively. The groundwater was introduced into the columns directly from the fracture zone without contact with the atmosphere. The hydrostatic pressure of the groundwater supplied to the columns was reduced from the ~2.4 MPa in the fracture zone to ~ 0.7 MPa using a pressure reducing valve. The groundwater flow was controlled with solenoid valves located downstream from the speciation train. After terminating the migration experiments, the columns were frozen, the column material removed and cut into twenty 1-cm thick sections and each section analyzed by gamma spectrometry.

The pH, Eh and conductivity of the groundwater supplied to the columns were monitored hourly and had values of 9, -330 mV and 1440 mS/cm, respectively. Stability of the groundwater composition during the experimental period was excellent.

Static sorption/desorption experiments with neptunium were performed in the controlled atmosphere chamber at the surface laboratory under a N_2 atmosphere containing < 0.5 ppm O_2 on fractions of the same crushed and wet-sieved granite as used in the column experiments. Individual contacting solutions containing ^{237}Np were prepared as described above for the injection solutions except that the addition of ^{3}HHO was omitted. The solid/liquid ratio was ~0.1g/mL. Terminal sorption experiments were performed in triplicate for 1-, 3- and 10-day contact periods. Following sorption, 10 mL volumes of groundwater were added to each reaction vessel for a 10-day desorption step.

RESULTS AND DISCUSSION

Elution profiles were obtained for ^{3}HHO but no ^{237}Np was detected in the eluent. No ^{237}Np was detected on any of the colloid filters or on the cation exchange resins. Only in the case of the highest flow rate, a very small amount (3.2×10^{-2} Bq) of ^{237}Np was found on the anion exchange resin. No ^{237}Np was detected on the other anion exchange resin columns. Almost all the injected ^{237}Np was strongly retained on the granite in the columns.

A one-dimensional transport model[3, 4] was fitted to the ^{3}HHO breakthrough curves to

obtain flow parameters for each of the three columns. The results of this fitting exercise are shown in Figure 1 and indicate that excellent flow stability was achieved with no significant channeling. The hydraulic properties of the columns obtained from this fitting exercise are listed in Table 1. The dispersion coefficient for the groundwater (Dw) decreases exponentially with decreasing flow velocity (Vw) (Figure 2).

The ^{237}Np activity profiles obtained for the three columns show a dependence on flow velocity (Figure 3). At a flow rate of 0.3 mL/h, the ^{237}Np remaining in the column was limited to 3 cm from the inlet of the column. At a flow rate of 1.0 mL/h, the transport of the ^{237}Np in the column was limited to 5 cm. Only in the case of the highest flow rate, 3.0 mL/h, was the ^{237}Np distributed along the entire length of the column. The fact that some ^{237}Np was detected near the outlet of the column agrees with the observation that some ^{237}Np was detected in the speciation train for this column.

To analyze the neptunium transport under deep geological conditions, a one-dimensional transport model was fitted to these neptunium profiles using Vw and the flow porosity obtained from curve fitting of the ^{3}HHO breakthrough curve. At the highest flow rate, the curve could be fitted to the first seven data points of the neptunium profile (see Column 3 of Figure 4), giving a distribution coefficient for neptunium (Kd) of 900 mL/g and a dispersion coefficient (Dn) of 7.3 x 10^{-8} m^2/s. The remaining part of the ^{237}Np profile could not be fitted using this approach. The ^{237}Np activity within the first 7 cm of the column corresponds to about 70 % of total activity in the column. Therefore, the calculated curve can be considered to represent the major amount of the neptunium in the column. This suggests that the location of the bulk of the neptunium in the column can be estimated with a reversible and linear 1-D sorption model. Using this assumption, however, the ^{237}Np profile obtained along the column at the highest flow rate suggests that more than one, presumably poorer sorbing, neptunium species was present in the column and appear to have traveled more rapidly than the predominant neptunium species. The nature of these species was not investigated in the course of these experiments.

At the intermediate flow rate, transport of ^{237}Np was limited to the first 5 cm of the column. It was not possible to fit a single curve to the five data points of the ^{237}Np profile obtained for the column, and the existence of two ^{237}Np species is again postulated. The first two data points were fitted to the 1-D curve, giving values for Kd of 3000 mL/g and Dn of 2.2 x 10^{-8} m^2/s for the ^{237}Np species with the largest Kd.

A total of about 5000 Bq of ^{237}Np was injected into each column. However, the total amount of a neptunium detected in the recovered material from the column at the lowest flow rate was about 2400 Bq and corresponds to about half of the total injected ^{237}Np activity. The remainder is postulated to have been firmly fixed on granite particles embedded in the porous Teflon sheets at the inlet of the column, although no supporting evidence is available. A similar observation was

made in a technetium migration experiment[5]. If this assumption is correct, the Kd value of the ^{237}Np species with the largest Kd in the column might be larger than those observed in the experiment performed at the intermediate flow rates.

The Kd and Dn values for neptunium for Columns 2 and 3 obtained by curve fitting are listed in Table 2.

Based on the assumptions that 1) the major species of neptunium in the three columns are the same and 2) the dispersion coefficient (Dn) will decrease exponentially with decreasing flow velocity (Vw) as in the case of relationship between Dw and Vw, a lower limit for Dn of nearly 1.2 x 10^{-8} m^2/sec is obtained when the velocity of the transport solution approaches zero.

The retardation factor (Rf) used in the 1-D transport model follows the standard form of

$$Rf = 1 + \frac{\rho\, Kd}{\theta}$$

where ρ is the bulk density of column material and θ is the volumetric water content. Rf values for the major neptunium species in Columns 2 and 3 are also listed in Table 2.

The relationship between the transport velocity of a radionuclide (Vn) to the groundwater velocity (Vw) is given by $Rf=Vw/Vn$. Values for Vn of 2.0 x 10^{-10} m/s and 1.9 x 10^{-9} m/s were obtained for Columns 2 and 3, respectively, a difference of one order magnitude. The difference in the velocity of transport solution between two columns is only a factor of 3. It should be kept in mind in a safety assessment that dependence of the Vn for neptunium on the velocity of groundwater is significant under deep geological conditions.

The results obtained in the sorption/desorption experiments showed highly irreversible sorption of neptunium on the geological material used in the columns. Only limited sorption (2.80 mL/g) was observed after a 10-day contact period. On the other hand, desorption Kd values ranged from 368 to 873 mL/g (average of triplicate samples) (Table 3). Sorption increased with increasing contact time. This increase is also reflected in the higher desorption Kd values and is consistent the observation that ^{237}Np sorbed in the columns was not readily eluted. The Kd values obtained by curve fitting are much higher than those obtained from static sorption experiments, including the desorption values. This difference may be attributed to differences in the chemical conditions of the batch sorption experiment in the anaerobic chamber and those in the columns. The presence of as little as 0.5 ppm O_2 in the controlled atmosphere chamber at the surface laboratory may have been sufficiently high to produce a chemical environment different to the in-situ conditions in the URL. To obtain reliable Kd values of neptunium under anoxic conditions, establishing truly anoxic conditions in an experimental system, both in the atmosphere and in mixtures of solutions and solids is required[5].

In our column experiments, small amounts of neptunium species with relatively low Rf

(and hence, *Kd*) values were observed at the higher flow rates. At low groundwater velocities, high *Kd* values of neptunium can be expected in the fracture zone under deep geological conditions. However, at higher flow velocities, neptunium species with a low *Kd* become more important. Further investigation is required to study the behaviour of these neptunium species under reducing conditions.

Recent speciation studies with neptunium have indicated that Np(IV) may form a strongly sorbing $Np(OH)_2(CO_3)_2^{2-}$ species in carbonate solutions under anoxic conditions [6-8]. The HCO_3 concentration in the groundwater used in this experiment was ~200 mg/L [1]. The formation of this strongly sorbing species may account for the high retardation under the in situ conditions of these experiments.

CONCLUSION

Almost all of the injected ^{237}Np was strongly retarded on crushed granite under geochemical conditions similar to those in a natural fracture zone. This retardation was much higher than predicted on the basis of the sorption coefficients obtained on similar geological material and may be due to different geochemical conditions between sorption and migration experiments even though the former were performed in a controlled atmosphere. Transport of ^{237}Np through the columns may have been controlled by a rapid sorption reaction, possibly by reduction of Np (V) to Np (IV) followed by a slow desorption step.

A one-dimensional flow model can be used to model the transport behaviour of the bulk of the ^{237}Np retained by the column over the duration of the experiment, but, multi-phase transport of neptunium needs to be invoked at higher flow rates.

A diffusion coefficient for the neptunium, of 1.6 x 10^{-8} m^2/sec, was estimated by extrapolation of the relationship obtained between the neptunium dispersion coefficient and the flow velocity.

Strong dependence of *Rf* and *Dn* on the flow velocity was observed. Based on the relation between *Rf* and the flow velocity, *Vn* for neptunium varied over one order of magnitude.

Further investigation of the transport behaviour of ^{237}Np under chemically reducing conditions is warranted.

ACKNOWLEDGMENTS

REFERENCES

(1) Kumata, M. and Vandergraaf, T.T., 1991. Nuclides Migration Tests Under Deep Geological Conditions, Proc. 3rd Int. Symp. on Advanced Nuclear Energy Research, 414-419.

(2) Kumata, M., Vandergraaf, T.T. and Takahashi, T., 1998. (to be published)

(3) Kimura, H., Takahashi, T., Shima, S., & Matsuzuru, H., 1992. A generic safety assessment code for geologic disposal of radioactive waste: GSRW computer code user's manual (JAERI-M No. 92-161). Japan Atomic Energy Research Institute Tokai Research Establishment.

(4) Kinzelbach, W., 1986. *GROUNDWATER MODELLING*, An Introduction with Sample Programs in BASIC. ELSEVIER Science Publishers B.V.(Amsterdam), Elsevier Science Publishing Company INC.(New York).

(5) Kumata, M. and Vandergraaf, T.T., 1993. Technetium behaviour under deep geological conditions, Radioactive Waste Management and the Nuclear Fuel Cycle, 17, 107-117.

(6) Yamaguchi, T., Pratopo, M.I., Moriyama, H. and Higashi, K., 1991. Adsorption of cesium and neptunium(V) on bentonite, Proc.3rd Int.Conf.on Nuclear Fuel Reprocessing and Waste Management, Japan, 2, 999-1004.

(7) Pratopo, M.I., Yamaguchi, T., Moriyama, H. and Higashi, K., 1991. Adsorption of Np(IV) on Quartz in carbonate solutions, Radiochimica Acta, 55, 209-213.

(8) Pratopo, M.I., Yamaguchi, T., Moriyama, H. and Higashi, K., 1993. Sorption and colloidal behavior of Np(IV) in a bentonite-carbonate solution system, J. of Nuclear Scie. Tech., 30, 560-566.

Table 1　Hydraulic Properties of the columns for the migration experiment

Column No.	Flow Velocity (m/s)	Dispersion Coefficient for the groundwater Dw (m^2/s)	Flow Porosity
1	3.5×10^{-7}	6.3×10^{-10}	0.503
2	1.1×10^{-6}	1.1×10^{-9}	0.592
3	3.2×10^{-6}	4.0×10^{-9}	0.578

Table 2　Kd values and Dispersion Coefficient for Neptunium

Column No.	Kd (mL/g)	Dispersion Coefficient Dn (m^2/s)	Retardation Factor Rf
2	3000	2.2×10^{-8}	5380
3	900	7.3×10^{-8}	1710

Table 3　Kd Values from Static Sorption/Desorption Experiment

Sorption Time (day)	Kd* (mL/g)	Desorption Time (day)	Kd* (mL/g)
1	0.63	10	368
3	1.70	10	497
10	2.80	10	668

* average of triplicate samples
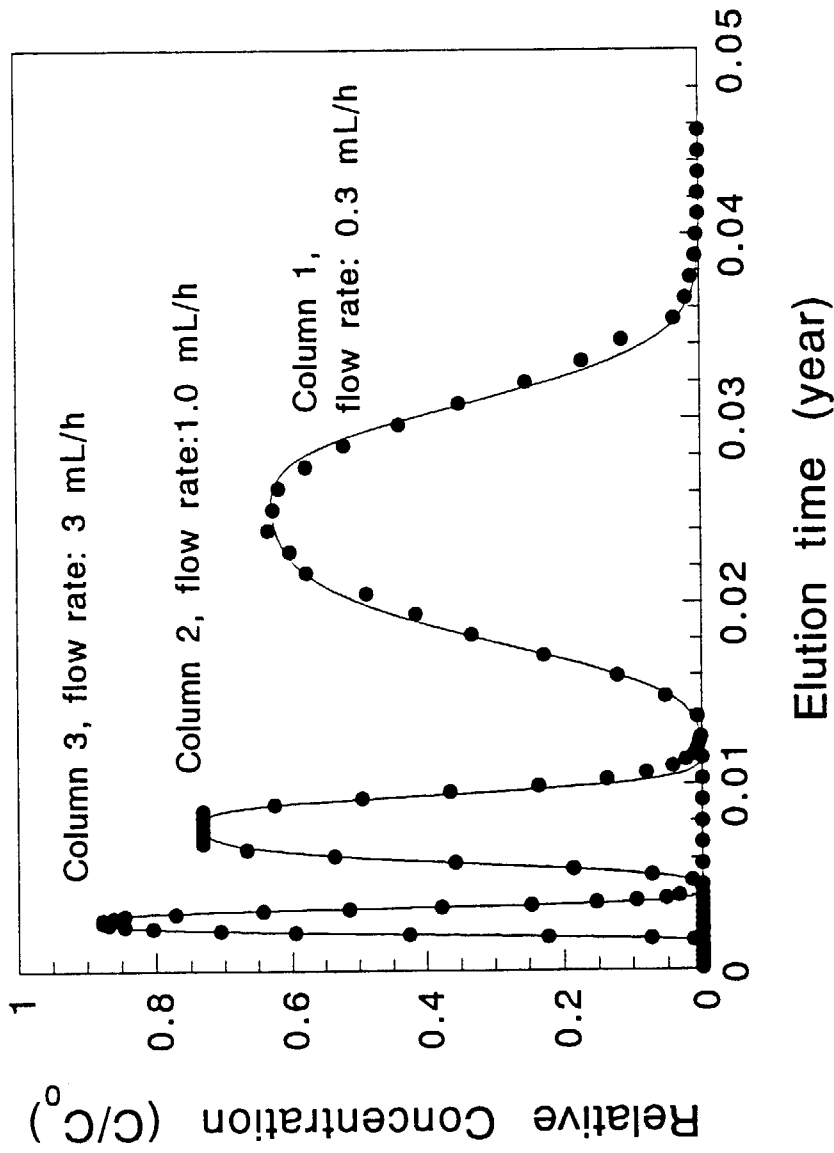
Figure 1 Breakthrough curves of ^{3}HHO for Column 1, 2 and 3.
Solid lines represent fitted curves for each breakthrough curves calculated by a one-dimensional transport model.
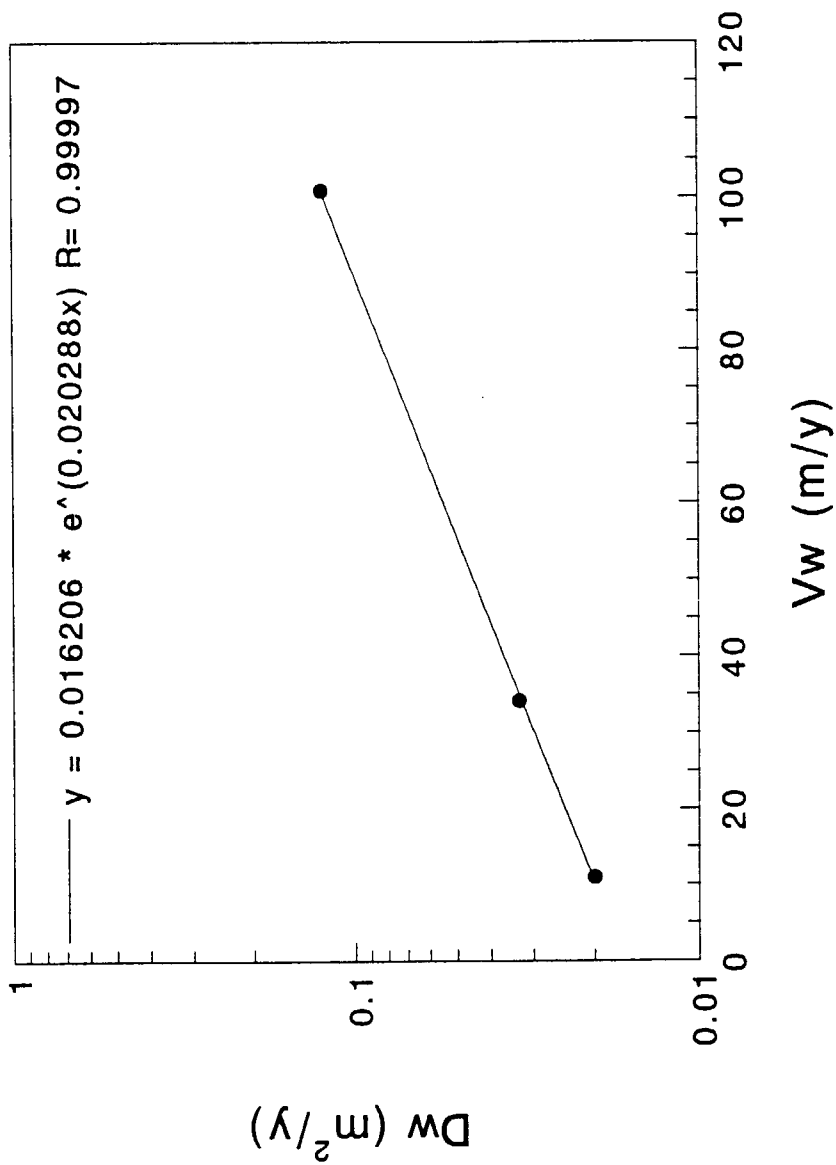
Figure 2　Relation between the flow velocity (*Vw*) and the dispersion coefficient for groundwater (*Dw*).
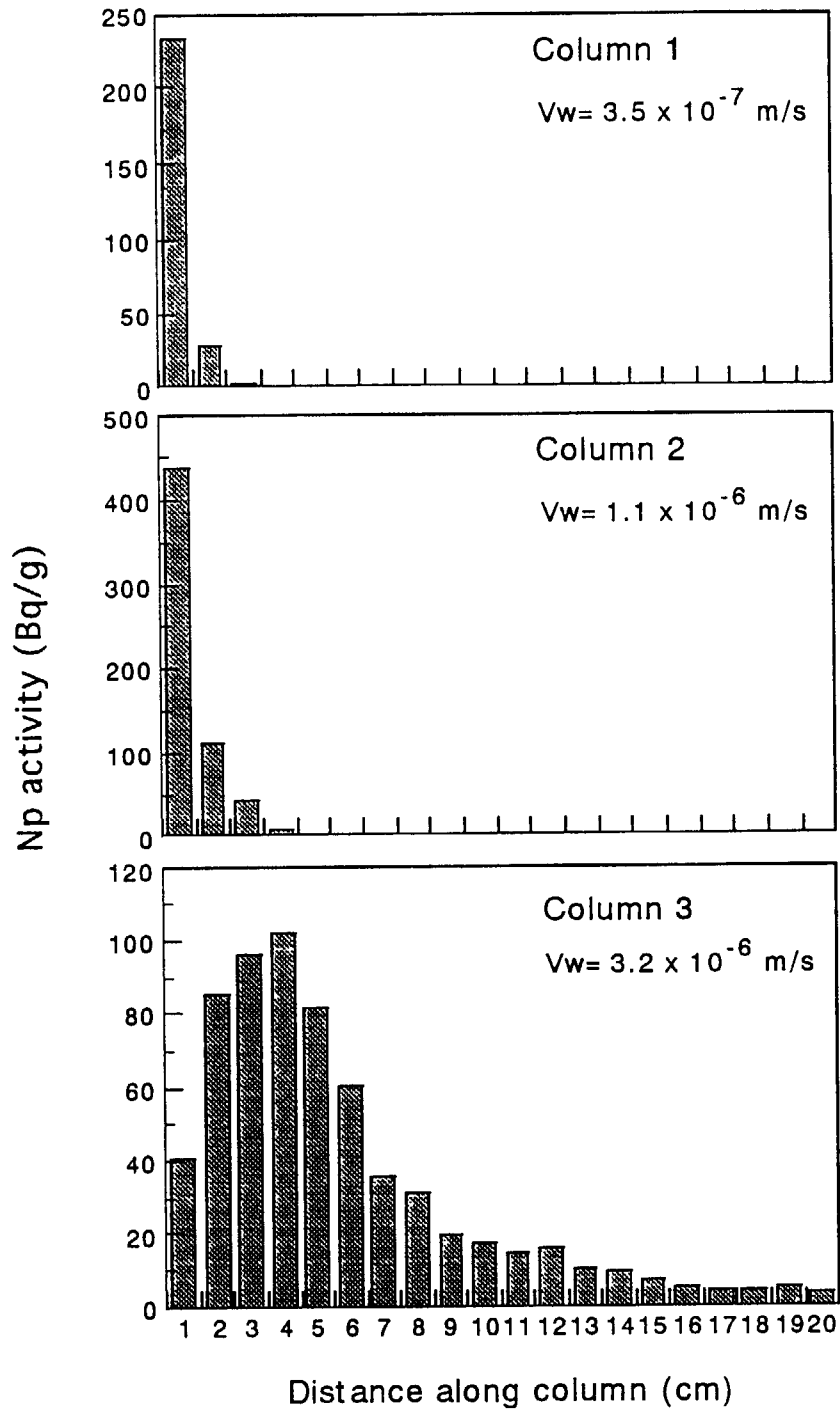
Figure 3 ^{237}Np distribution in each columns after 95 days continuous elution.
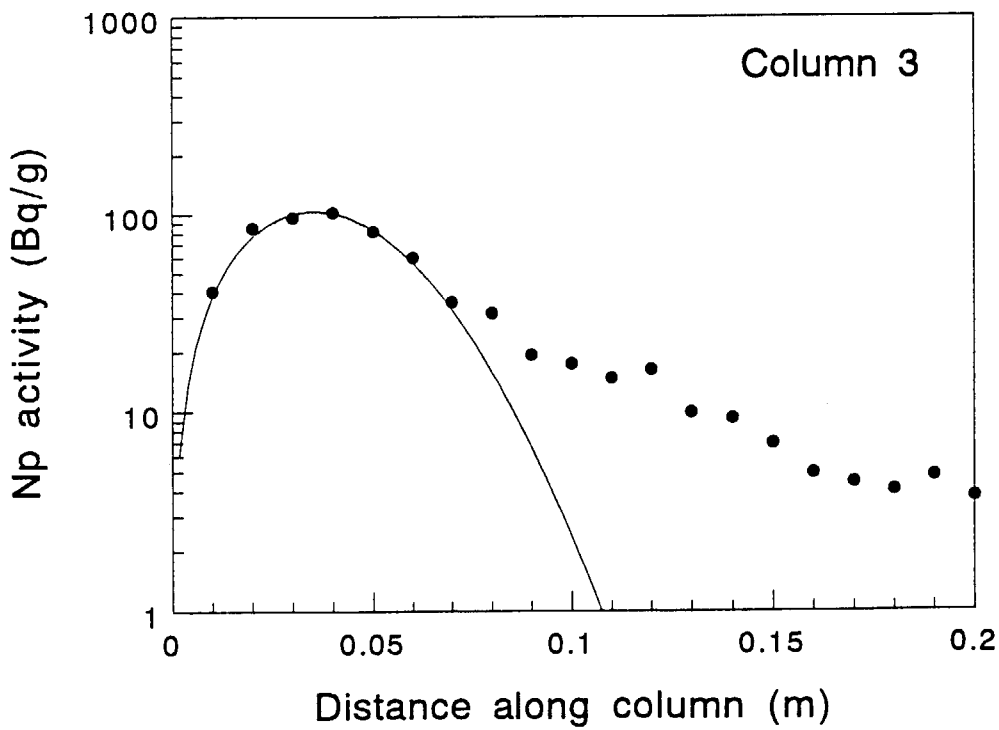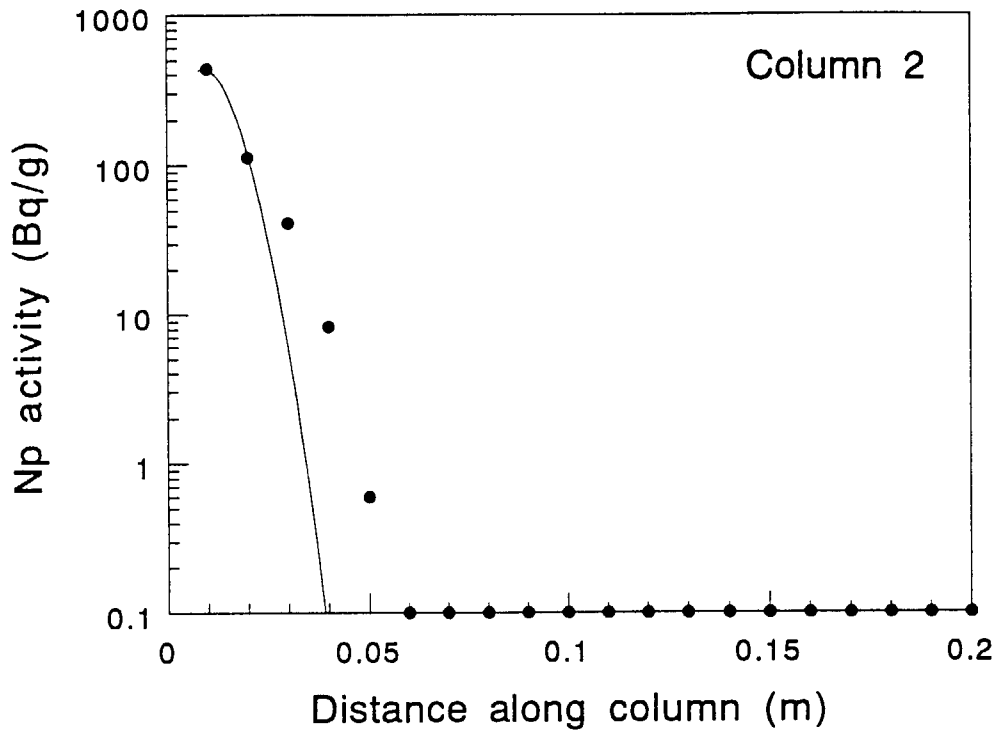
Figure 4   Curve fitting results for Np profiles in Column 2 and 3.

The curves were calculated using the one-dimensional transport model.

3.3 RADIONUCLIDE MIGRATION IN NATURAL FRACTURES UNDER IN SITU CONDITIONS

M.Kumata, S.Muraoka, T.T.Vandergraaf[3]

For the most reliable predictions of radioactive nuclide migration at depth, one needs to understand the actual behavior of the nuclides of interest under natural geochemical conditions. For this purpose, many relevant studies have been performed since 1987 under a collaborative program between the Japan Atomic Energy Research Institute and Atomic Energy of Canada Limited. In Phase I program (1987-1993), the need to perform radionuclide migration experiments under in situ conditions in the Underground Research Laboratory (URL) has been demonstrated[1]. This laboratory was excavated in a previously undisturbed granitic pluton, the Lac du Bonnet batholith, located in South-Eastern Manitoba. The results obtained from one-dimensional migration experiments performed in columns of crushed fracture infilling materials in the URL showed that retardation of radionuclides tended to be higher than predicted on the basis of static sorption data obtained under a controlled atmosphere[1,2].

To obtain data for nuclide migration through fractured rocks such as crystalline rocks, radionuclide migration experiments in natural fractures under in situ conditions are being performed at the URL. A new experimental room, the Quarried Block Radionuclide Migration Facility (QBRMF), was excavated to provide access to a subvertical joint zone at the 240 level of the URL that had not been exposed to the atmosphere. Blocks of granite, with dimensions of ~1 x ~1 x ~0.7 m, each containing a natural fracture have been excavated from that joint zone using a diamond wire saw. Prior to removing the blocks from their location along the wall of the excavated area, stainless steel straps were wrapped around the blocks and tightened mechanically to prevent the fracture from separating. The surfaces of the blocks were immediately sealed using a silicone-based sealant, and stainless steel plates, each containing three inlet/outlet ports were mounted on each of the four faces that were intersected by the fracture (Figure 1). Groundwater from the joint zone (pH of ~8.5 and an Eh of ~ -200 mV) was used as drilling and cutting fluid to minimize contamination of the fractures and is also used as the transport solution for migration experiments in the natural fractures in these blocks to maintain in situ geochemical conditions. A more detailed description of the excavation and preparation of the blocks were presented at the 4th International Conference on Nuclear and Radiochemistry, St. Malo, France September 8-13, 1996[3].

Two excavated blocks have been selected for the migration experiments. Hydrological characterization of the fractures has been carried out by injecting groundwater into inlet/outlet ports located at the periphery of the fracture where it intersects the outer surfaces of the block[3]. Based on

---

[3] Whiteshell Laboratories, AECL, Pinawa, Manitoba R0E 1L0 Canada

the hydraulic data the most appropriate flow path for radioisotope migration experiments was selected. One block was used for in situ geochemical conditions. For comparison, for the other block the groundwater was artificially oxygenated to produce oxidizing conditions. Groundwater spiked with ^3H_2O, ^{85}Sr, ^{237}Np, ^{238}Pu and $^{95m+99}Tc$ was injected into the fracture at a flow rate of 5 mL/h in four separate migration experiments. Some preliminary results were presented at the Migration '97, Sendai Japan, October 27-31, 1997[4].

These experiments will be followed by migration experiments using colloidal material. At the completion of these experiments, the blocks will be separated at the fracture and the surfaces analyzed radiometrically.

REFERENCES

(1) Kumata,M. and Vandergraaf,T.T. : Technetium behaviour under deep geological conditions, Radioactive Waste Management and the Nuclear Fuel Cycle. **17(2)**, pp. 107-117 (1993).

(2) Kumata,M. and Vandergraaf,T.T. : Experimental Study on Neptunium Migration under In Situ Geochemical Conditions, Migration '97, Sendai Japan, October 27-31 (1997).

(3) Vandergraaf,T.T., Drew,D.J., Kumata,M. and Nakayama,S. : Design, Construction and Operation of an Underground Facility to Study the Migration of Radioisotopes in Natural Fractures under In Situ Conditions, the 4th International Conference on Nuclear and Radiochemistry, St.Malo, France, September 8-13 (1996).

(4) Vandergraaf,T.T., Drew,D.J., Kumata,M. and Nakayama,S. : Migration Experiments in Natural Fractures in Quarried Granite Blocks under In Situ Conditions, Migration '97, Sendai Japan, October 27-31 (1997).
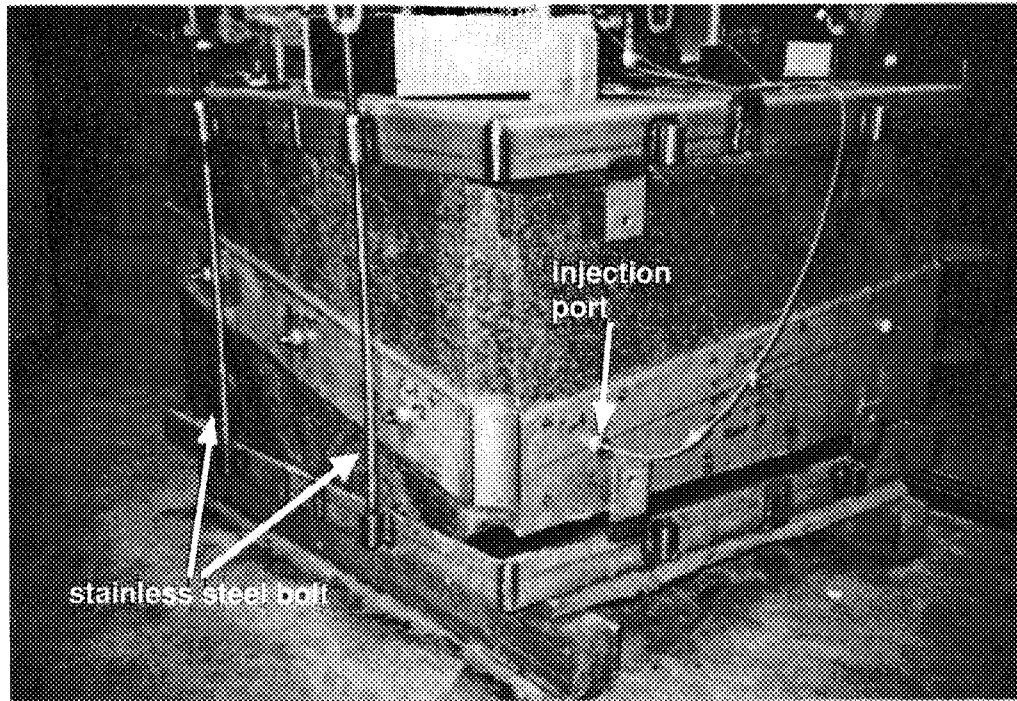
Figure 1 Quarried Block Radionuclide Migration Experiment

A large block of granite containing part of natural water-bearing fracture was excavated from the fracture zone at the 240 level of the URL, Canada. The block sized about 1 x 1 x 0.7 m was tightened up by stainless steel bolts and coated with silicon glue to keep original in-situ conditions. Twelve ports were equipped on the block surfaces to inject solutions into the fracture. Hydrologic characterization of the fracture was carried out. After that, the groundwater spiked with Np and Pu was injected into the fracture.

3.4 Study on crystallization of neodymium-containing ferric gels in aqueous solutions by X-ray diffractometry

Tetsushi NAGANO, Hisayoshi MITAMURA and Shinichi NAKAYAMA

INTRODUCTION

In a geological repository for high-level nuclear waste forms, iron minerals will be generated as a result of corrosion of engineered barrier materials and weathering of natural iron-containing minerals. These iron minerals are expected to fix some hazardous radionuclides released from the waste forms and to retard the migration of these radionuclides in ground water. The freshly formed iron minerals are amorphous, and have a large capacity of sorption and/or incorporation of foreign elements (Sakamoto and Senoo, 1994). Under the redox conditions prevailing near the surface of the earth, the amorphous iron minerals are likely to crystallize into more stable phases, e.g. goethite or hematite (Schwertmann and Murad, 1983). These crystalline phases may have a smaller surface area and less capacity for sorption than their amorphous precursors (Payne et al., 1994). During the re-crystallization process, an adsorbate may be partially released into the ground water. In addition, the crystal structure of iron minerals may be influenced by the presence of foreign elements.

In pedogenic environments, iron minerals have a large pigmenting ability (ranging from red to yellow (Schwertmann, 1993)) and consequently play an important role in coloring of aerobic soils, and also in the fixation of trace anions and cations (Schwertmann and Taylor, 1989). For instance, an aluminum ion (Al^{3+}) can be substituted for Fe^{3+} at the octahedral site of the goethite structure as it has the same valence and a similar ionic radius (Schulze, 1984: Schulze and Schwertmann, 1984: Schulze and Schwertmann, 1987).

Transuranium (TRU) elements such as neptunium, plutonium and americium have various ionic radii and valences (III to VII), and may be incorporated into iron minerals by other fixation mechanisms (compared to aluminum), and these mechanisms would also depend on redox conditions and temperature. However, until now there have been few studies of the fixation

mechanisms of these elements, and of their modes of incorporation into crystalline iron minerals.

In the present paper, we investigate the effect of the presence of neodymium (Nd) on the re-crystallization mechanisms of ferric gels to produce iron minerals. Neodymium was chosen as a simulant of trivalent TRU elements because it is considered to have a similar chemical behavior having a similar ionic radius. For this reason, the results of experiments involving Nd may be extrapolated to these TRU elements in their trivalent state.

EXPERIMENTAL METHODS

Preparation process

Aqueous solutions of ferric nitrate (0.2 M) and neodymium nitrate (0.2 M) were mixed so as to attain molar Nd/(Nd+Fe) ratios of 0, 2, 5, 7, 10, 15, 20 and 30% in a standard experimental volume of 200 mL. The mixtures were hydrolyzed by adjusting the pH to ~7.5 with aqueous ammonia. The mixtures were poured into a dialysis tube, and then the resulting precipitates were washed with distilled water in a 1-L beaker at 15 °C. The conductivity of the water was measured and the water was replaced with freshly-distilled water daily. After dialyzing for 10 days, the conductivity of the wash water became almost constant. The resulting precipitates were X-ray amorphous at this stage. In a preliminary experiment using neodymium nitrate alone, the hydrolysis products above pH 9 consisted mainly of crystalline neodymium hydroxide ($Nd(OH)_3$), and neodymium was not detected in solution. These observations imply that neodymium was coprecipitated with iron at pH~7.5 rather than being precipitated as a separate crystalline phase, since the precipitate in the mixed system was amorphous.

Deionized water was added to the dialyzed suspension sample to compensate for the volume reduction during the dialysis. This suspension was then divided into two portions. A 0.2 M aqueous solution of sodium nitrate was added to one portion of the suspension to achieve ionic strength of 0.1, and then the pH of the mixture was adjusted to ~ 9.2 with aqueous ammonia. This mixture was aged in a thermostated oven at 70 °C for 9 days in a polyethylene bottle. Under this condition, both goethite and hematite form from pure ferric gels.

A 2 M solution of sodium hydroxide was added to the other portion of the suspension until the amount of excess OH⁻ exceeded 0.3 M. This mixture was then subdivided into several parts which were placed in polyethylene bottles. One sub-sample was aged in an oven at 40 °C for 10 days, and the remainder were aged at 25 °C for duration ranging from 6 hours to 20 days. These conditions are favorable for formation of goethite alone.

Resulting precipitates consisting of poorly-crystallized iron minerals were washed with deionized water before centrifuged at 4000 rpm for 30 minutes and dried at 40 °C. On the other hand, for well-crystallized samples the washing procedure was omitted because they were considered to be suspended in solutions even after the centrifugation.

Characterization method

The sediments were subjected to powder X-ray diffractometry (XRD) (Rigaku, Geigerflex). Diffraction data were collected using $CoK\alpha$ radiation at 40 kV and 20 mA. A small amount of silicon powder from National Bureau of Standards was added to some samples as an internal standard. Peak positions and areas in XRD patterns were determined using a PC-based software "GRAMS", which generally fits a spectrum to a curve that consists of Lorentzian, Gaussian, or the convolution of both elements.

RESULTS AND DISCUSSION

1. Aging products in samples aged with 0.3 M excess OH⁻ at 40 °C

Figure 1 shows the XRD patterns of precipitates aged with 0.3 M excess OH⁻ at 40 °C for 10 days. Diffraction data were accumulated at an interval of 0.02 °2θ with a dwell time of 7 seconds. The inhibition by Nd of the crystallization of iron minerals is demonstrated by the data in Figure 1. Strong reflections at 33.2 and 55.6 °2θ were due to silicon mixed as an internal standard, and the other lines were due to goethite. The crystallinity of goethite (based on peak areas at 24.7 °2θ) decreased with increasing Nd ratio (Figure 2), confirmed the inhibiting effect of Nd on goethite

formation. The full width at the half maximum (FWHM) of the goethite peaks became smaller with increased Nd, which implies that the aging products had a larger particle size with higher Nd content (Schulze, 1984).

The lattice parameters of goethite were calculated from the d-values for *130, 021, 111* and *140* reflections. Peak positions of these reflections were calibrated by the two lines due to silicon (Figure 1). As a reference, the lattice parameters of synthesized aluminum-substituted goethite were also calculated using previously published d-values for the above four reflections (Thiel, 1963). A correction for the crystal size was not carried out because the lattice parameters were not significantly influenced by particle size when the FWHM at *130* and *140* lines were below 0.8 and 0.7 °2θ, respectively (Nagano, 1996). A simple computer program using VISUAL BASIC was written to calculate the lattice parameters of goethites, which minimized $\Sigma[d(2\theta)-d(hkl)]^2$ for measured $d(2\theta)$ ($=\lambda/(2\cdot\sin\theta)$) and estimated $d(hkl)$ ($=[(h/a)^2 + (k/b)^2 + (l/c)^2]^{-1/2}$). Here λ is the wave length of X-ray used, the values (*hkl*) are Miller indices of the lattice plane, and *a, b* and *c* are lattice parameters.

In Figure 3, the lattice parameters of goethite aged with 0.3 *M* excess OH⁻ at 40 °C for 10 days are plotted as a function of the Nd content of the parent solutions. This figure also includes data for aluminum-substituted goethite (Thiel, 1963). Whereas the lattice parameters of Al-substituted goethite decrease linearly with increasing Al content, those of goethite in the experiments with Nd are almost constant, apart from a slight decrease in the *a*-value with increasing Nd content up to 7 mol% above which it becomes constant. Schulze (1984) postulated that this phenomenon may have been due to defects in the lattice. This is consistent with the larger ionic radius of the Nd^{3+} ion (for a given coordination number) compared to the Fe^{3+} and Al^{3+} ions (Shannon, 1976), although there is no published information on the isomorphous substitution of Nd^{3+} into the octahedral Fe^{3+} site of the goethite structure.

2. Aging products at pH 9.2 and 70 °C

X-ray diffraction patterns of the precipitates aged at pH 9.2 and 70 °C for 9 days are shown in

Figure 4. Intensity measurements were made at intervals of 0.02 °2θ with a dwell time of one second.

Figure 5 shows that the dominant iron mineral phases in the aging products depended on the Nd/(Nd+Fe) ratios of the parent solutions. With a Nd/(Nd+Fe) ratio of 0-7%, both goethite and hematite were present, whereas only goethite was observed for Nd/(Nd+Fe) ratios of 10-15%. For the highest amount of Nd, only amorphous material was present. Peaks at 34.3 °2θ in the XRD patterns are due to sodium nitrate which was added when adjusting the ionic strength and remained in the precipitates because washing procedure was omitted.

Figure 5 shows the relationship between the crystallinity of iron minerals and the Nd/(Nd+Fe) ratios of the parent solutions. The crystallinity of these minerals was determined based on the peak areas at 24.7 °2θ (_110_) for goethite, 28.1 °2θ (_012_) for hematite, and 38.8 °2θ for total iron minerals. The latter line is a combination of goethite and hematite. The crystallinity was normalized using the maximum peak area at each line.

As shown in Figure 5, the crystallinity of hematite decreased with increasing Nd content and was negligible at 10% Nd. This indicates that the formation of hematite was inhibited by the presence of Nd. On the other hand, the crystallinity of goethite increased with increasing Nd ratio up to 10%, and then decreased to zero at 20 mol% of Nd. The changes in crystallinity of the two minerals between 0 and 10 mol% of Nd support the competitive formation model, which suggests that favorable conditions for the formation of goethite are unfavorable for hematite formation, and vice versa (Schwertmann and Murad, 1983). Figure 5 implies that Nd generally prevents the formation of crystalline iron minerals, with greater inhibition of the formation of hematite than that of goethite.

In order to calculate the lattice parameters of hematite, samples which contained hematite ($NF_0 \sim NF_7$) were re-subjected to XRD at an interval of 0.02 °2θ with a dwell time of 7 seconds after mixed with a small amount of silicon powder (Si). The d-values of _110_, _113_ and _024_ reflections (see Figure 4) were used for the calculation. The peak positions were calibrated by two peaks due to Si (see Figure 1). The calculation method was the same as that for the goethite crystal except an estimation equation of $d(hkl)$ ($=[4 \cdot (h^2 + h \cdot k + k^2)/3a^2 + l^2/c^2]^{-1/2}$) for the hexagonal crystal. Figure

6 shows a and c values of the hematite as a function of Nd content of the parent solutions, and also contains a linear relationship for Al-substituted hematite (Vegard rule) as a reference. The lattice parameters from the present study appear to gradually increase with increasing Nd content and hence it is possible that Nd was incorporated in the hematite structure because Nd^{3+} has a larger ionic radius than Fe^{3+}. However, the parameters of goethite were not calculated because peak intensities were small and some peaks were overlapped by those of hematite.

3. Nd inhibition mechanism for crystallization of iron minerals from Nd-containing ferric gels

The results described above provide information about an inhibition mechanism of Nd for the formation of the pure iron minerals, that are closely related to the crystallization mechanisms of Fe minerals. Previous studies have revealed that hematite and goethite crystallize from ferric gels through different competition pathways (Feitknecht and Michaelis, 1962: Schwertmann and Fischer, 1966: Cornell et al., 1989). Hematite grows through dehydration and/or rearrangement of ferrihydrite, whereas goethite grows through dissolution of ferrihydrite and consecutive reprecipitation of the Fe ion as goethite. In the case of a system having silicate species, the inhibition of the crystallization of iron minerals is considered to be due to formation of a rigid network of ferrihydrite, which is enhanced by the coexistence of Si (Cornell et al., 1987). In the present study, we assumed that the Fe ion in the Nd-containing ferric gels be more strongly restrained to the Nd ion before aging, so the iron in the Nd-containing ferric gels may probably become less mobile with increasing Nd ratio of the parent solutions.

Formation of Nd-substituted hematite was postulated from the fact that the lattice parameters of hematite in the present study gradually increased with increasing Nd content (Figure 6). During the formation of hematite through dehydration and/or rearrangement of ferrihydrite, it is considered that Nd ions was not released outside the amorphous phase but incorporated into the hematite structure. However, formation of Nd-substituted hematite may have been inhibited because rearrangement of the ferrihydrite was getting harder by the presence of Nd.

In order to form goethite, Fe ions in the ferrihydrite must detach against O-Fe bonding to

cause dissolution of the ferrihydrite. As assumed above, the Fe ion was more difficult to detach from the ferric gels containing higher Nd contents, and this may be attributed to the restraining effect of the Nd ion on the detachment of the Fe. During reprecipitation of the Fe as goethite after detachment from the ferrihydrite, since there is scarcely Nd in the solutions due to its low solubility, the non-substituted goethite may have formed. The non-substituted goethite was also reported by Gerth (1989) who examined goethite synthesized from thorium- or uranium-containing ferric gels. These actinide elements were unable to substitute for the Fe^{3+} ion in the octahedral site of goethite.

The crystallization of the two iron minerals may have been inhibited through these mechanisms. Furthermore, the fact that Nd more strongly influenced the formation of hematite than that of goethite (see Figure 5) suggests that the detachment of the Fe ions from the ferrihydrite should be easier than the rearrangement toward Nd-substituted hematite from the ferrihydrite.

During the goethite formation process, nucleation is likely to occur both near the ferrihydrite and in solution, which leads to the formation of crystals having different morphology (Cornell et al., 1986). The lower mobility of the Fe in the NF_{30} sample may have caused a low degree of supersaturation and reduction of the goethite nucleation rate and number after the dissolution of the ferrihydrite. Consequently, the goethite in the NF_{30} sample was larger in particle size than that in the NF_5.

REFERENCES

Cornell, R. M. and Giovanoli, R. 1986. Factors that govern the formation of multidomainic goethites. Clays Clay Miner 34:557-564.

Cornell, R. M., Giovanoli, R. and Schindler, P. W. 1987. Effect of silicate species on the transformation of ferrihydrite into goethite and hematite in alkaline media. Clays Clay Miner 35:21-28.

Cornell, R. M., Giovanoli, R. and Schneider, W. 1989. Review of the hydrolysis of iron (III) and the crystallization of amorphous iron (III) hydroxide hydrate. J Chem Tech Biotechnol 46:115-34.

Feitknecht, W. and Michaelis, W. 1962. Uber die hydrolyse von Eisen (III) perchlorat-Losungen.

Helv Chim Acta 45:212-24.

Gerth, J. 1990. Unit-cell dimensions of pure and trace metal-associated goethites. Geochim Cosmochim Acta 54:363-371.

Nagano, T. 1996. Estimation of peak shifts in powder X-ray diffraction pattern for goethite crystallites having different sizes. JAERI-memo 08-140, Japan Atomic Energy Research Institute, Tokai, Naka, Ibaraki, Japan (Private communication) (in Japanese).

Payne, T.E., Davis, J.A. and Waite, T.D. 1994. Uranium retention by weathered schists - the role of iron minerals. Radiochim Acta 66/67:297-303.

Sakamoto, Y. and Senoo, M. 1994. Redistribution of Strontium during Crystallization of Amorphous Ferrihydrite to Goethite. Radioactive Waste Management and Environmental Restoration 18:265-280.

Shannon, R. D. 1976. Revised Effective Ionic Radii and Systematic? Studies of Interatomic Distances in Halides and Chalcogenides. Acta Cryst A32:751-767

Schulze, D. G. 1984. The influence of aluminum on iron oxides. VIII. Unit-cell dimensions of Al-substituted goethites and estimation of Al from them. Clays Clay Miner 32:36-44.

Schulze, D. G. and Schwertmann U. 1984. The influence of aluminum on iron oxides: X. Properties of Al-substituted goethites. Clay Miner 19:521-539.

Schulze, D. G. and Schwertmann U. 1987. The influence of aluminum on iron oxides: XIII. Properties of goethites synthesized in 0.3 M KOH at 25 °C. Clay Miner 22:83-92.

Schwertmann, U. 1993 Relations between iron oxides, soil color, and soil formation. In: SSSA Special Publication 31:51-70.

Schwertmann, U. and Fischer, W. R. 1966. Zur Bildung von α-FeOOH und α-Fe$_2$O$_3$ aus amorphous Eisen(III)-hydroxid III. Z Anorg Allg Chem 346:137-142.

Schwertmann, U. and Murad, E. 1983. Effect of pH on the formation of goethite and hematite from ferrihydrite. Clays Clay Miner 31:277-284.

Schwertmann, U. and Taylor, R. M. 1989. Iron oxides. In: Minerals in Soil Environments (2nd Ed.). Soil Sci Soc Amer Book Series 1:379-438.

Thiel, R. 1963. Zum System α-FeOOH- α-AlOOH. Anorg Allg Chem 326:70-78.
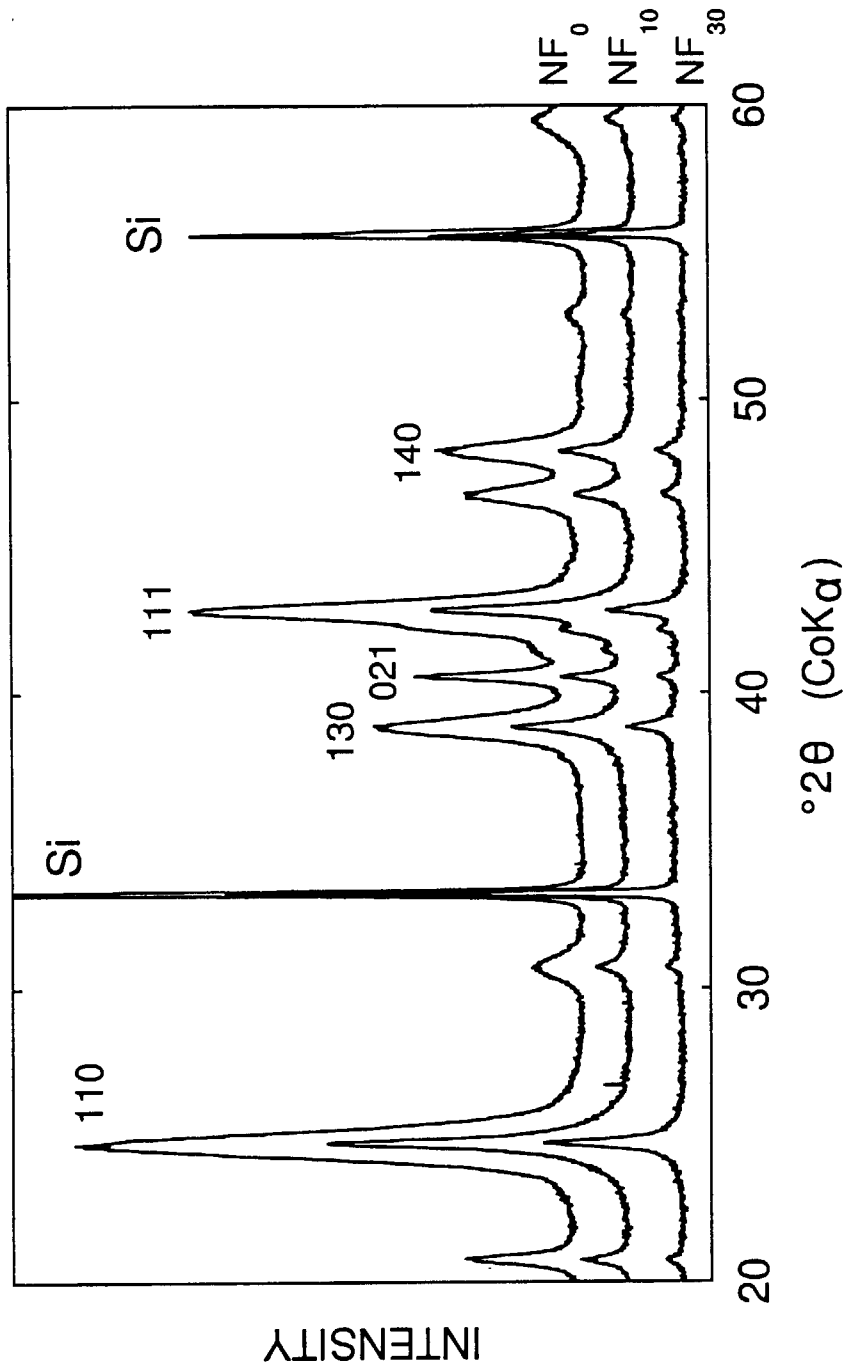
Figure 1 X-ray diffraction patterns of Nd-containing ferric gels aged at 0.3 M excess OH^- and 40 °C. The mark of "Si" indicates peaks from silicon metal powder mixed as an internal standard. The other peaks are due to goethite.
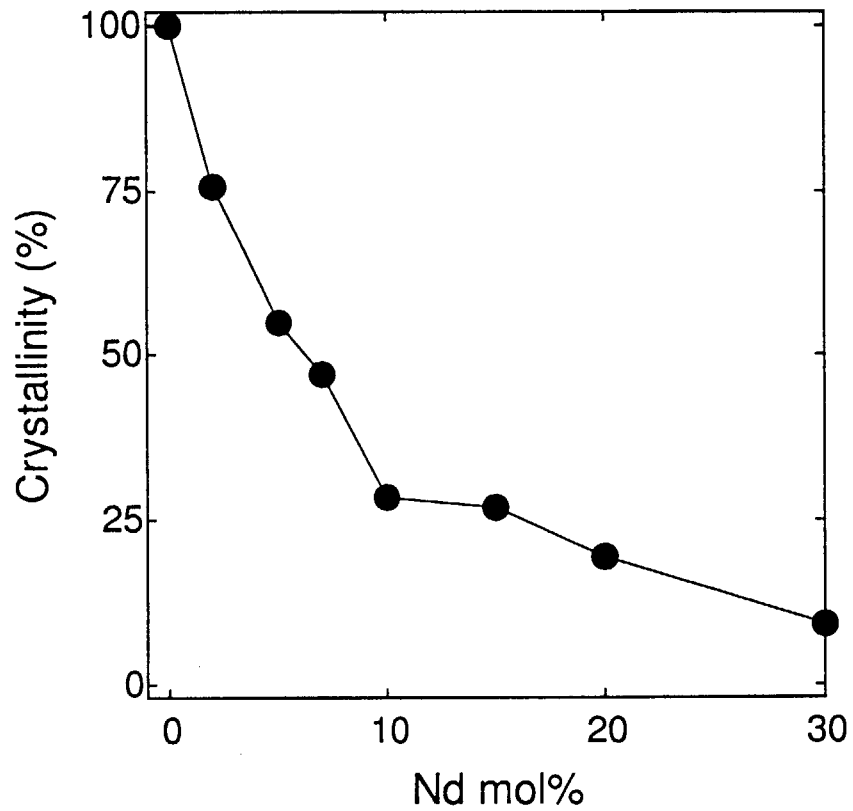
Figure 2 Relationship between crystallinity of iron minerals and Nd/(Nd+Fe) ratio. The crystallinity was determined based on peak areas of (110) reflection in Figure 1, and normalized using the maximum peak area.
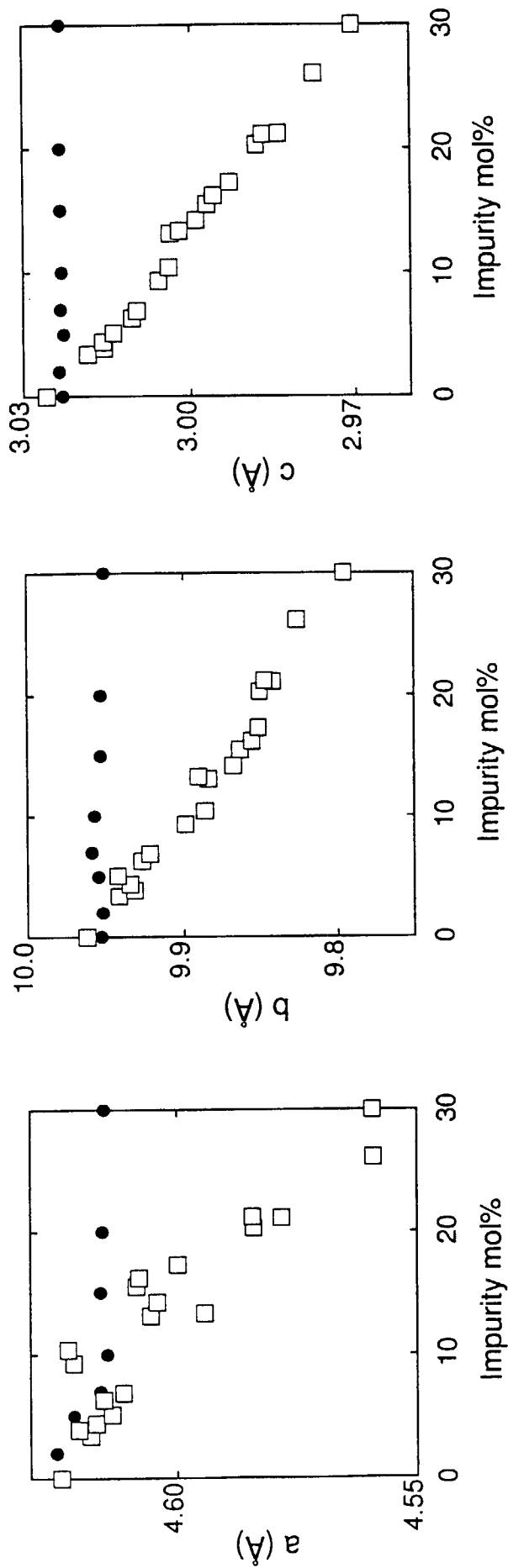
Figure 3 Lattice parameters of synthetic goethite as a function of impurity contents. The sings of ●
and □ indicate the data from the present study and Thiel (1963), respectively. The former used Nd
as an impurity, and the latter did Al.
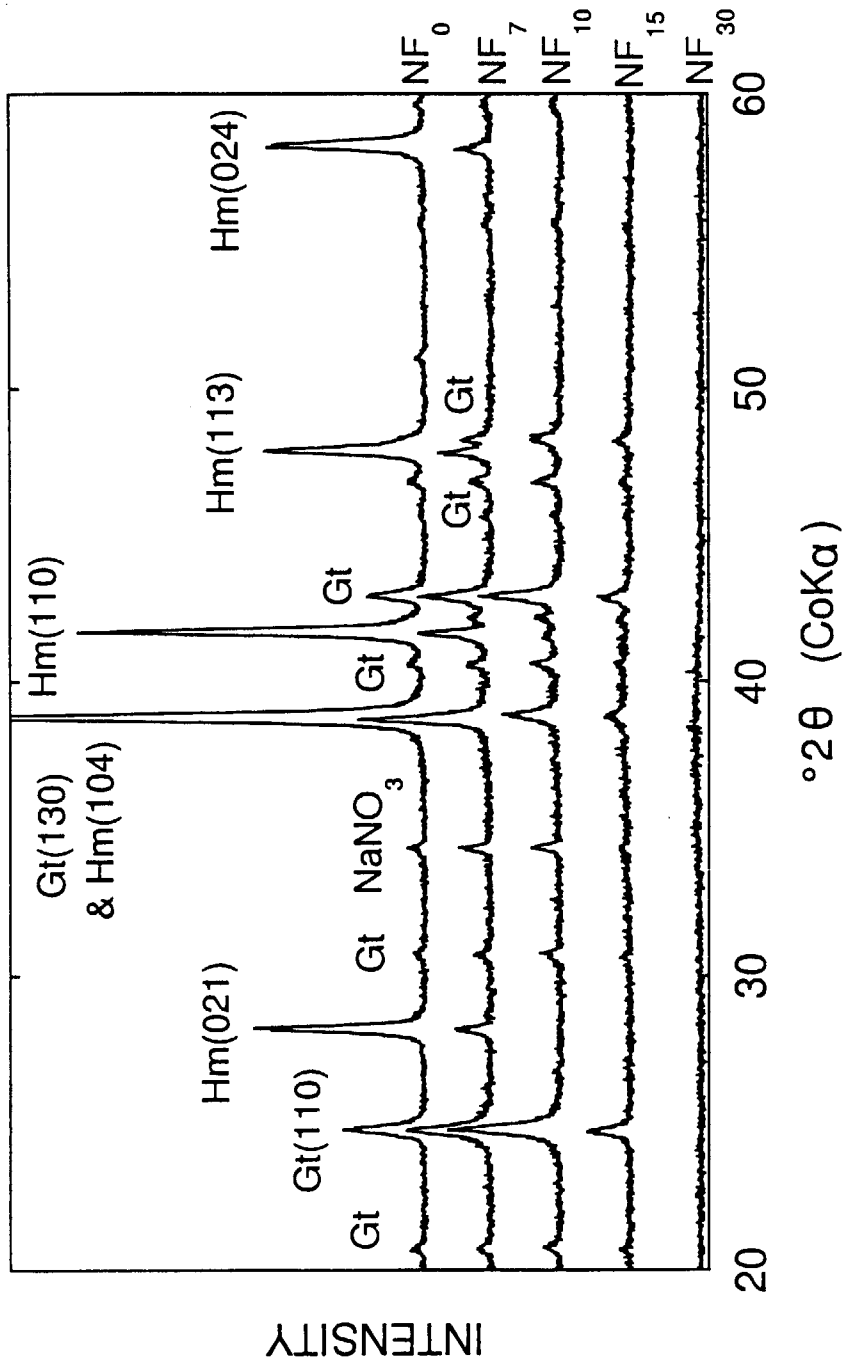
Figure 4 Powder X-ray diffraction patterns of Nd-containing ferric gels aged at pH 9.2 and 70 °C.

Products from a solution having x mol% of Nd/(Nd+Fe) ratio are also labeled as NF_x. The marks of

"Gt" and "Hm" indicate peaks from goethite and hematite, respectively.
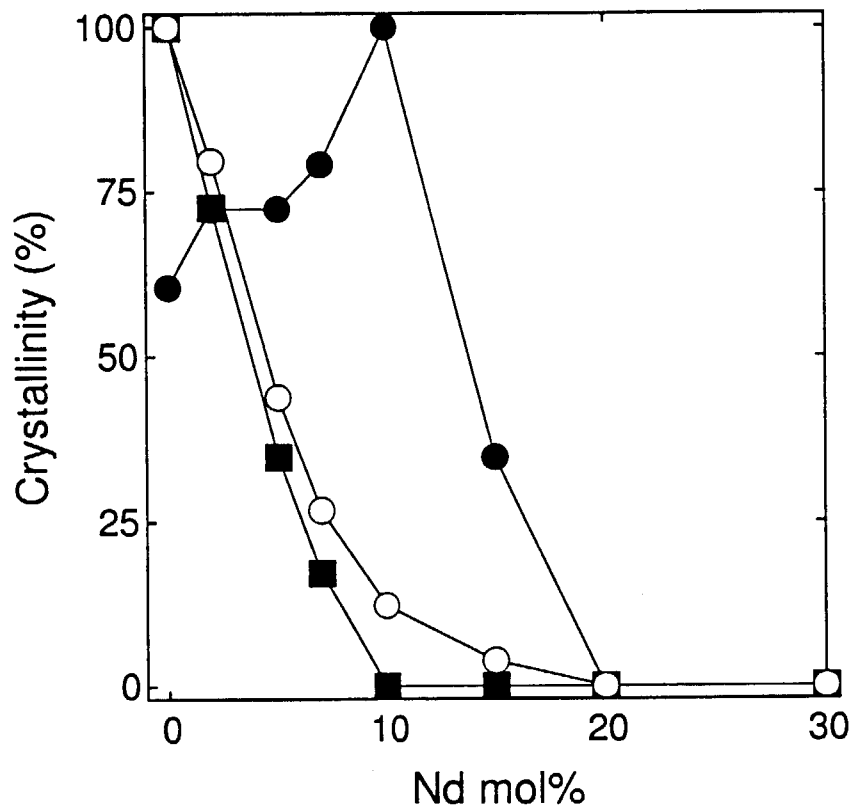
Figure 5 Relationship between crystallinity of iron minerals and Nd/(Nd+Fe) ratio. The crystallinity was determined based on peak areas in Figure 4 and normalized using the maximum peak area at each reflection line. The signs of ●, ■ and ○ indicate goethite (24.7 °2θ), hematite (28.1 °2θ), and goethite & hematite (38.8 °2θ), respectively.
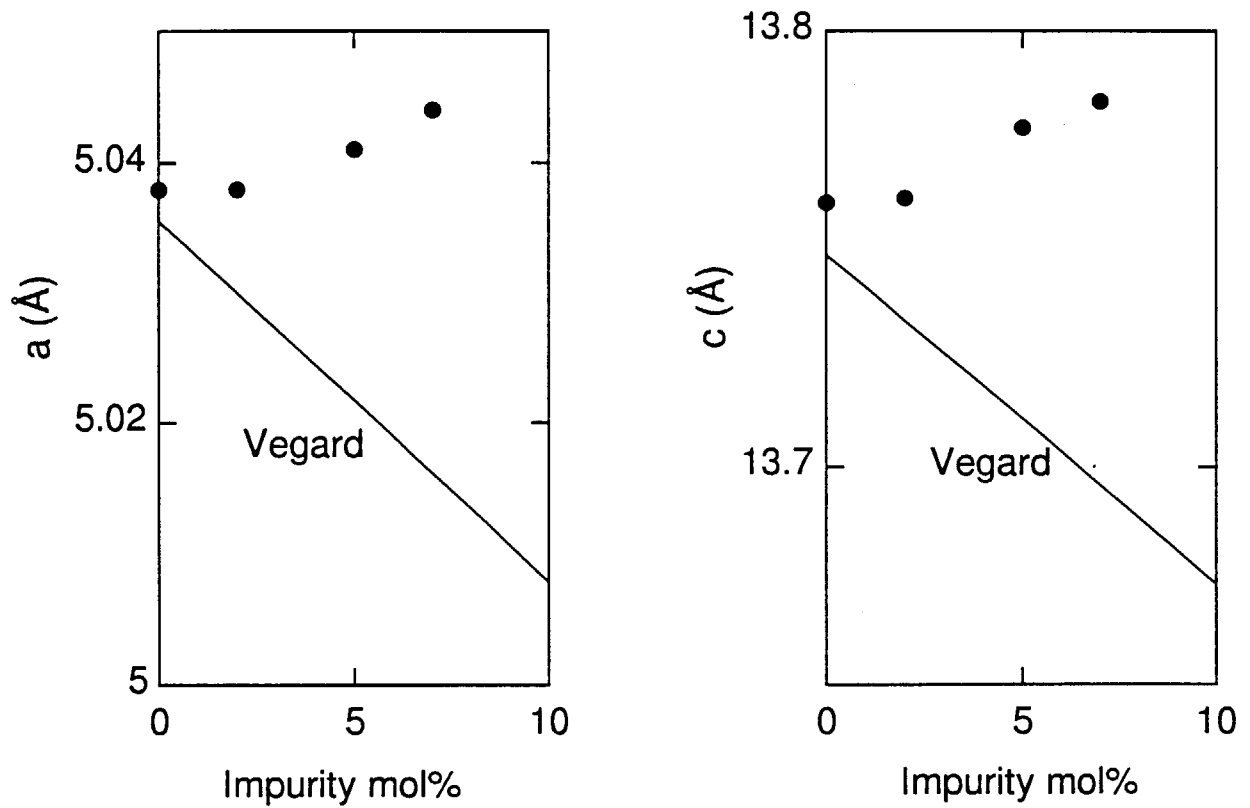
Figure 6 Lattice parameters of synthetic hematite as a function of impurity contents. Solid lines show linear relationship for Al-substituted hematite (Vegard rule) as a reference.

3.5 Natural Analogue Studies on the Koongarra Uranium Deposit, Australia: Behavior of Uranium and Decay Products in the Environment

Hiroshi ISOBE*, Nobuyuki YANASE, Tsutomu SATO, Yoshihisa IIDA and Toshihiko OHNUKI

Department of Environmental Safety Research
Japan Atomic Energy Research Institute
Tokai, Ibaraki, 319-1195, JAPAN
e-mail address

ABSTRACT

Natural analogue studies were carried out on the Koongarra uranium deposit, Australia, under the international collaborative projects. In the projects, Environmental Geochemistry Laboratory of Japan Atomic Energy Research Institute obtained much information on behavior of uranium and decay products in geosphere. The most essential result is that uranium is more strongly fixed by several ways in nature than the simple adsorption on minerals observed in laboratories. Fixation mechanisms of uranium are coprecipitation with iron minerals and precipitation of uranium minerals through alteration of the host rock and uranium minerals. These are direct evidences of uranium migration and fixation in near surface condition. Natural analogue studies can provide us not only direct contribution to the performance assessment of scenario on the nuclear waste disposal, but also securities for various natural systems through general understanding of geological processes.

INTRODUCTION

For the accurate safety assessment of the nuclear waste disposal, we have to understand the long-term migration behavior of radionuclides in geosphere. Quantitative evaluation and modeling of processes that occur in nature enables us application for prediction of migration behavior of elements in nuclear waste repositories. For these purposes, studies on natural systems have been carried out as natural analogue studies on migration of radioactive nuclides.

The most important processes regarding to migration are dissolution, transportation and fixation of elements. In nature, these are common processes of ore deposit formation. Remobilization of elements in ore deposits can be considered good analogue to the migration phenomena of nuclides from radioactive waste repository. Especially,

evolution of uranium ore deposits has unique and significant value because uranium is not only a direct analogue to trans uranium elements (TRU) in radioactive waste but also uranium and related elements have various geochemical and geochronological characters. We can extract key processes for migration and fixation of elements from studies on the uranium ore deposits. Based on the observation on nature, we can build models that represent the natural processes, and evaluate how accurate it is. In this paper, the natural analogue studies on the Koongarra uranium deposit, Northern Territory, Australia, carried out by our laboratory are introduced briefly.

Koongarra uranium deposit, Australia

Koongarra deposit is located 220 km east from Darwin, and it is in the Kakadu national park (Figure 1). In the region, several uranium deposits were found and some of them are under mining operation. Among them, Koongarra deposit has quite characteristic features on uranium migration. Formation of the Koongarra deposit is estimated to be approximately 1.6 billion years ago in quartz chlorite schist, an iron-rich low-grade metamorphic rock [1]. After that, the ore body was under relatively stable geological setting. However, gradual erosion of ground surface let the depth of the ore body getting shallow. At approximately 2 million years ago, oxidized surface water began to affect to the ore body.

The current Koongarra deposit has three distinct sections (Figure 2). The deeper zone is the unweathered, primary ore region where uraninite (uranium oxide) and uranyl silicate minerals are dominant. The shallower zone is the weathered, secondary ore region where uranium occurs as uranyl phosphate minerals or absorbant on iron and clay minerals [2]. Border of the weathered and unweathered zones is the transition zone where redox condition changes drastically.

Main oxidized alteration products of the host rock are kaolinite and iron minerals. Iron minerals have high sorption capacity of elements from ground water. Flow of the oxidized surface water dissolved the upper part of the ore body and moved uranium downstream, then precipitated the secondary ore body. This feature makes the Koongarra deposit to be significant and unique natural analogue site for migration of nuclides in surface condition. We can observe migration and fixation mechanisms of uranium occurred in nature.

To study the above features of Koongarra, the deposit is subject to international natural analogue studies for more than ten years. In 1987, Alligator Rivers Analogue Project (ARAP) was organized as a multilateral project sponsored by OECD/NEA. Japan Atomic Energy Research Institute (JAERI) joined the project and kept

contributing to the next project, Analogue Studies in the Alligator Rivers Region (ASARR).

RESULTS OF NATURAL ANALOGUE STUDIES

Distribution and disequilibrium of uranium

Distribution of uranium in the ore body was determined by measurement of radioactivity coupled with sequential selective extraction techniques [3,4]. Uranium in the primary ore body is attributed to uranyl minerals or uranium oxide minerals. In the secondary ore body, majority of uranium coexists with crystalline iron minerals (Figure 3). The residual phases like quartz and kaolinite in the secondary ore body have extraordinary higher activity ratio of $^{234}U/^{238}U$ than unity [4]. This disequilibrium on uranium series nuclides also means that uranium in the weathered zone is related to iron minerals coating quartz. Disequilibrium of uranium series nuclides can provide us information concerning migration rates of uranium in several hundred thousand years.

Weathering of host rock and fixation of uranium by iron minerals

Detailed mineralogical observation on weathering process of the host rock was carried out [5-9]. Main mineral of the host rock, chlorite, altered to kaolinite through vermiculite by oxidized ground water (Figure 4). In this process, iron in the chlorite is oxidized and released, then iron minerals such as amorphous ferrihydrite and goethite precipitated. Magnesium and silicon are also released during alteration of chlorite to the ground water. These elements play important role on the fixation of uranium. Migration rate of uranium to the secondary ore body may depend on weathering rate controlled by the alteration of chlorite.

In the central region of the current secondary ore body, iron minerals play the most important role to fix and keep uranium by their high sorption capacity on dissolved species. Observations by high-resolution transmission electron microscopy, nanocrystals of uranyl phosphate minerals were observed [10-12]. Precipitation of uranium minerals from low concentration ground water is conducted by catalytic reaction by iron minerals. This process may have a key role on fixation of uranium.

Alteration of uranium minerals

In the primary ore body of the Koongarra deposit, alteration of uranium minerals determines distribution and migration of uranium [13]. The initial uranium mineral of the deposit is uraninite (UO_{2+x}) precipitated just below the graphite layer of the host rock. Uraninite is still found in the limited area of the primary ore body (Figure 5). The

most dominant uranium mineral in the current primary ore body is sklodowskite, uranyl Mg silicate minerals. Alteration processes of uraninite to uranyl silicate minerals through uranyl lead oxide minerals (mainly curite) are controlled by migration of lead and uranium (Figure 6).

At the bottom of the secondary ore body, replacement by a uranyl phosphate mineral (saleeite) with a uranyl silicate mineral or a calcium phosphate mineral (apatite) occurred [14,15]. These processes are also evidences of precipitation of uranium minerals from unsaturated ground water.

Fixation of uranium at the redox front

In the transition zone, the redox front between weathered and unweathered zones, growing grains and layers of uranium minerals are observed [16] (Figure 7). These minerals are reduced products of dissolved uranyl ion in ground water by reducing minerals such as graphite (C) and pyrite (FeS_2). This is the direct evidence of fixation of uranium from ground water by reducing reaction in the natural system.

Hydrological data at Koongarra suggest that complete reduction and fixation of uranyl ion at the transition zone dose not conflict with weathering rate assumed by alteration processes of the host rock. Reduction of uranyl ion by graphite and sulfide minerals may be universal process at the redox front.

Modeling of uranium migration regarding fixation

Based on the observations of alterations of the host rock and distribution of uranium, a model of uranium migration that contains fixation of uranium by secondary minerals was constructed [17,18]. The calculated distribution by the model is well concordant with one-dimensional distribution of uranium in the Koongarra deposit, while conventional sorption model with experimental retardation factors can not reproduce the distribution of uranium (Figure 8). The uranium migration is governed by fixation mechanisms rather than simple adsorption observed in laboratories.

CONCLUSION

The results of the natural analogue studies on the Koongarra deposit revealed important information on radionuclide migration, especially distribution and fixation mechanisms of uranium in nature. We observed evidences of uranium migration and fixation in near surface condition. Coupling of mineralogical observation with measurement of uranium series disequilibrium has possibility to provide us constraint on migration rates of uranium in nature. Observation of natural analogue sites can provide us not only direct contribution to the performance assessment of the particular

scenario on the nuclear waste disposal, but also securities for various natural systems through general understanding of geological processes.

References

1. Snelling, A. A. (1992): ARAP Final Report, Vol. 2, Geological setting, DOE/HMI/PR/92/072, p. 118, Australian Nuclear Science and Technology Organisation.

2. Snelling, A. A. (1980): Uraninite and its alteration products, Koongarra uranium deposit. In: Ferguson, J. and Goleby, A. B. (ed.) *Uranium in the Pine Creek Geosyncline*, IAEA, Vienna, pp. 487-498.

3. Yanase, N, Nightingale, T., Payne, T. E. and Duerden P. : Uranium distribution in mineral phases of rock by sequential extraction procedure. *Radiochimica Acta*, **52/53**, 387-393. (1991).

4. Yanase, N. and Sekine, K. : Measurement of uranium series radionuclides in rock and groundwater at the Koongarra ore deposit, Australia, by gamma spectrometry, *Sci. Basis for Nucl. Waste Manag. XVIII*. Mater. Res. Soc. Symp.Proc., **353**, 1235-1242. (1995).

5. Murakami, T., Isobe, H. and Edis, R.: Effects of chlorite alteration on uranium redistribution in Koongarra, Australia., *Sci. Basis for Nucl. Waste Manag. XIV* Mater. Res. Soc. Symp.Proc., **212**, 741-748. (1991)

6. Murakami, T., Isobe, H., Nagano T. and Nakashima, S.: Uranium redistribution and fixation during chlorite weathering at Koongarra, Australia, *Sci. Basis for Nucl. Waste Manag. XV* Mater. Res. Soc. Symp. Proc., **257**, 473-480. (1992)

7. Murakami, T., Isobe, H., Ohnuki, T., Yanase, N., Sato, T., Kimura, H., Sekine, K., Edis, R., Koppi, A.J., Klessa, D.A., Coneley, C., Nagano, T., Nakashima, S. and Ewing, R.C.: Weathering and its effects on uranium redistribution, *Alligator Rivers Analogue Project Final Report*, Vol. 9, p138. (1993)

8. Murakami, T., Ohnuki, T., Isobe, H., Sato, T., Yanase, N. and Kimura, H.: Significance of the effect of mineral alteration on nuclide migration, *Sci. Basis for Nucl. Waste Manag. XVII* Mater. Res. Soc. Symp.Proc., **333**, 645-652. (1994)

9. Murakami, T., Isobe, H., Sato, T. and Ohnuki, T.: Weathering of chlorite in a quartz-chlorite schist: I. Mineralogical and chemical changes, *Clays Clay Miner.*, **44**, 244-256. (1996).

10. Murakami, T., Tsuzuki, T., Sato, T., Isobe, H. and Ohnuki, T.: Uranium fixation during uranium migration under an oxidizing condition, *Sci. Basis for Nucl. Waste Manag. XVIII*. Mater. Res. Soc. Symp.Proc., **353**, 1219-1226. (1995).

11. Murakami, T., Ohnuki, T., Isobe, H., and Sato, T.: Mobility of uranium during weathring, *American Mineralogist*, **82**, 888-899 (1997)

12. Sato, T., Murakami, T., Yanase, N., Isobe, H., Payne, T. E. and Airey, P. L.: Iron nodules scavenging uranium from groundwater, *Environmental Science and Technology*, **31**, 2854-2858 (1997).

13. Isobe, H. Murakami, T. and Ewing, R.C.: Alteration of uranium minerals in the Koongarra deposit, Australia: Unweathered zone, *J. Nucl. Mater.* **190**, 174-187. (1992).

14. Isobe, H., Ewing, R.C. and Murakami, T.: Formation of secondary uranium minerals in the Koongarra deposit, Australia, *Sci. Basis for Nucl. Waste Manag. XVII* Mater. Res. Soc. Symp.Proc., **333**, 653-660. (1994)

15. Murakami, T., Isobe, H., Ohnuki, T., Sato, T., Yanase, N. and Kiyoshige, J.: Mechanism of saléeite formation at the Koongarra secondary ore body, *Sci. Basis for Nucl. Waste Manag. XIX.* Mater. Res. Soc. Symp.Proc., **412**, 809-816. (1996).

16. Isobe, H., Ohnuki, T. and Murakami, T. : The fixation of uranium from ground water by redox reaction at the redox front, Abstract for Migration 97, Sendai, Japan, 95, (1997).

17. Ohnuki, T., Murakami, T., Isobe, H., Sato, T. and Yanase, N.: Modelling study on uranium migration in rocks under weathering condition, *Sci. Basis for Nucl. Waste Manag. XVIII.* Mater. Res. Soc. Symp.Proc., **353**, 1227-1234. (1995).

18. Ohnuki, T., Murakami, T. and Isobe, H.: Retardation mechanism of uranium migration at Koongarra, Australia, Abstract for Sci. Basis for Nucl. Waste Manag. XXI, Davos, Switzerland, 357-258, (1997).
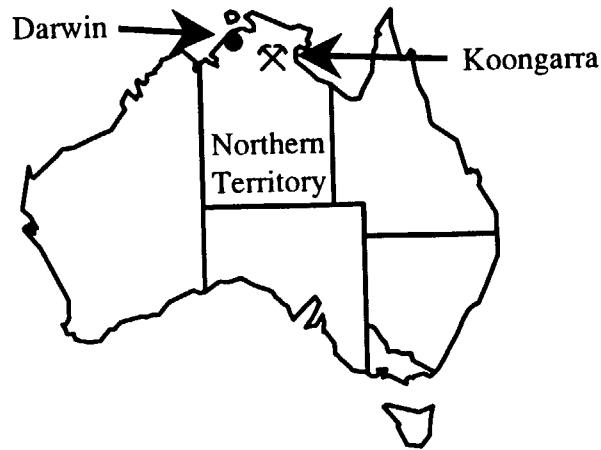
Fig. 1 Location of the Koongarra deposit.
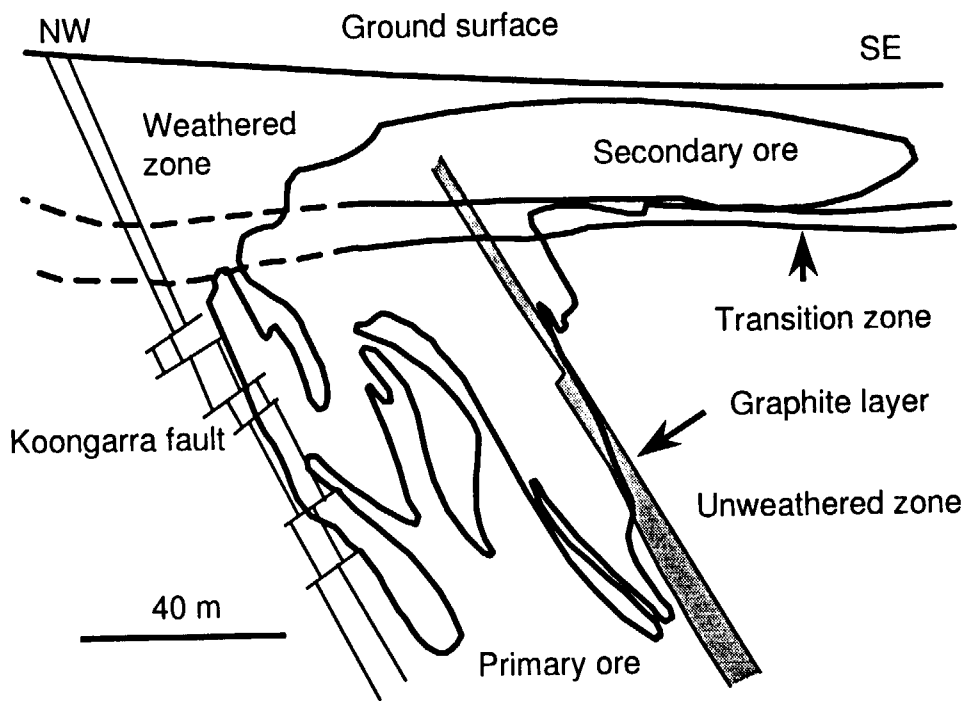
Figure 2   Schematic vertical cross section of the Koongarra deposit (NW-SE) modified after Snelling (1980). Ground water flow from NW to SE formed the secondary ore as a dispersion fan.

Morgan's (adsorbed, carbonate)
TAO (amorphous Fe, secondary U minerals)
CDB (crystalline Fe minerals)
6 M HCl (clay, U oxides)
Fusion (residual minerals)

Primary ore body

U extracted (%)

80
60
40
20
0

DDH1, 19.4-20.5   DDH2, 33.0-34.3
Drill hole and depth (m)

Secondary ore body

U extracted (%)

100
80
60
40
20
0

DDH1, 4.7   DDH3, 16.3-17.5   DDH4, 14.0-15.2
Drill hole and depth (m)
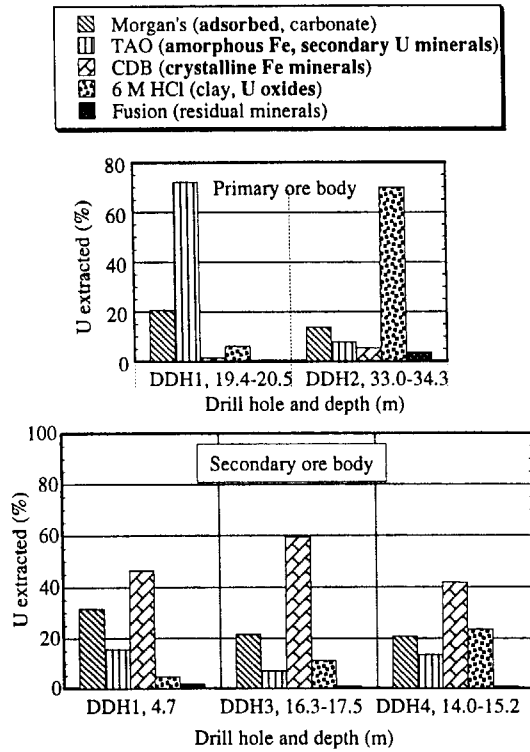
Figure 3   Fraction of uranium extracted by sequential extraction technique

oxidation
primary uraninite ⟶

uranyl lead oxide
curite,
wölsendorfite

Pb enrich

Si, Mg ⟶

uranyl Mg silicate   uranyl Pb silicate
sklodowskite ⟷ kasolite

radiogenic Pb

*reduction by graphite and
pyrite at the transition zone*
secondary uraninite

secondary ore

uranyl Mg phosphate
saléeite

*replacing apatite and sklodowskite
micro crystals in iron minerals*
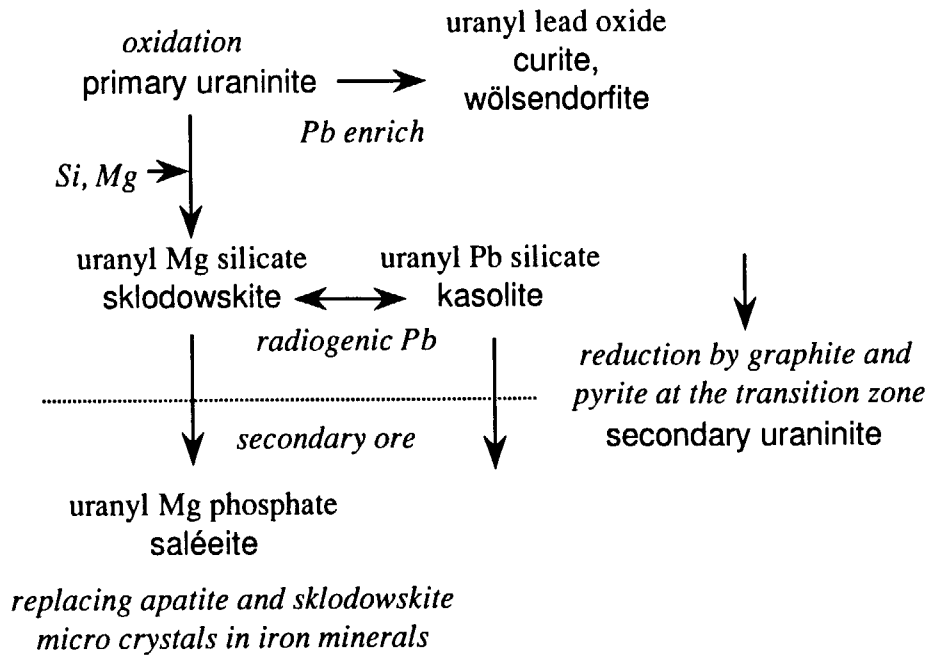
Figure 4 Schematic alteration path of chlorite weathering.

Figure 5　Sample of the primary ore body. Uraninite (U) is surrounded by curite (C), and sklodowskite (Sk) veins.

Chlorite
$(Mg_{2.24}Fe^{2+}_{2.61}Al_{1.214})(Si_{2.89}Al_{1.11})O_{10}(OH)_8$

$\longrightarrow$ Mg^{2+}, Ferrihydrite

Vermiculite
$(Mg_{1.36}Fe^{3+}_{0.95}Al_{0.64})(Si_{2.89}Al_{1.11})O_{10}(OH)_2$

$\longrightarrow$ Mg^{2+}, Si^{4+}, Ferrihydrite

Kaolinite $Al_2Si_2O_5(OH)_4$ (ideal)
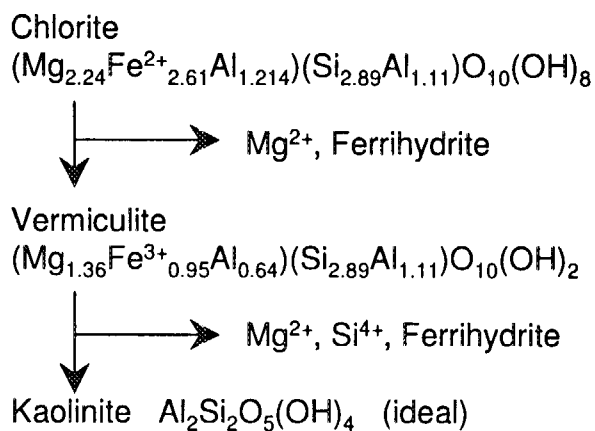
Figure 6　Schematic alteration path of uranium minerals in the Koongarra deposit. uranium and lead are retained in the system.
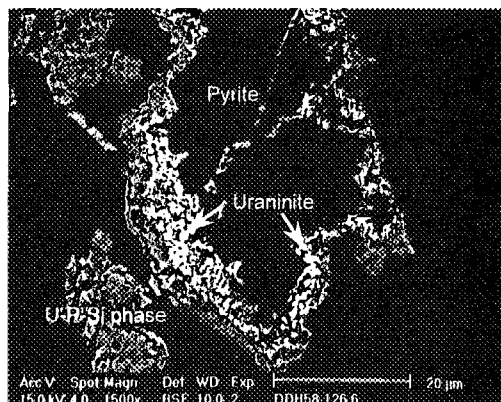
Figure 7　SEM image of pyrite in the transition zone. Layer of U-P-Si mineral with submicron uraninite grains occurs around pyrite.
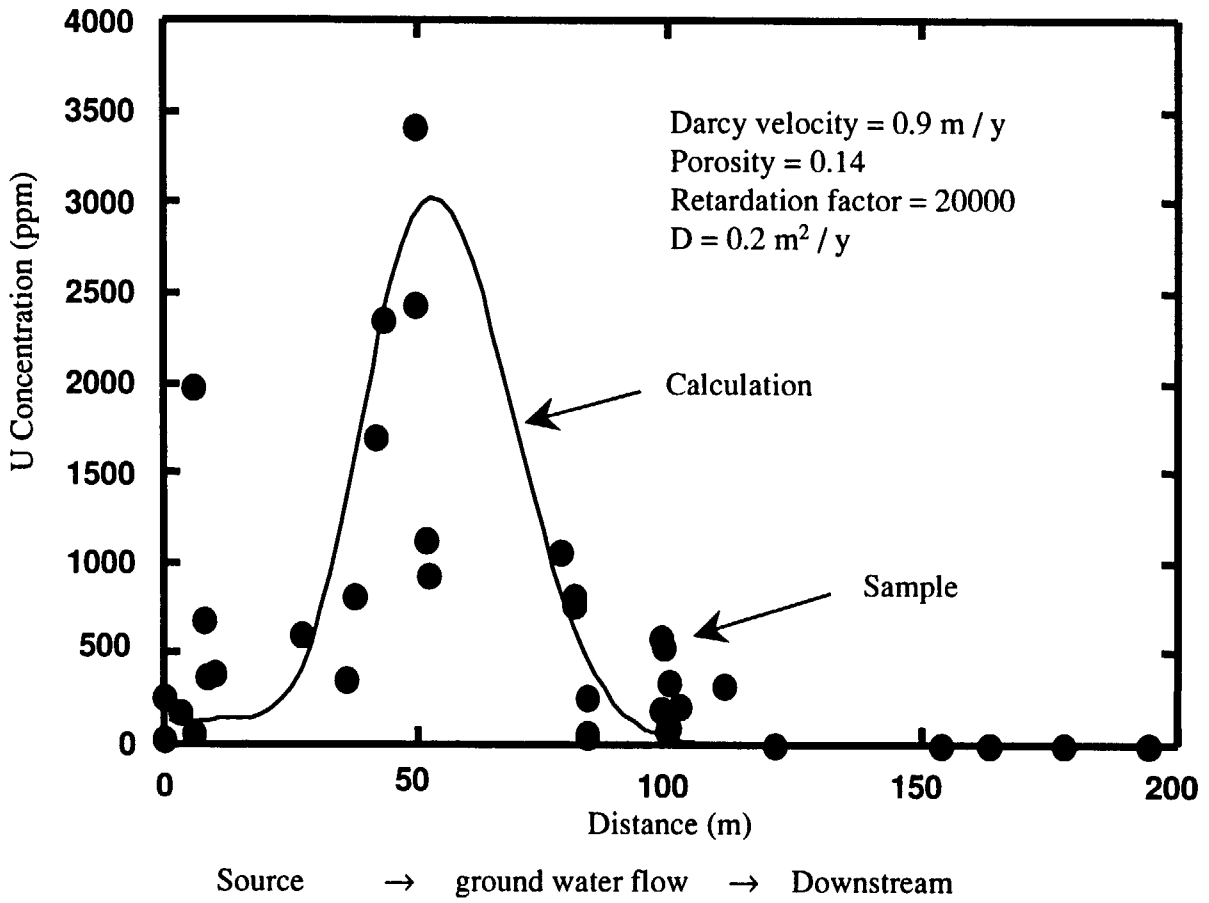
Figure 8   Comparison of calculated uranium concentration with observed ones.   The most fitted calculation (shown here) needs retardation factor more than 20 times higher than that is obtained by laboratory experiments on the media.

3.6 Iron Nodules with High Uranium Retention Capacity and the Retention Mechanisms

Tsutomu Sato*, Takashi Murakami[2], Nobuyuki Yanase[1], Hiroshi Isobe[1],
Timothy E. Payne[3], and Peter L. Airey[3]

[1] Department of Environmental Safety Research, Japan Atomic Energy Research
Institute, Tokai, Ibaraki 319-11, Japan
[2] Mineralogical Institute, University of Tokyo, Bunkyo-ku, Tokyo 113, Japan
[3] Australian Nuclear Science and Technology Organisation, PMB 1, Menai, NSW 2234,
Australia

Introduction

Under oxidizing conditions, uranium (U) is much more mobile in the environment than it is in reducing conditions. However, the mobility of dissolved U in groundwater can be retarded by precipitation of U-bearing materials and, particularly at low U concentrations, by adsorption to various geomaterials. For the modeling of U transport, it is important to determine the relative importance of these two mechanisms. Numerous studies have reported that U is generally associated with iron (Fe)-oxides, hydroxides and oxyhydroxides (hereafter grouped generically as Fe-oxides) in the subsurface environment (1-13). An understanding of the interaction between U and Fe-oxides is therefore important for assessing the retardation capacity of geological systems into which U may be disposed, such as U mine waste dumps and radioactive waste repositories. Although most of the previous studies have emphasized the importance of Fe-phases in adsorption of U, less attention has been paid to their capacity for U uptake, and to the post-adsorption behavior of U in Fe-oxides.

The Koongarra U ore deposit in Australia, from which U has been mobilized by water-rock interactions in the past 1-3 million years (14, 15), is a suitable site to follow the fate of U in circumstances where groundwater U concentrations are relatively high. At Koongarra, both re-precipitation of mobilized U as secondary minerals and association of U with Fe-oxides are observed (14). Here we focus on the U associated with Fe-oxides and report on: (i) the extent to which U has accumulated in the various types of Fe-oxides (fissure fillings, clay coatings, and nodules), and (ii) the chemical form of U associated with Fe-nodules.

Sampling Sites and Experimental

The Koongarra uranium deposit lies about 225 km east of Darwin in the Northern Territory of Australia. As a result of the leaching of the primary ore zone and transport of U by groundwater, a tongue-like "dispersion fan", a region of ore-grade material has formed in the most recent 1-3 million years (Figure 1). Within the primary ore zone, uranyl silicates (sklodowskite) have been produced by in-situ oxidation and alteration. The secondary mineralization in the zone above the primary ore is characterized by uranyl phosphates (saléeite), which are frequently found as aggregates observable with the naked eye. The weathering of uraninite to secondary U-bearing minerals has occurred concurrently with alteration of chlorite $((Mg, Fe, Al)_6(Al, Si)_4O_{10}(OH)_8)$ to clays and iron oxides. Downstream of the primary ore-zone, the U is associated with weathering products, especially the Fe-oxides in the dispersed ore zone *(4, 10-13)*.

The rock samples used in this study were collected from diamond-drill cores (DDH) drilled at an angle of about 50° from the horizontal to facilitate core recovery and intersect strata. The samples were collected at intervals of three meters in depth (from 3 to 30 meters) and analyzed mineralogically and radiochemically.

Polished thin sections of the samples were examined by optical microscopy, followed by scanning electron microscopy (SEM) with energy dispersive X-ray analysis (EDX), analytical electron microscopy (AEM), micro-infrared and visible (micro-IR and VIS) spectroscopies to identify the mineral species and to examine the textures of the samples. For quantitative element analysis, the EDX spectra were collected for 200 seconds at an operating voltage of 20 kV and a beam current of 0.1 nA. The analyses were corrected for matrix effects (atomic number, absorption and fluorescence) using a standard routine. Powdered bulk samples were examined by gamma spectrometry to measure the uranium contents (see *(16)* for further details).

Results and Discussion

Previous mineralogical studies at Koongarra have shown that goethite (α-FeOOH), hematite (α-Fe$_2$O$_3$) and ferrihydrite (Fe$_5$HO$_8$·4H$_2$O) are the major Fe-minerals in the weathered zone *(11-13)*. Sub-micrometer sized grains of Fe-oxides are found at domain boundaries, and larger accumulations are located within grain boundaries, fissures and the voids produced during mineral dissolution. The accumulated Fe-minerals occur in particular morphological features such as fissure fillings, dispersed clay coatings and nodules. Most of the Fe-nodules are surrounded by kaolinite (Al$_2$Si$_2$O$_5$(OH)$_4$), a weathering product of the host rock. The U distribution is controlled by the mineralogy; the Fe-nodules contain high concentrations of U, whereas the kaolinite has virtually no

U (Figure 2).

Quantitative analysis of the Fe-oxides by SEM/EDX shows that there is a considerable variation in the amount of U associated with each form of Fe-oxide. The nodules usually have high U contents (up to approximately 8 wt. % as UO_3) compared to the other Fe-forms (Table 1). Fe-oxides are ubiquitous in the dispersion fan, and also the surrounding weathered rocks. However, Fe-nodules are restricted to the center of the dispersion fan (Figure 1), which is also an area of high U content. The U in the groundwater is only 10-100 ppb in the vicinity of secondary ore deposit (13, 17), and is undersaturated with respect to the U minerals which are present (18). The high U content of the solid phase in the center of dispersion fan is therefore largely attributable to the U-rich Fe-nodules. This suggests that the Fe-nodules play a key role in the scavenging and retention of U downgradient of the secondary ore zone, where no uranyl silicates and phosphates have been observed.

Within the Fe-nodules, the U content is variable and is related to the color of Fe-materials. It is greatest in the yellow zones, then decreasingly found in the orange, brown, and black zones (Table 1). Micro-IR and VIS spectroscopies showed that the yellow material is goethite and the black zone contains an amorphous Fe-material (probably ferrihydrite). The brown and orange zones are probably intermediate phases, and include a small amount of hematite. The order of decreasing U-content therefore corresponds to the order of decreasing crystallinity of the Fe-oxides. Generally, amorphous Fe-oxides, precursor materials of crystalline Fe-oxides, have a higher adsorption capacity than the crystalline phases due to their larger specific surface areas, as shown by the enrichment factors for U adsorption under the same experimental conditions (e.g., amorphous Fe-oxides; 1.1-2.7×10^6, natural goethite; 4×10^3) (4). However, at Koongarra, the goethite in the nodules has a higher U content than the amorphous Fe-oxides in the coatings and fissures (Table 1). This result suggests that the U enrichment in the goethite cannot be explained by adsorption alone.

The SEM/EDS examination showed that the U-rich Fe-nodules contain aluminum, silicon, phosphorus (P), copper (Cu), and occasionally magnesium, titanium, vanadium, chromium, manganese, and nickel. Of these elements, the U content of the nodules is positively correlated only with P and Cu (Figure 3), suggesting the formation of a phase containing these elements.

In common with uranyl, phosphate and Cu ions are strongly adsorbed on Fe-oxides (19-27). The uptake of phosphate generally induces an increase in the cation exchange capacity by the creation of additional negative charge. However, Cu ions compete against uranyl ions in adsorption, therefore, the presence of Cu may interfere

with U adsorption on Fe-oxides. The positive correlation of U content with both Cu and P in the Fe-nodules suggests that the U retention may be due to precipitation rather than adsorption, possibly as copper uranyl phosphate, i.e., torbernite or metatorbernite $(Cu(UO_2)_2(PO_4)_2 \cdot 8\text{-}12H_2O)$.

In order to observe the U-bearing phases, Fe-nodules in sample DDH60 15.2m were examined further by AEM which has a superior spatial resolution to SEM/EDX. Although phases containing only U, P and Cu were not detected, scattered domains (about 20 nm) with high U, P and Cu were observed in the matrices of the large Fe-oxide particles. This observation strongly indicates that U associated with P and Cu was not only adsorbed on the surfaces of the individual Fe-particles, but incorporated as microcrystalline torbernite or metatorbernite scattered in the matrices of the Fe-oxides.

Saléeite $(Mg(UO_2)_2(PO_4)_2 \cdot 8\text{-}10H2O)$ is present at the upstream edge of the secondary ore deposit (Figure 1), as visible crystals which are not associated with iron minerals. In this region close to the primary ore-body, U concentrations in the groundwater are relatively high, and the Mg concentrations greatly exceed those of other cations due to the weathering of Mg-rich chlorite. Phosphate concentrations are also relatively high close to the primary ore-zone (13). Consequently, the saléeite appears to have formed by direct precipitation, which is a different mechanism to that proposed for the formation of torbernite or metatorbernite within the Fe-nodules. Fe-oxides strongly bind Cu, P and U in the circumneutral pH range (19-27), whereas adsorption of Mg is weaker and occurs in the pH range above 7 (28). Consequently, when the contacting groundwater contains Cu, the microcrystalline phase forming within the Fe-nodules is a copper uranyl phosphate mineral rather than a Mg-containing phase such as saléeite. Although the contacting groundwater is currently undersaturated with respect to torbernite or metatorbernite, several experimental and theoretical studies have shown that the surface of various oxides may induce precipitation when the bulk solution is still undersaturated with respect to the precipitated phase (29, 30). The precipitation of torbernite or metatorbernite in the Fe-nodules would be consistent with these results.

Textural relationships in the samples suggest that the crystalline Fe-minerals in the nodules result from conversion of the amorphous materials. As mentioned above, most of the Fe-nodules we observed were surrounded by kaolinite (Figure 2). The peripheral kaolinite appears to play an important role in producing the physico/chemical conditions conducive to this conversion. Further work is required to elucidate the mechanism of the development of Fe-nodules, and to study the role of the peripheral kaolinite.

In this paper, we have shown that the Fe-nodules are important in immobilizing U in the Koongarra dispersion fan. In previous studies of the association between U and Fe-oxides, the reported levels of U scavenged by Fe-oxides are commonly in the ppm range *(3, 31)* but occasionally approach 0.1 to 1 percent *(5, 8)* under environmental conditions. The Fe-nodules at Koongarra, with approximately 8% of U, therefore have a remarkably high scavenging capacity, even allowing for the large amount of uranium available by weathering of the primary U ore. The ability of the Fe-nodules to enrich U (10^6 times higher than the groundwater) is also very high. The enrichment factor of the Fe-nodules exceeds those of other natural scavengers such as micro-organisms (10^3 times) *(32)*, marine ferro-manganese nodules (10^3 times) *(3, 31)*, and suspended particulates in river (10^3-10^5 times) *(33)*.

The initial interaction of U with Fe-oxides is probably by adsorption, but there is a subsequent mineralization process leading to the formation of U-bearing phases with very high U contents in the Fe-nodules. This post-adsorption process occurs during aging and conversion of Fe-oxides. This process is an important immobilization mechanism leading to the long-term retardation of U in the system. In the absence of these processes occurring in the weathered zone of Koongarra, the U would have presumably been dispersed much more widely. Many previous studies have focused on the types and amounts of adsorbing materials for radionuclide immobilization in geological systems. This study illustrates that, even if all possible sorbing phases are considered, long-term predictions as to the fate of U are incomplete without an understanding of post adsorption processes related to evolution of the associated materials over the long-term.

Acknowledgment

Literature Cited

(1) Koons, R.D.; Helmke, P.A.; Jackson, M.L. *Soil Sci. Soc. Am. J.* **1980**, *44*, 155-159.

(2) Gueniot, B.; Guillet, B.; Souchier, B. *C.R.Acad.Sci. Ser. 2* **1982**, *251*, 31-36.

(3) Kunzendorf, H.; Glasby, G.P.; Plüger, W.L.; Friedrich, G.H. *Uranium* **1982**, *1*, 19-36.

(4) Gray, D.J. Ph.D. Dissertation, University of Sydney, 1986.

(5) Guthrie, V.A.; Kleeman, J.D. *Chem. Geol.* **1986**, *54*, 113-126.

(6) Smellie, J.A.T.; MacKenzie, A.B.; Scott, R.D. *Chem. Geol.* **1986**, *55*, 233-254.

(7) Zielinski, R.A.; Bush, C.A.; Spengler, R.W.; Szabo, B.J. *Uranium* **1986**, *2*, 361-386.

(8) Ilani, S.; Kronfeld, J.; Pinchasov, A. *Uranium* **1987**, *4*, 159-174.

(9) Milton, G.M.; Brown, R.M. *Can. J. Earth Sci.* **1987**, *24*, 1321-1328.

(10) Yanase, N.; Nightingale, T.; Payne, T.E.; Duerden, P. *Radiochim. Acta* **1991**, *52/53*, 387-393.

(11) Edis, R. et al. *Alligator Rivers Analogue Project Final Report*, Vol. 8 ISBN 0-642-59934-3, Sydney, 1992.

(12) Murakami, T. et al. *Alligator Rivers Analogue Project Final Report*, Vol. 9 ISBN 0-642-59935-1, Sydney, 1992.

(13) Payne, T.E. et al. *Alligator Rivers Analogue Project Final Report*, Vol. 7 ISBN 0-642-59933-5, Sydney, 1992.

(14) Snelling, A.A. *Alligator Rivers Analogue Project Final Report*, Vol. 2 ISBN 0-642-59928-9, Sydney, 1992.

(15) Airey, P.L. *Chem. Geol.* **1986**, *55*, 255-268.

(16) Yanase, N.; Sekine, K. Mat. Res. Soc. Symp. Proc. *353*; Mat. Res. Soc. **1995**, 1235-1242.

(17) Yanase, N.; Payne, T.E.; Sekine, K. *Geochem J* **1995**, *29*, 1-29.

(18) Sverjensky, D.A. *Alligator Rivers Analogue Project Final Report*, Vol. 12 ISBN 0-642-59938-6, Sydney, 1992.

(19) Hingston, D.D.; Atkinson, R.J.; Posner, A.M.; Quirk, J.P. *Trans. Int. Congr. Soil Sci., 9th* **1968**, I, 669-678.

(20) Atkinson, R.J.; Posner, A.M.; Quirk, J.P.J. *Inorg. Nucl. Chem.* **1972**, *34*, 2201-2209.

(21) Russell, J.D.; Parfitt, R.L.; Fraser, A.R.; Farmer, V.C. *Nature* **1974**, *248*, 220-221.

(22) MacKenzie, R.M. *Aust. J. Soil Res.* **1980**, *18*, 61-73.

(23) Sigg, L.; Stumm, W. *Colloids Surf.* **1981**, *2*, 101-117.

(24) Padmanabham, M. *Aust. J. Soil Res.* **1983**, *21*, 309-320.

(25) Padmanabham, M. *Aust. J. Soil Res.* **1983**, *21*, 515-525.

(26) Dzombak, D.A.; Morel, F.M.M. Surface complexation modeling, John Wiley & Sons, New York 1990.

(27) Payne, T.E.; Davis, J.A; Waite, T.D. Radiochim. Acta 1996, *74*, 239-243.

(28) Balistrieri and Murray, Am. J. Sci. **1981**, *281*, 788-806.

(29) James, R.O.; Healy, T.W. *J. Colloid Interface Sci.* **1972**, *40*, 42-52.

(30) James, R.O.; Healy, T.W. *J. Colloid Interface Sci.* **1972**, *40*, 65-81.

(31) Huh, C.A.; Ku, T.L. *Geochim. Cosmochim. Acta* **1984**, *48*, 951-963.

(32) Strandberg, G.W.; Shumate, S.T.; Parrott, J.R.J. *Appl. Environ. Microbiol.* **1981**, *41*, 237-245.

(33) Mann, H.; Fyfe, W.S. *Uranium* **1987**, *4*, 175-192.

Table 1 Comparison of uranium contents among various iron forms.

Iron forms	Nodules							Coatings			Fissures	
DDH No.	58			60			87	58			60	
Depth [m]	18.2			15.2			15.2	12.1			15.2	12.1
U in bulk [ppm]*	4543			2172			773	1688			2172	1173
Measuring point[†]	1	2	3	4	5	6	NS	7	8	9	NS	NS
UO_3 [wt%][‡]	1.9	4.3	7.7	2.4	2.9	4.6	1.6	0.7	0.5	0.6	0.5	ND
Color	Br	O	Y	RBr	RBr	O	RBr	Bk	Bk	Bk	Bk	Bk

*: Uranium contents of bulk samples were measured by gamma-spectrometry. †: Measuring points are shown by corresponding numbers in figure 2. ‡: Uranium contents were measured by SEM/EDX. These values are weight percentages of UO_3. Key: DDH No. = diamond drill hole number; NS = position not shown in figure 2; ND = not detected; Br, brown; O, orange; Y, yellow; Rbr, reddish brown; and Bk, black.
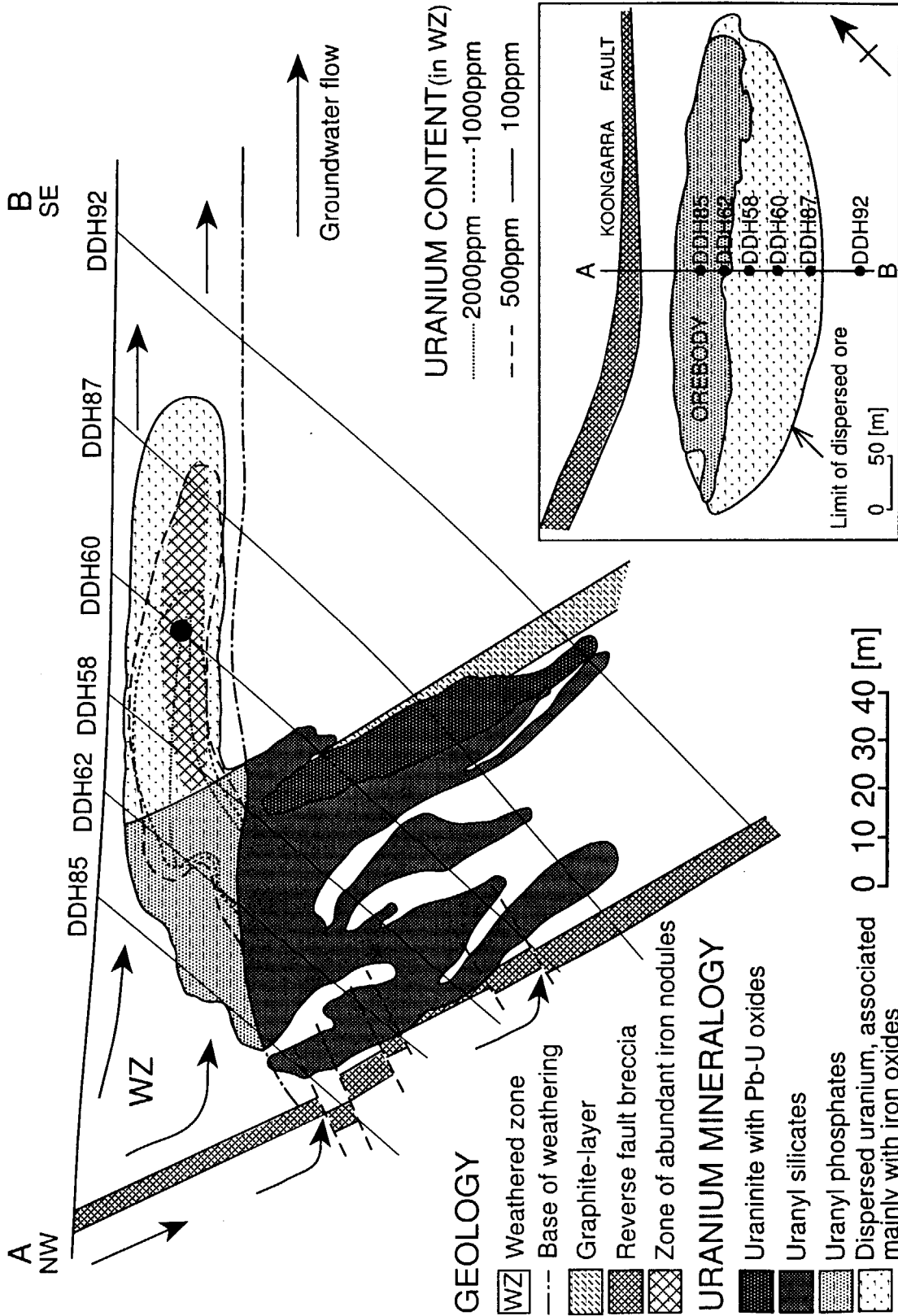
Figure 1 Cross-section of the Koongarra orebody showing the geology, distribution of uranium minerals, zone of abundant iron nodules, and contours of uranium contents in weathered bulk samples. The insert in the bottom right-hand corner shows locations of the holes from which the samples were collected (plan view).
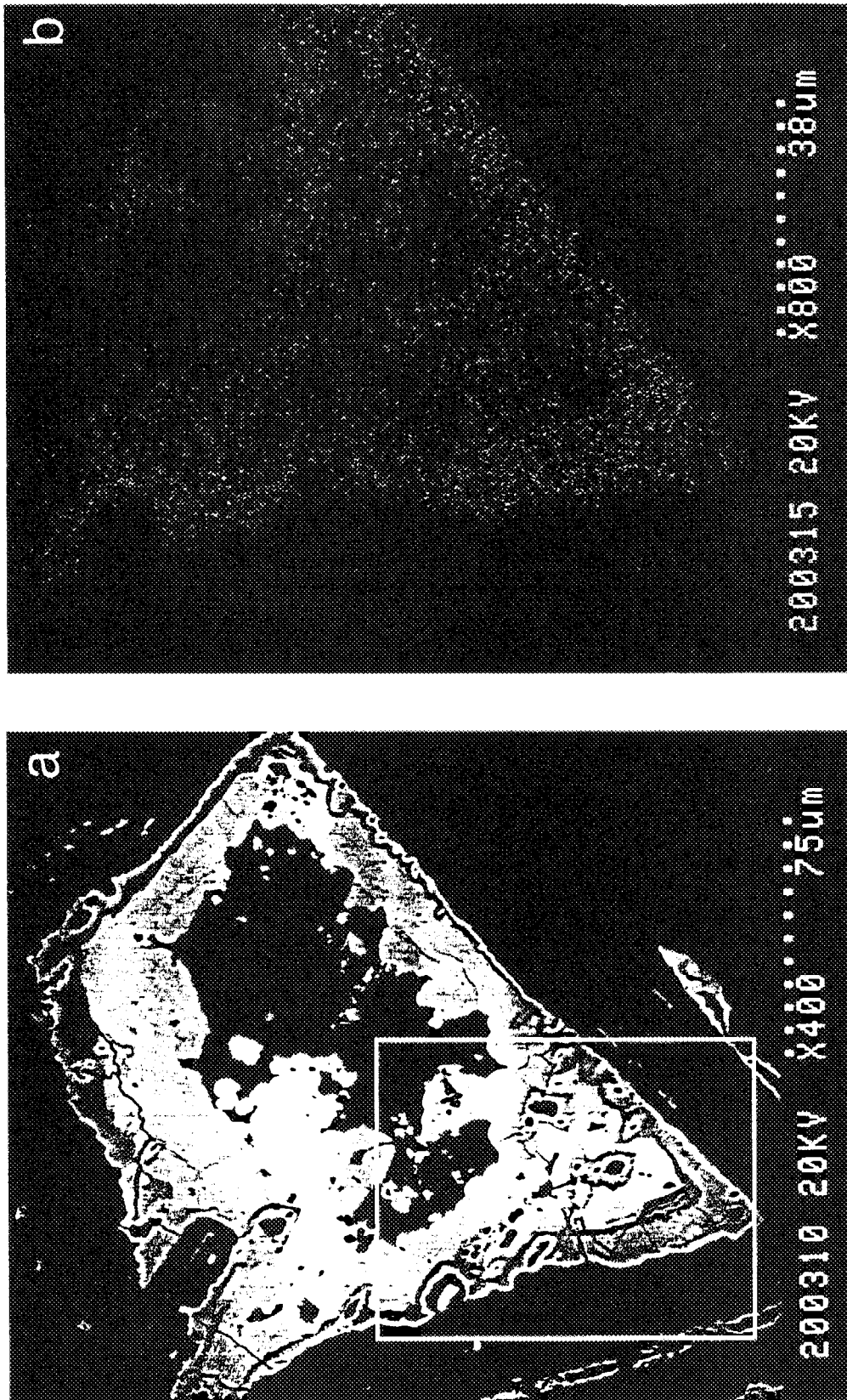
Figure 2 Backscattered electron (BSE) image (a) and X-ray map of uranium (b) of iron nodules from DDH58 18.2m. White and black areas in the BSE image correspond with Fe-minerals and kaolinites, respectively. The X-ray map was obtained by wavelength dispersive spectrometry from the enclosed area with a rectangle in BSE image. The regions of higher uranium content correspond with a higher density of dots in the X-ray map.
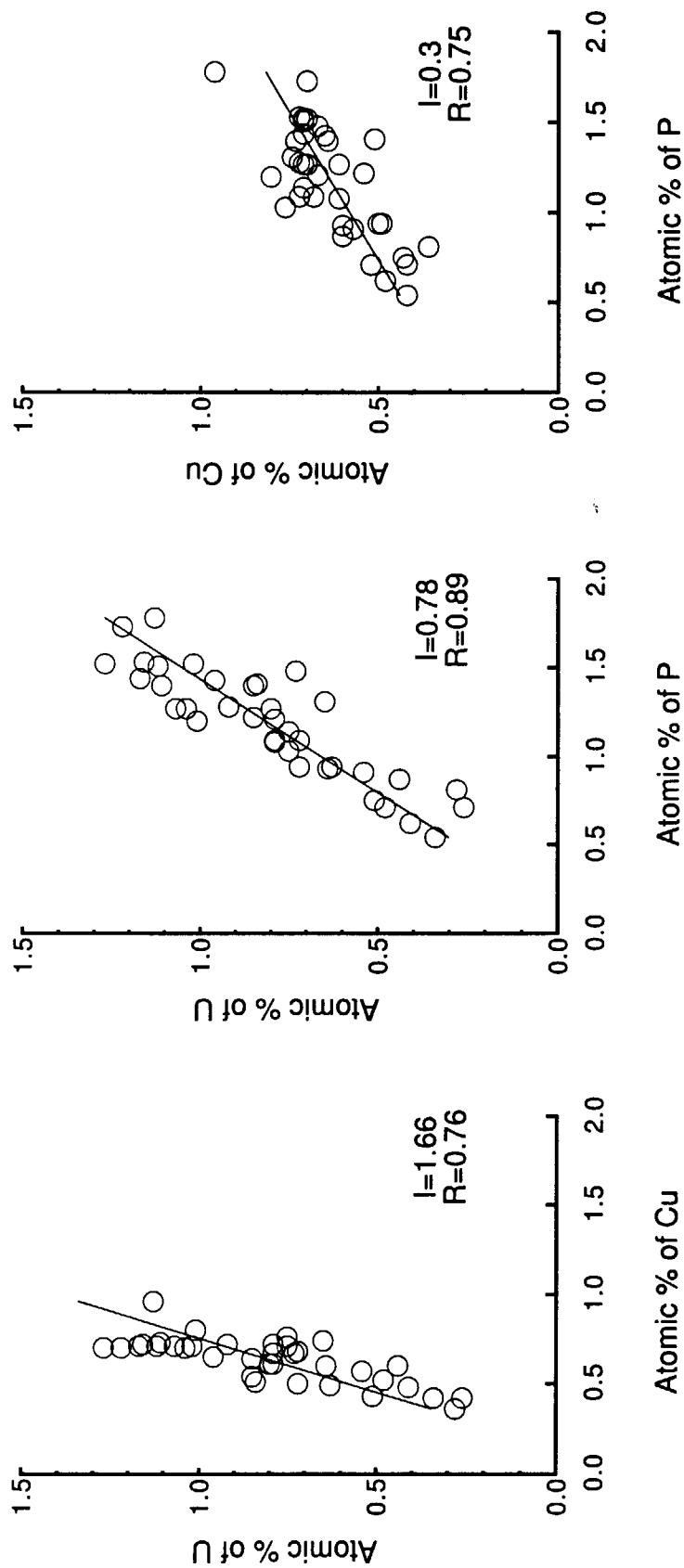
Figure 3 Relationships between atomic percentage of uranium (U) and copper (Cu), U and phosphorus (P), and Cu and P in the iron nodules of DDH58 18.2m. The atomic percentages of each element were measured by SEM/EDX. The values of I and R in each figure are the inclination and the coefficient of correlation of fitting line, respectively. Each of the correlations shown in the figure is significant at the $p < 0.001$ level. There were no significant correlations observed between any other elements contained in the Fe-nodules.

3.7 CARBON AGE OF THE GROUNDWATER

M.Kumata, J.Shimada[4] and T.Nakamura[5]

INTRODUCTION

Some times the concept of groundwater age has little significant. However, differences in apparent ages between two sampling points A and B in a homogeneous aquifer make it possible to obtain an idea of the flow rates along the direction A to B.

Carbon-14, the long-lived carbon isotope, has a half-life of 5730 ± 30 years. ^{14}C is produced naturally in the upper atmosphere by secondary neutrons from cosmic-ray interaction with ^{14}N in the $^{14}N(n,p)^{14}C$ reaction. Free ^{14}C rapidly reacts with O_2 to form CO_2 and enters the carbon cycle.

Since the isotopic ratio of $^{12}C : ^{13}C : ^{14}C$ in the atmosphere is $0.989 : 0.011 : 1.2 \times 10^{-12}$, a 50 to 100 liter water sample was required for measurement of ^{14}C activity in groundwater by using gas-proportional counting or liquid scintillation counting[1]. ^{14}C in groundwater is sampled by removing all carbon species from by precipitating them in alkaline media. Tandem accelerators have recently been used to measure ^{14}C concentrations directly by mass spectrometer. A great advantage of accelerator techniques is the very small sample size needed - about 100 mL water of a few milligrams of carbon.

^{14}C activities in the groundwaters sampled from a stydy area were measured by using Tandetron AMS for groundwater age determination.

STUDY AREA

The study area is located in the northern part of Kanto area at central part of Japan. This area is geographically an alluvial fan of Daiya river. Since groundwater flow is active in an alluvial fan, and a large groundwater movement is expected in the basement rock, this area was selected for one of the deep groundwater flow study area.

Basement rock of this area is constituted of tertiary rocks of rhyolite, andesite and tuff. Alluvial sediments are consisted of mainly sand and gravel layers. The surface is widely covered by tephra with pumice, scoria and volcanic ash.

Groundwater were sampled from two deep boreholes drilled into the basement. A borehole named IMHS have been drilled at around the top of the fan, and the other borehole named IMOS have been drilled at close to the end of the fan. The depth of the boreholes are 205 m and 207 m

---

[4] Tsukuba University

[5] Nagoya University

respectively. The distance of two boreholes is about 12 km. Five different depth are selected for each borehole to take deep groundwater in the basement rock.

GROUNDWATER SAMPLE

Since about 30 liters of dead volume was in the groundwater sampling system, about 100 liters of groundwater were taken from the basement rock and wasted before one liter or 200 ml of sample for ^{14}C measurements at each sampling point. Accordingly, ten groundwater samples were taken from the basement rock from these two boreholes. Additionally, for the comparison, one groundwater sample from gravel layer lying on the basement rock was taken from each borehole. In case of 1 liter sampling, samples were carried to laboratory to obtain ^{14}C as $SrCO_3$ precipitation. Then about a 200 ml sample was separated to a flask from the one liter polyethren bottle in a grove box under carbon free conditions. After that a 5 ml $SrCl_2$ solution was added to the groundwater sample in the flask. The flask was kept in the grove box under carbon free conditions about 3 days. In case of 200 ml sampling, the strontium solution was added immediately into the groundwater sample in-situ and bottle neck was sealed tightly. After that precipitations in the flask was selected by wasting the head of the solution. Then 5 ml phosphoric acid was poured into the precipitation under vacuum conditions. Generated gas phase, CO_2, was purified and yield was measured. The CO_2 gas was reduced by hydrogen to obtain carbon on the surfaces of pure iron powder as targets of AMS. ^{14}C content was measure on this targets by the accelerator mass spectrometer at Nagoya University.

^{14}C AGE OF GROUNDWATER

The time function is provided by the radioactive decay of a radioactive isotope according to the low of radioactivity:

$$t = \frac{\tau}{\ln 2} \ln \frac{A_0}{A}$$

where A is the ^{14}C activity of the sample,

A0 is the initial ^{14}C activity of a standard

τ is the half-life of ^{14}C (5730 · 40a).

The results are shown in Table 1. There are three data set. Each data set consists of ^{14}C age of groundwater sample taken from boreholes A(IMOS) and B(IMHS). In each data set, ^{14}C age of groundwater from basement rock in borehole B showed 3000~7000 a. On the other hand, at the borehole A, ^{14}C age of groundwater of basement rock showed 1300~2100 except the third data set.

All deep groundwater sampled from the borehole A showed relatively younger than the deep groundwater from borehole B.

In case of the third sampling, borehole A have been opened for shallow land groundwater for about one year. Since groundwater potential in the basement rock is slightly smaller than the hydrostatic pressure, deep groundwater was well contaminated by groundwater from shallow land.

Borehole A is located at near the end of the fan, and situated at downstream. Based on the results of ^{14}C age of groundwater, not simple but complex groundwater flow was suggested between two boreholes in the basement rock. Further investivations are under going.

REFERENCE
(1) M.A.Geyh and H.Schleicher, Springer-Verlag, (1990).

Table 1 Apparent groundwater age in Imaichi area
Boreholes A (IMOS) and B (IMHS)

Data Set No.	Sample No.	Depth(m)	Sampling Date	TDIC* (mmol/l)	δ ^{13}C (permil)	^{14}C-Age
I	IMHS-GR	43.5-49.0	1994/10/20	0.880	-16.2	-
	IMHS-01	99.5-104.2	1995/1/14	1.150	-15.3	4954
	IMHS-02	105.3-110.0	1995/1/15	1.130	-14.7	3462
	IMHS-03	114.0-118.7	1995/1/15	0.930	-13.2	6163
	IMHS-04	126.5-131.2	1995/1/16	0.960	-14.4	3769
	IMHS-05	138.5-143.0	1995/1/22	1.140	-15.3	3756
	IMOS-GR	38.5-44.0	1994/10/29	1.500	-17.4	-
	IMOS-1	89.0-93.7	1995/2/23	1.380	-16.3	222
	IMOS-3	121.0-125.7	1995/2/24	1.230	-16.2	2115
	IMOS-5	195.0-207.0	1995/2/25	1.960	-16.8	1927
II	IMHS-GR	43.5-49.0	1995/8/7	1.027	-18.0	-
	IMHS-01	99.5-104.2	1995/8/10	1.188	-14.3	3713
	IMHS-02	105.3-110.0	1995/8/10	1.129	-14.7	2696
	IMHS-03	114.0-118.7	1995/8/11	0.963	-12.1	5960
	IMHS-04	126.5-131.2	1995/8/11	0.994	-12.6	5247
	IMHS-05	138.5-143.0	1995/8/12	1.091	-13.2	5372
	IMOS-GR	38.5-44.0	1995/8/10	1.603	-19.1	-
	IMOS-01	89.0-93.7	1995/8/6	1.379	-17.6	1315
	IMOS-02	102.0-106.7	1995/8/7	1.329	-16.5	1382
	IMOS-03	121.0-125.7	1995/8/7	1.413	-17.6	1293
	IMOS-04	153.0-157.7	1995/8/8	1.535	-18.6	-
III	IMHS-01	99.5-104.2	1996/8/24	0.970	-12.0	7654
	IMHS-02	105.3-110.0	1996/8/24	0.954	-11.7	5869
	IMHS-03	114.0-118.7	1996/8/25	0.936	-11.4	6493
	IMHS-04	126.5-131.2	1996/8/25	0.938	-11.7	5729
	IMHS-05	138.5-143.0	1996/8/26	0.797	-11.5	6088
	IMOS-01	89.0-93.7	1996/8/21	1.577	-19.0	-
	IMOS-02	102.0-106.7	1996/8/21	1.613	-19.1	-
	IMOS-03	121.0-125.7	1996/8/22	1.486	-18.8	-
	IMOS-04	153.0-157.7	1996/8/22	1.590	-19.1	-
	IMOS-05	202.3-207.0	1996/8/22	1.579	-19.1	-

TDIC* : Total dissolved inorganic carbon.

- : not older than present time.

IMHS-GR (IMOS-GR): Sample taken from the gravel layer laying on the basement rock.

国際単位系 (SI) と換算表

表1　SI基本単位および補助単位

量	名　称	記号
長　　さ	メ ー ト ル	m
質　　量	キ ロ グ ラ ム	kg
時　　間	秒	s
電　　流	ア ン ペ ア	A
熱力学温度	ケ ル ビ ン	K
物 質 量	モ ル	mol
光　　度	カ ン デ ラ	cd
平 面 角	ラ ジ ア ン	rad
立 体 角	ス テ ラ ジ ア ン	sr

表3　固有の名称をもつSI組立単位

量	名　称	記号	他のSI単位による表現
周 波 数	ヘ ル ツ	Hz	s^{-1}
力	ニ ュ ー ト ン	N	$m \cdot kg/s^2$
圧 力, 応 力	パ ス カ ル	Pa	N/m^2
エネルギー, 仕事, 熱量	ジ ュ ー ル	J	$N \cdot m$
工 率, 放 射 束	ワ ッ ト	W	J/s
電 気 量, 電 荷	ク ー ロ ン	C	$A \cdot s$
電位, 電圧, 起電力	ボ ル ト	V	W/A
静 電 容 量	フ ァ ラ ド	F	C/V
電 気 抵 抗	オ ー ム	Ω	V/A
コンダクタンス	ジ ー メ ン ス	S	A/V
磁 束	ウ ェ ー バ	Wb	$V \cdot s$
磁 束 密 度	テ ス ラ	T	Wb/m^2
インダクタンス	ヘ ン リ ー	H	Wb/A
セ ル シ ウ ス 温 度	セルシウス度	℃	
光 束	ル ー メ ン	lm	$cd \cdot sr$
照 度	ル ク ス	lx	lm/m^2
放 射 能	ベ ク レ ル	Bq	s^{-1}
吸 収 線 量	グ レ イ	Gy	J/kg
線 量 当 量	シ ー ベ ル ト	Sv	J/kg

表2　SIと併用される単位

名　称	記　号
分, 時, 日	min, h, d
度, 分, 秒	°, ′, ″
リ ッ ト ル	l, L
ト ン	t
電 子 ボ ル ト	eV
原 子 質 量 単 位	u

$1 \text{ eV} = 1.60218 \times 10^{-19} \text{ J}$

$1 \text{ u} = 1.66054 \times 10^{-27} \text{ kg}$

表4　SIと共に暫定的に維持される単位

名　称	記　号
オングストローム	Å
バ ー ン	b
バ ー ル	bar
ガ ル	Gal
キ ュ リ ー	Ci
レ ン ト ゲ ン	R
ラ ド	rad
レ ム	rem

$1 \text{ Å} = 0.1 \text{ nm} = 10^{-10} \text{ m}$

$1 \text{ b} = 100 \text{ fm}^2 = 10^{-28} \text{ m}^2$

$1 \text{ bar} = 0.1 \text{ MPa} = 10^5 \text{ Pa}$

$1 \text{ Gal} = 1 \text{ cm/s}^2 = 10^{-2} \text{ m/s}^2$

$1 \text{ Ci} = 3.7 \times 10^{10} \text{ Bq}$

$1 \text{ R} = 2.58 \times 10^{-4} \text{ C/kg}$

$1 \text{ rad} = 1 \text{ cGy} = 10^{-2} \text{ Gy}$

$1 \text{ rem} = 1 \text{ cSv} = 10^{-2} \text{ Sv}$

表5　SI接頭語

倍数	接頭語	記号
10^{18}	エ ク サ	E
10^{15}	ペ タ	P
10^{12}	テ ラ	T
10^{9}	ギ ガ	G
10^{6}	メ ガ	M
10^{3}	キ ロ	k
10^{2}	ヘ ク ト	h
10^{1}	デ カ	da
10^{-1}	デ シ	d
10^{-2}	セ ン チ	c
10^{-3}	ミ リ	m
10^{-6}	マ イ ク ロ	μ
10^{-9}	ナ ノ	n
10^{-12}	ピ コ	p
10^{-15}	フ ェ ム ト	f
10^{-18}	ア ト	a

（注）

1. 表1－5は「国際単位系」第5版, 国際度量衡局 1985年刊行による。ただし, 1 eV および1 uの値はCODATAの1986年推奨値によった。
2. 表4には海里, ノット, アール, ヘクタールも含まれているが日常の単位なのでここでは省略した。
3. barは, JISでは流体の圧力を表わす場合に限り表2のカテゴリーに分類されている。
4. EC閣僚理事会指令ではbar, barnおよび「血圧の単位」mmHgを表2のカテゴリーに入れている。

換　算　表

力	N(=10^5dyn)	kgf	lbf
	1	0.101972	0.224809
	9.80665	1	2.20462
	4.44822	0.453592	1

粘　度　$1 \text{ Pa·s}(N \cdot s/m^2) = 10 \text{ P}$(ポアズ)$(g/(cm \cdot s))$

動粘度　$1 \text{ m}^2/s = 10^4 \text{ St}$(ストークス)$(cm^2/s)$

圧力	MPa(=10 bar)	kgf/cm²	atm	mmHg(Torr)	lbf/in²(psi)
	1	10.1972	9.86923	7.50062×10^3	145.038
	0.0980665	1	0.967841	735.559	14.2233
	0.101325	1.03323	1	760	14.6959
	1.33322×10^{-4}	1.35951×10^{-3}	1.31579×10^{-3}	1	1.93368×10^{-2}
	6.89476×10^{-3}	7.03070×10^{-2}	6.80460×10^{-2}	51.7149	1

エネルギー・仕事・熱量	J(=10^7erg)	kgf·m	kW·h	cal(計量法)	Btu	ft·lbf	eV
	1	0.101972	2.77778×10^{-7}	0.238889	9.47813×10^{-4}	0.737562	6.24150×10^{18}
	9.80665	1	2.72407×10^{-6}	2.34270	9.29487×10^{-3}	7.23301	6.12082×10^{19}
	3.6×10^6	3.67098×10^5	1	8.59999×10^5	3412.13	2.65522×10^6	2.24694×10^{25}
	4.18605	0.426858	1.16279×10^{-6}	1	3.96759×10^{-3}	3.08747	2.61272×10^{19}
	1055.06	107.586	2.93072×10^{-4}	252.042	1	778.172	6.58515×10^{21}
	1.35582	0.138255	3.76616×10^{-7}	0.323890	1.28506×10^{-3}	1	8.46233×10^{18}
	1.60218×10^{-19}	1.63377×10^{-20}	4.45050×10^{-26}	3.82743×10^{-20}	1.51857×10^{-22}	1.18171×10^{-19}	1

$1 \text{ cal} = 4.18605 \text{ J}$（計量法）

$\phantom{1 \text{ cal}} = 4.184 \text{ J}$　（熱化学）

$\phantom{1 \text{ cal}} = 4.1855 \text{ J}$　（15 ℃）

$\phantom{1 \text{ cal}} = 4.1868 \text{ J}$（国際蒸気表）

仕事率　1 PS（仏馬力）

$ = 75 \text{ kgf·m/s}$

$ = 735.499 \text{ W}$

放射能	Bq	Ci
	1	2.70270×10^{-11}
	3.7×10^{10}	1

吸収線量	Gy	rad
	1	100
	0.01	1

照射線量	C/kg	R
	1	3876
	2.58×10^{-4}	1

線量当量	Sv	rem
	1	100
	0.01	1

PROGRESS REPORT ON SAFETY RESEARCH ON RADIOACTIVE WASTE MANAGEMENT FOR THE PERIOD APRIL 1996 TO MARCH 1998